Low-dimensional controllability of complex networks and applications to the human brain

Rémy Ben Messaoud

Sorbonne Université
Ecole doctorale Informatique, Télécomunications et Eléctronique,
EDITE de Paris

Low-dimensional controllability of complex networks and applications to the human brain

Dissertation in applied mathematics

by Remy Ben Messaoud

supervised by Fabrizio de Vico Fallani
and co-supervised by Mario Chavez

to be defended on 30/11/2023

Members of the jury:
- Carlos Canudas-de-Wit, directeur de recherche, HDR, rapporteur & président du jury
- Laura Marzetti, professeur, HDR, rapporteur
- Maria Giulia Preti, maître de conférence, examinateur
- Fabrizio de Vico Fallani, directeur de recherche, HDR, directeur de thèse

"Does the brain control you or are you controlling the brain? I don't know if I'm in charge of mine."

– Karl Pilkington

Acknowledgements

First, I would like to thank my thesis director and supervisor Fabrizio de Vico Fallani. It was an honor to work with him. He taught me a lot during these last 3 years. It was also a pleasure to exchange with him on non-scientific subjects and confront our different senses of humor. I also thank my co-supervisor, Mario Chavez, for his help and precious insights along the project. More importantly, Mario gave me my chance when I was finishing my studies and recruited me as a research intern before the Ph.D. I consider myself very lucky that I was present at the Imperial College of London that precise day for Mario's talk on Machine Learning based predictions of epilepsy seizures. That afternoon, I asked him for an internship at the Paris Brain Institute which paved the way for the four following years of my life.

The Institute was a wonderful place to work at because of its interdisciplinary teams and I had the chance to collaborate with great people. I express special thanks to Louis Cousyn, a neurologist whom I met during my early days at the Institute and who is now a friend. I thank Paolo Bartolomeo and Brigitte Charlotte Kaufmann for our collaborations. Paolo and Brigitte are two neuroscientists with whom I collaborated for the application of my work to real structural brain networks. Their participation was a real upgrade for the project. They brought the expertise and knowledge of brain cognition essential to interpreting our results.

We had to analyze a large-scale neuro-imaging dataset, the UK-biobank, to have those results. I thank Baptiste Couvy-du-chene for his precious help during that process. Thanks to Baptiste, I am no longer afraid of bash scripts! I thank my colleague Vincent Ledu who developed the tractography pipeline that enabled extracting the 6k brain networks that constituted the core materials of my work. That would have not been possible without the Institute's computing facilities and the support of the IT team.

The working environment was so great and it was a pleasure being part of the ARAMIS team for three years. I thank the whole team for the passionate lunch discussions and relaxing after-work drinks. Special thanks to Charley Presigny and Tristan Venot, my close sailing comrades during this adventure.

Every Ph.D. student would say it: "Doctoral research can be hard sometimes". I thank my girlfriend, friends, and family for making it easier on me, especially when they fainted to understand what I was doing.

Abstract

Controllability and optimal control are specific fields of mathematics that have been developed since the Industrial Revolution in order to command engineered systems. Nowadays, many systems are interconnected and form networks like the World Wide Web, transportation networks, or power grids. The biological world is also full of networks: vascular networks, gene regulation, and brain connectivity networks. Gaining control over these large and complex interconnected systems is challenging.

During the last decade, there has been an explosion of studies applying controllability theory to networks. Some breakthroughs were made in characterizing the minimum number of controlled nodes and their placement. However, the state-of-the art metrics have some pit-falls for undirected and/or large networks. In addition, practically controlling networks and steering them toward specific configurations remains challenging mainly when a small fraction of nodes is controlled which is a common constraint, especially for biological networks.

This dissertation aims to explore the limit where only one single node is allowed to be driven by external input as it would certainly be the case for brain stimulation perspectives. We observed in practice that one driver node can only control five target nodes. This practical limitation was previously observed and documented. In order to overcome it, we developed a way to aggregate the states of large networks into a few representative components. We decided to take advantage of the Laplacian eigenmaps method which was already successfully applied in graph embedding and dimensionality reduction techniques. By controlling a few output components, we reduced drastically the number of terminal constraints and ensured that the problem is well-conditioned. We described trade-offs between the precision of the output control and the representativeness of the original high dimensional network state and compared our approach to other outputs. We called our method low-dimensional network control. We tested and validated it with synthetic networks.

We found that it can be adapted to build a controllability metric that is well-scaled and does not suffer from the numerical issues which arise in high dimensions. We applied our method to a large dataset of structural brain networks (N > 6k) of healthy participants deriving a detailed map of single-driver controllability for 9 large-scale networks that support human cognition. Our findings were in line with previous literature and brought additional knowledge to the lateralization of cognitive networks. More importantly, our framework enabled a comprehensive integration of controllability at the level of these aforementioned cognitive networks. This integration showed how brain wiring deferentially facilitates the influence they can have on one another.

Scientific production

Papers:

• Ben Messaoud R., Ledu V., Kaufmann B. C, Baptiste Couvy-Duchesne, Lara Migliaccio, Bartolomeo P., Chavez M., De Vico Fallani F., Low-dimensional controllability of complex brain networks. https://arxiv.org/abs/2311.11132

Side colalborations

• Cousyn, L, Messaoud, RB, Lehongre, K, Frazzini, V, Lambrecq, V, Adam, C, et al. Daily resting-state intracranial EEG connectivity for seizure risk forecasts. Epilepsia. 2023; 64: e23–e29. https://doi.org/10.1111/epi.17480

• Lucas Baudouin, Noémie Adès, Kadia Kanté, Corinne Bachelin, Hatem Hmidan, Cyrille Deboux, Radmila Panic, Rémy Ben Messaoud, Yoan Velut, Soumia Hamada, Cédric Pionneau, Kévin Duarte, Sandrine Poëa-Guyon, Jean-Vianney Barnier, Brahim Nait Oumesmar, Lamia Bouslama-Oueghlani bioRxiv 2023.10.16.555467; doi: https://doi.org/10.1101/2023.10.16.555467

Talks:

• Oral presentation at « International School and Conference on Network Science », July 10-14, Vienna, Austria, https://netsci2023.wixsite.com/netsci2023

• Oral presentation at « Network Neuroscience » satellite of Netsci23, July 10-11, Vienna, Austria, https://networkneuroscience.github.io

Posters

• Poster at the Conference on Complex Systems CCS2022, Oct. 17-21, Palma de Mallorca, https://www.ccs2022.org/, Ben Messaoud R, Kaufmann B. C., Bartolomeo P., De Vico Fallani F., Right and left hemispheres of the human brain compete for centrality. https://cnrs.hal.science/hal-03997857/

Contents

List of Figures

List of Tables

Introduction 1

1.1 A bit of history

Let us dive into the mathematical journey and the history of network controllability to put this dissertation in its global context. The first contributions that relate to network science can be traced back to the 18th century when mathematician Leonard Euler resolved the famous problem of the seven bridges of Königsberg where the task is to devise a walk through the city that would cross each bridge once and only once. This laid the foundations of graph theory which is closely connected to network science. Overall, graph theory focuses on developing algorithms to solve topological problems like finding shortest paths, matchings, or spanning trees in a graph [1].

However, network science is focused on understanding the statistical properties of networks, uncovering the mechanisms that favor certain topologies, and ultimately explaining how the functions of real-world systems relate to their underlying structures. And this field is relatively new. Many agree that the cooperation, in the fifties and sixties, of Hungarian mathematician Paul Erdős and statistician Alfred Rényi to explore the properties of random graphs marked the beginning of network science [2].

Around that same time, another Hungarian mathematician, Rudolf Emil Kálmán, made major contributions to the theory of optimal control. It is a framework that seeks to find the best possible control inputs to a system in order to steer it to a desired state while optimizing a certain criterion typically expressed as a cost function. Mostly known for his digital filters that revolutionized guidance and control of many engineered systems, Kálmán also introduced the notion of controllability which denotes the ability to move a system around its possible configurations that are called state space [3].

These two sub-fields of mathematics stayed unrelated until Ching-Tai Lin combined them almost fifteen years later. He introduced the concepts of structure and structural controllability for linear time-invariant systems. His paper of 1974 [4] marked the beginning of the sub field of network controllability. One has to imagine a system of interconnected agents with linear dynamics and the goal is to understand the role of the underlying network structure in the controllability of the whole system.

1.2 Network controllability: today

Nowadays, almost fifty years later, network controllability is still a challenging field of research. It has been applied to a variety of networks: technological such as power grids [6] or transportation networks [7], or biological like gene regulation networks [8] or brain networks [9]. For

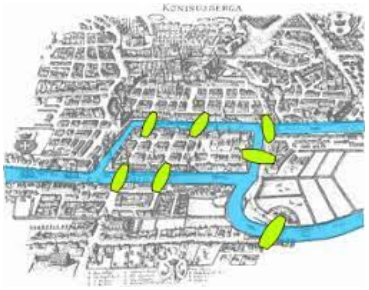

Figure 1.1: The seven bridges of Königsberg. Image from https://en.wikipedia.org/wiki/Seven_Bridges_of_K%C3%B6nigsberg. This image is under the "Creative Commons" licence.

[1]: Bondy et al. (2008), *Graph Theory*

[2]: Paul Erdos et al. (1959), 'On random graphs I'

[3]: Kálmán (1960), 'Contributions to the Theory of Optimal Control'

[4]: Lin (1974), 'Structural controllability'

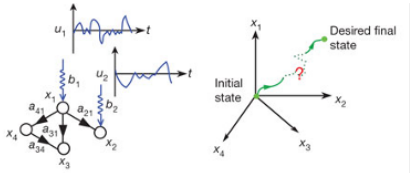

Figure 1.2: Sketch of the network controllability framework. Figure reproduced from [5] with permission of the rights holder, Springer Nature.

[5]: Liu et al. (2011), 'Controllability of complex networks'

[6]: Summers et al. (2016), 'On Submodularity and Controllability in Complex Dynamical Networks'

[7]: Rinaldi (2018), 'Controllability of transportation networks'

[8]: Li et al. (2019), 'Control principles for complex biological networks'

example, in brain network controllability, the goal can be to understand the ability of single regions to influence the rest or part of the network [9]. The perspective of such studies can be to gain information on endogenous control processes that happen during cognitive tasks [10] or also to help guide exogenous interventions like electrical or magnetic brain stimulation [11]. The study of brain network controllability could help in designing targeted and individualized interventions.

[9]: Gu et al. (2015), 'Controllability of structural brain networks'
[10]: Medaglia (2019), 'Clarifying cognitive control and the controllable connectome'
[11]: Menardi et al. (2022), 'Maximizing brain networks engagement via individualized connectome-wide target search'

Network controllability can be unfolded in two parts: Where is the external input to be placed? And how do we calculate it? In other terms how many driver nodes (which each receive an input) are needed in order to achieve theoretical controllability and what is their location? Once the driver nodes are selected, how do we practically calculate the input to steer the network toward a desired final state? These questions have been tackled progressively during the last decades using different techniques. However, there are still challenges and that is why network controllability is still being investigated. Indeed, in 2013, Sun & Motter showed that even though a network is theoretically controllable regarding the Kalman criterion, steering it to a desired state fails in practice if too few drivers are used (below a fraction of 0.2) [12]. This was a tipping point as it showed the limits of the theory and put the practicality of the control at the center of attention.

[12]: Sun et al. (2013), 'Controllability Transition and Nonlocality in Network Control'

In fact, if not enough driver nodes are allowed, the problem of finding a control input for a given state transition becomes ill-posed. In other terms, the problem cannot be solved precisely because the solution will be dominated by round-off errors. On top of that, very often, the number of drivers is constrained. If we take the example of brain networks, it is not technologically realistic to consider multiple and simultaneous stimulations. Most transcranial magnetic stimulation protocols use one single coil [11] and recently 2-coil devices have been tested [13]. This constituted the departing point of the research question we investigated during this PhD project.

[13]: Kavanaugh et al. (2018), 'Neurocognitive Effects of Repetitive Transcranial Magnetic Stimulation With a 2-Coil Device in Treatment-Resistant Major Depressive Disorder'

We ultimately wanted to find a way to select driver nodes that would best control a given target subnetwork by avoiding numerical discrepancies. To summarize our approach, as it is often impossible to increase the number of drivers, we preferred to focus on the target and reduce its dimensionality. The idea is to control just an aggregate measure of the states of the target nodes. We proposed to use the Laplacian eigenvectors as a basis to project the target states onto a lower dimensional space. This way, we decrease the number of terminal constraints and solve a well-posed. The use of a network output that is directly derived from the Laplacian ensures that we aggregate the network state by taking account of its underlying topology. We finally, applied our method to a large database of healthy participants from which we extracted their structural connectomes.

Our framework is original, because it permitted us to study the controllability of large networks without the computational limitations that arise from the curse of dimension. An addition to reliably selecting driver nodes, the other important aspect of this work is that with classical metrics one cannot compare the controllability of heterogeneous targets of different sizes. By projecting the targeted networks into spaces of low and fixed dimension, we obtained a harmonized, or normalized

controllability metric. As a result, we were the first to dress a map of system-level controllability of the brain and to interpret it from a cognitive perspective.

In this dissertation, we first explain, in Chapter 2, in which ways network controllability can help understand and better manipulate brain networks. We then introduce, in Chapter 3, basic concepts of network controllability and try to dress an extensive and comprehensive review of the literature. In Chapter 4, we introduce our contribution and its validation. In Chapter 5, we present its application to brain networks in a large dataset and integrate the results at the system-level in Chapter 7. We further examined this dataset in Chapter 7 in order to highlight the hemispheric differences in structural brain networks. Finally, in Chapter 8, we draw conclusions about our work and discuss its limitations and potential future directions.

Network Neuroscience and controllability

2

2.1 Network neuroscience

Network neuroscience is a flourishing field of research that focuses on understanding the intricate and complex relationships among brain regions by modeling them as interconnected networks. This approach capitalizes on concepts from graph theory and complex systems to unravel the fundamental principles governing brain function and dynamics. The field has rapidly evolved into an official area of investigation due to several key steps [14].

[14]: Bassett et al. (2017), 'Network neuroscience'

Advancements in Brain Imaging: The development of advanced neuroimaging techniques, such as functional Magnetic Resonance Imaging (fMRI), Electroencephalography (EEG), and Magnetoencephalography (MEG), enabled researchers to non-invasively observe and measure brain activity with high spatial and temporal resolution.

Graph Theory and Complex Systems The application of graph theory to brain research paved the way for representing brain regions as nodes and their connections as edges in a network. This approach allowed researchers to quantify various network properties, such as node centrality, modularity, and small-worldness, providing a novel framework for characterizing brain organization.

Data Sharing and Collaboration The establishment of large-scale collaborative initiatives, like the Human Connectome Project, facilitated the collection and sharing of extensive neuroimaging data from diverse populations. This collaborative spirit fostered the development of standardized methodologies and analytical tools, promoting the growth of network neuroscience.

Interdisciplinary Approach Network neuroscience thrives at the intersection of neuroscience, physics, mathematics, and computer science. This interdisciplinary approach has attracted researchers with diverse expertise, leading to innovative techniques and insights.

Relevance to Brain Disorders The potential of network neuroscience to uncover altered connectivity patterns in various brain disorders, such as Alzheimer's disease, schizophrenia, and epilepsy, has garnered significant attention from the medical and clinical communities. These insights hold promise for developing new diagnostic and therapeutic strategies.

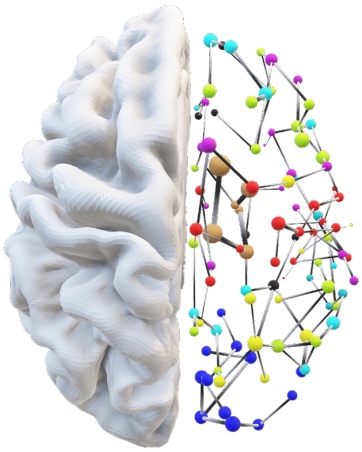

Figure 2.1: backbone of a structural connectome.

Network neuroscience presents a highly promising tool for understanding brain dynamics due to its ability to capture the complex interactions between brain regions and their roles in cognition, behavior, and dysfunction. By viewing the brain as a network, we can uncover emergent properties that would be challenging to discern using traditional reductionist approaches [14]. The network perspective provides a holistic understanding of brain function, revealing how information flows, how

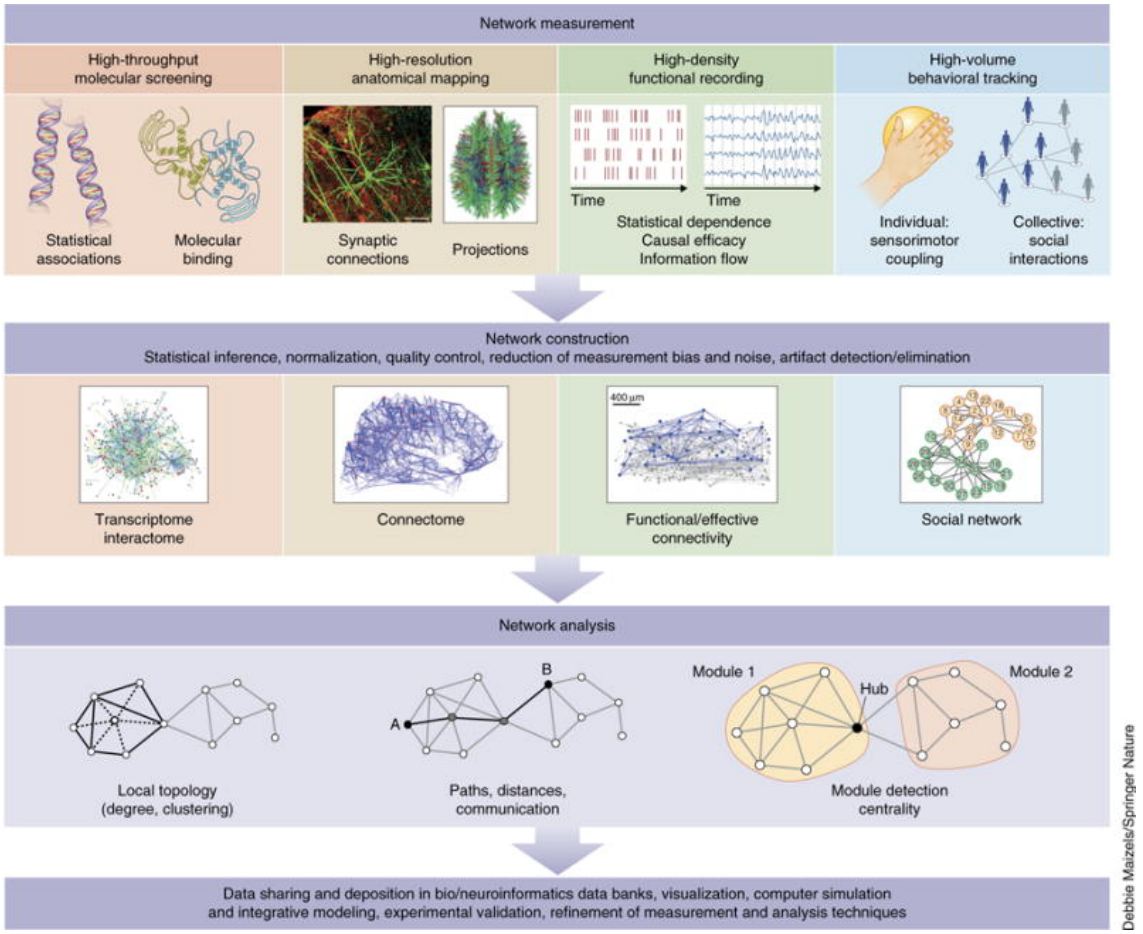

Figure 2.2: Network measurement, construction and analysis: figure reproduced from [14] with permission of right holders, Springer Nature.

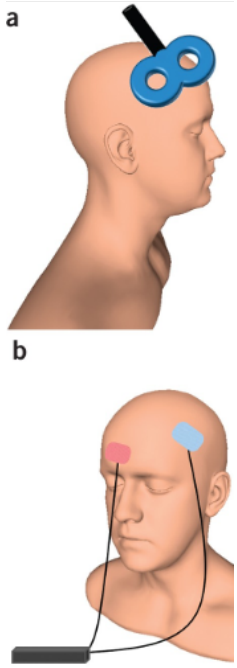

Figure 2.3: NIBS: a) TMS, b) tDCS, figure reproduced from [16] with permission of rights holders, Springer Nature.

[15]: Kringelbach et al. (2007), 'Translational principles of deep brain stimulation'

different regions collaborate, and how disruptions in connectivity can lead to cognitive deficits or neurological disorders. As our knowledge of network neuroscience continues to grow, it holds the potential to revolutionize our understanding of the brain's intricate workings and open up new avenues for targeted interventions and treatments.

2.2 Network controllability: a promising tool for brain stimulation

Deep brain stimulation has been approved by the Food and Drugs Administration in 1997 for the treatment of Parkinson's disease. It is now a mature technology that can also be used to treat dystonia, obsessive-compulsive disorder (OCD) and epilepsy [15]. However it is an invasive technique that involves a major surgery and regular monitoring.

In the last two decades, there has also been a tremendous development of noninvasive brain stimulation techniques (NIBS). The most commonly used are transcranial magnetic stimulation (TMS; Fig2.3a)) and transcranial direct current stimulation (tDCS; Fig2.3b)) The development of neuroimaging techniques opened the possibility to study not only the clinical and long-term effects of brain stimulation but also its immediate

electrophysiological impact on the brain and how its induced perturbations propagate through its underlying structural connectivity [16, 17]. Moreover, this technique has gained popularity and proved to be efficient in curing psychiatric diseases like depression [11] or in improving motor or cognitive recovery after a stroke for example[18, 19]. In this context, a theory that would explain or predict the effects of brain stimulation on functional network activity was needed. Presumably, network control theory is the best candidate that can integrate both static features of brain networks and their complex dynamical activity [20]. To our knowledge, there is one study [21] that confronted network control theory (NCT) with experimental physiological testable hypotheses. They used Electrocorticography (ECoG), a type of intracranial electroencephalography (iEEG) to stimulate and monitor brain activity during memory tasks. They quantified the role of white matter tract architecture in guiding direct electrical stimulation and reported positive conclusions regarding the power of NCT in predicting brain response to stimulation.

[16]: Dayan et al. (2013), 'Noninvasive brain stimulation'
[17]: Polanía et al. (2018), 'Studying and modifying brain function with non-invasive brain stimulation'
[18]: Smith et al. (2016), 'Transcranial magnetic stimulation (TMS) in stroke'
[19]: Medaglia et al. (2021), 'Language Tasks and the Network Control Role of the Left Inferior Frontal Gyrus'
[20]: Lynn et al. (2019), 'The physics of brain network structure, function and control'
[21]: Stiso et al. (2019), 'White Matter Network Architecture Guides Direct Electrical Stimulation through Optimal State Transitions'

Additionally, when using TMS, the general goal is to engage certain areas of the brain. For example, there are protocols and guidelines to find specific "hotspots" responsible for muscle representations [22]. Very often, when used for therapeutic objectives, like for depression, cognitive enhancement, or rehabilitation purposes, the point is to engage brain networks that are composed of many regions that are sometimes sparsely distributed in the brain. A recent study [23], demonstrated the fact that applying TMS to generic "hotspots" will have different effects depending on the specific functional neuroanatomy of the subject. Indeed, they first showed that there is variability in the network organization of functional networks, and thus the electrical field of the TMS will certainly cover off-target regions. Therefore, they suggested an automated and personalized method for coil placement. However, they assumed in the paper that it was important to maximize the electrical field within the target network and they also discussed that it is not known a priori which of the regions composing the network would give the best results. Regarding this matter, another study also conducted in silico experiments on structural brain connectomes [11]. They used NCT to find individual regions that maximize the engagement of known functional networks and showed a large variability in the selected brain regions.

[22]: Sivaramakrishnan et al. (2016), 'Spatial localization and distribution of the TMS-related 'hotspot' of the tibialis anterior muscle representation in the healthy and post-stroke motor cortex'

[23]: Lynch et al. (2022), 'Automated optimization of TMS coil placement for personalized functional network engagement'

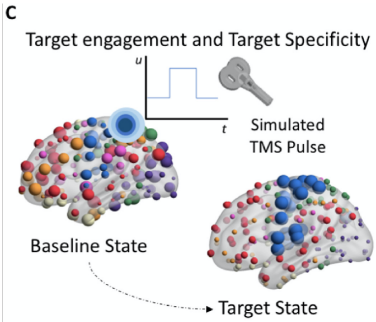

Figure 2.4: Somatomotor network engagement, Image adapted from [11] under license CC-BY-NC-ND.

[11]: Menardi et al. (2022), 'Maximizing brain networks engagement via individualized connectome-wide target search'

Taken together, the results of these two studies show the importance of personalized methods [11, 23]. Indeed, each individual has its own anatomy, its own functional network organization, and its own white matter tract architecture that are very likely to change the effects of brain stimulation.

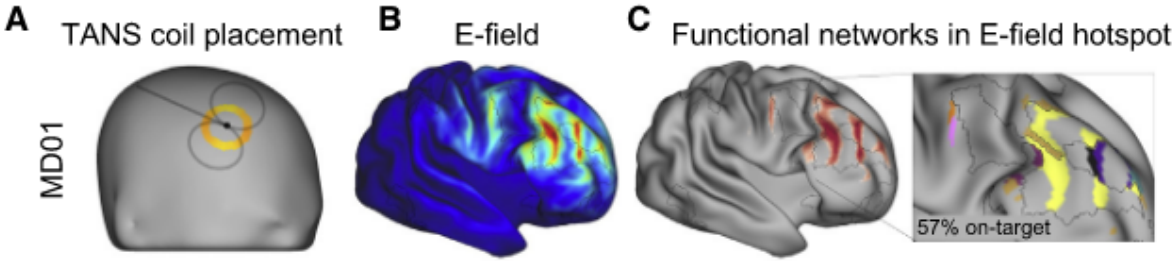

Figure 2.5: Coil placement and variability in functional network stimulation. The target is the frontoparietal network in yellow. Figure reproduced from [23] under the licence CC-BY-NC-ND

2.3 Brain controllability supports cognition and captures disease fingerprints

[9]: Gu et al. (2015), 'Controllability of structural brain networks'

The first study which focused on the controllability of structural brain networks, (Gu, et.al [9]) differentiated two types of controllability: average and modal controllability. The former, informs on the capacity to "drive" the network toward "easy to reach states" and the latter for "hard to reach states". The main conclusion of this paper is that hubs of average controllability were located in the parietal lobe whereas those for modal controllability were mostly in the frontal lobe involving the default mode network (DMN) and the executive control network (ECN). This result constituted the first promise of the NCT since these two networks are specifically those engaged in higher-order tasks such as those demanding intelligence and creativity [10, 24].

[10]: Medaglia (2019), 'Clarifying cognitive control and the controllable connectome'

[24]: Kenett et al. (2018), 'Driving the brain towards creativity and intelligence'

[25]: Cornblath et al. (2020), 'Temporal sequences of brain activity at rest are constrained by white matter structure and modulated by cognitive demands'

[26]: Cui et al. (2020), 'Optimization of energy state transition trajectory supports the development of executive function during youth'

[27]: Lee et al. (2020), 'Heritability and Cognitive Relevance of Structural Brain Controllability'

Since then, a lot of studies were conducted to analyze brain controllability and show its relevance to cognitive functions [10][26]. The data and experiments would suggest that network controllability of participants brain would account for 50% of their cognitive performances [27]. Moreover, specific aspects of cognition were then studied such as language that is known to be a left lateralized function was related through NCT to the left inferior frontal gyrus [19]. Memory was also studied and NCT permitted to unravel mechanistic state transitions and to better understand the

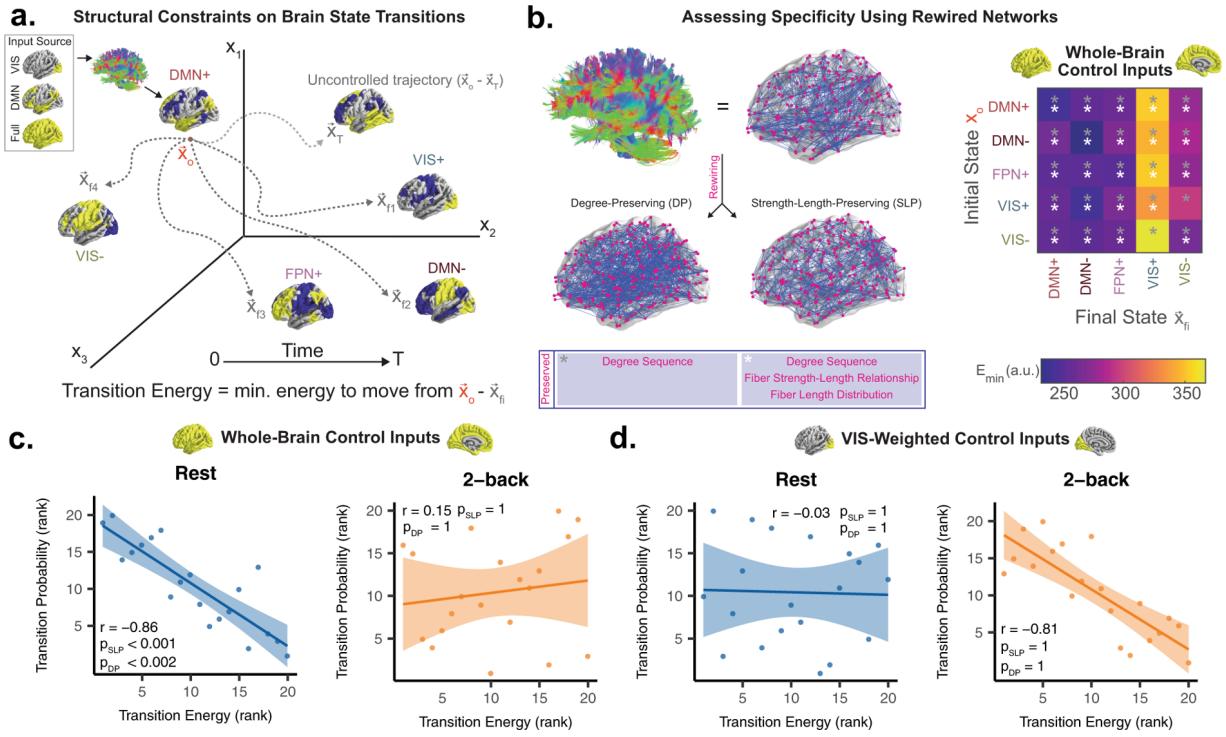

Figure 2.6: Figure and caption reproduced from [25] under license Creative Commons CC BY **: Linear dynamics along white matter explain brain state transition probabilities. a**, Schematic demonstrating calculation of minimum control energy needed to move a linear dynamical system defined by white matter connectivity from some initial state x_0 to some final state x_f over a time horizon T. **b**, Schematic of network null models (left) preserving different spatial and topological features of networks defined by white matter connectivity. The energies (Emin) required to maintain or transition between each state are lower in real brain networks compared to these null models (right). **c**, and **d** Spearman correlation between structure-based transition energy prediction (x-axis) and empirically derived transition probability (y-axis) for resting state (left) and the 2-back condition of the n-back task (right), using inputs weighted evenly throughout the whole brain c or weighted positively towards the visual system **d**,. Linear fit of rank values are shown due to the monotonic, non-linear relationships in the data.

dialogue between the visual system the DMN and the ECN during 2-back memory tasks.

Furthermore, efforts were made to assess the controllability of individuals with neurological alterations. It was shown for example that NCT captured alterations caused by schizophrenia of the energetic landscape of functional state transitions during memory tasks [28]. Other studies focused on epilepsy. It was shown that modal controllability accumulated specifically in the focal epileptic brain regions [29]. And Ref.[30] analyzed time-evolving effective connectivity during epileptic seizures and studied the controllability of implanted electrodes to assess control strategies in order to drive the network to seizure-free states.

[19]: Medaglia et al. (2021), 'Language Tasks and the Network Control Role of the Left Inferior Frontal Gyrus'

[28]: Braun et al. (2021), 'Brain network dynamics during working memory are modulated by dopamine and diminished in schizophrenia'

[29]: Chari et al. (2022), 'Drug-resistant focal epilepsy in children is associated with increased modal controllability of the whole brain and epileptogenic regions'

2.4 Conclusion

Network controllability offers a highly promising framework for studying brain dynamics due to its ability to unveil crucial aspects of neural information processing. By assessing how well we can steer the activity of the brain's interconnected regions it provides unique perspectives for designing individualized interventions and stimulations. This approach captures how the brain's intricate wiring supports cognition, identifying critical nodes and pathways that govern the control of information flow. Moreover, network controllability could serve as a potential bio-marker for neurological diseases. Changes in a network's controllability profile might indicate alterations in brain function, offering an early diagnostic tool and paving the way for tailored treatments that address specific disruptions in neural circuits. In essence, network controllability stands at the forefront of neuroscience, presenting a holistic understanding of brain dynamics.

Network controllability: concepts and state-of-the-art

3

3.1 From systems controllability to networks controllability

The concept of controllability is fundamental in engineered systems and has been extended to the realm of networked systems. In spite of some similarities, there are also notable differences between the controllability of an engineered system and network controllability.

In engineered systems, the plant parameters and dynamics are very often known and can be tuned. The state equation involves state variables that fully describe the system and are often velocities or voltages for example. The seminal work, by Kalman in 1960 [3], established the controllability criterion for linear time-invariant systems, known as the Kalman controllability matrix. This criterion ensures that a system is controllable if and only if its controllability matrix has full rank. Additionally, the controllability of engineered systems focuses on designing feedback control laws and implementing closed-loop controllers.

[3]: Kálmán (1960), 'Contributions to the Theory of Optimal Control'

In contrast, network controllability addresses the control of complex systems composed of interconnected elements. It seeks to investigate how the structure of a network affects the ability to control its dynamics by manipulating a subset of nodes as control inputs. The pioneering work of Ching-Tai made the first step toward it by introducing the concept of structural controllability in 1974 [4] and showed that finding driver nodes can be reduced to finding spanning cacti structures in the network. Building upon that, (Liu et.al) added the missing brick in 2011 and mapped the algebraic problem of determining ranks of the Kalman matrix for a prohibitive number of driver configurations to a graph-based problem [5]. They proved that a network can be fully controlled if drivers are selected as the unmatched nodes in a maximum cardinality matching.

[4]: Lin (1974), 'Structural controllability'

[5]: Liu et al. (2011), 'Controllability of complex networks'

In conclusion, the difference between engineered systems controllability and network controllability lies in their scope and methodology. Engineered system controllability focuses on the control of individual systems based on their internal dynamics, whereas network controllability examines the ability to control the collective behavior of interconnected elements in complex systems. The emergence of network controllability as a field of research has provided new insights into the control of complex systems, offering a novel perspective for understanding and influencing their behavior.

3.2 Network control theory

Let us consider a structured system that is described as a network (or graph) in which the nodes (or vertices) are entities that interact through links (or edges). The dynamics of the system are described by the following equation: 3.2.

$$\begin{aligned} \dot{x}(t) &= Ax(t) + Bu(t) \\ y(t) &= Cx(t) \end{aligned} \tag{3.1}$$

Here, the networked system, of size n, is described by the matrix A $(n \times n)$ and the vector x $(n \times 1)$ contains the states of the nodes. The second term in the state equation is the external action on the system. B $(n \times n_d)$ is the input matrix and denotes where the input signal u(t) is injected. The nodes to which we inject the input are called driver nodes. One can be interested in controlling the states $x(t)$ or an output $y(t)$. The output $y(t)$ can be any linear combination $Cx(t)$ and C $(r \times n)$ is called the output matrix. Some definitions [31]:

[31]: Kalman (2011), 'Lectures on Controllability and Observability'

Definition 3.2.1 *the system (A, B) is controllable if, for any initial state x_0 and any final state x_f, there exists an input $u(t)$ that achieves the state transition in finite time t_f.*

Definition 3.2.2 *The energy of the control input is defined as*
$E(u, t_f) = \int_0^{t_f} u(t) \,.\, u(t)^T \, \mathrm{d}t.$

Let us summarize important results from linear systems controllability [31]:

Theorem 3.2.1 *the following statements are equivalent*

(i) The system (A, B) is controllable.

(ii) The $n \times n.n$ Controllability matrix $\mathcal{K} = [B \; AB \; A^2B ... \; A^{n-1}B]$ has full rank (Kalman criterion).

(iii) The $n \times (n + p)$ matrix $[A - \lambda.I \quad B]$ has full row rank for each λ eigenvalue of A (PBH criterion).

(iv) The $n \times n$ controllability Gramian $\mathcal{W} = \int_0^{t_f} e^{A\tau} \, BB^T \, e^{A^T\tau} \, \mathrm{d}\tau$ is non-singular (Gramian criterion).

Theorem 3.2.2 *If (A,B) is controllable, then the control input that steers the system from x_0 to x_f in time t_f with minimum energy is*

$u(t) = -B.e^{A(t_f - t)}.\mathcal{W}^{-1}(t_f).[e^{A(t_f - t_0)}.x_0 \; - \; x_f]$

and substituting into equation 3.2 we have
$x(t) = e^{A.t}.x_0 \; + \; \int_0^t e^{A.(t-\tau)} \, B.u(\tau) \, \mathrm{d}\tau.$

Let us denote G the adjacency matrix of the considered network, meaning

that G_{ij} contains the weight of the directed link going from node j to node i.

Remark 3.2.1

Stabilization and normalization:
Typically, we obtain the matrix A by stabilizing the matrix G as follows.

$$A = G - \lambda_{max}(G).I \tag{3.2}$$

where $\lambda_{max}(G)$ denotes the largest eigenvalue of G.

Indeed, all eigenvalues of A must have negative real parts for system 3.2 to be stable. Matrix A can also be said Hurwirtz in that case as in [32, 33]. This is a sufficient condition for the existence of the controllability Gramian.

Another possibility is presented in [21, 34]:

$$A = \frac{G}{\lambda_{max}(G) + c} - I \tag{3.3}$$

that implies this new parameter c that tunes the degree of stability.

[32]: Casadei et al. (2018), 'Controllability of Large-Scale Networks'
[33]: Casadei et al. (2020), 'Model Reduction Based Approximation of the Output Controllability Gramian in Large-Scale Networks'

[21]: Stiso et al. (2019), 'White Matter Network Architecture Guides Direct Electrical Stimulation through Optimal State Transitions'
[34]: Karrer et al. (2020), 'A practical guide to methodological considerations in the controllability of structural brain networks'

Finally, the input matrix is typically composed of zeros and N_d elements equal to one that establishes a one-to-one relationship between each input signal component and each driver node.

3.3 Network controllability: different approaches and metrics

This section guides the reader through the timeline of contributions to the field. We specify the main used approaches that led to different types of controllability that have been addressed: structural, exact, target, and output controllability. We also review the main controllability metrics.

3.3.1 Structural controllability

Structural controllability was introduced to overcome the fact that many real-world networks are only known to a certain extent. Very often the weights of the network are estimated and are thus practically known with a certain error margin and that led to this formulation [35].

[35]: Lee et al. (1967), *Foundations of optimal control theory*

Proposition 3.3.1 *The pair (A_0, B_0) is structurally controllable if and only if $\forall \epsilon > 0$, there exists a completely controllable pair (A_1, B_1) of the same structure as (A_0, B_0) such that $\|A_1 - A_0\| < \epsilon$ and $\|BA_1 - B_0\| < \epsilon$.*

[4]: Lin (1974), 'Structural controllability'

Further, the work of Ching-Tai in 1974 [4] established an equivalence between the algebraic Kalman rank condition and two conditions on the underlying graph.

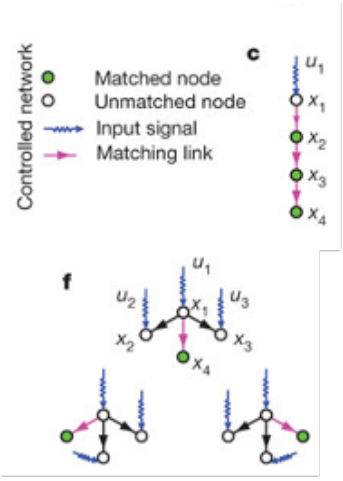

Figure 3.1: control of unmatched nodes, figure from [5] with permission of the rights holder, Springer Nature.

[5]: Liu et al. (2011), 'Controllability of complex networks'

[36]: Yuan et al. (2013), 'Exact controllability of complex networks'

[12]: Sun et al. (2013), 'Controllability Transition and Nonlocality in Network Control'

[37]: Pasqualetti et al. (2014), 'Controllability Metrics, Limitations and Algorithms for Complex Networks'

[38]: Müller et al. (1972), 'Analysis and optimization of certain qualities of controllability and observability for linear dynamical systems'

Theorem 3.3.2 *The following properties are equivalent*

(i) The pair (A, B) *is structurally controllable.*

(ii) The graph (A, B) *contains no non-accessible node and no dilation.*

(iii) The pair (A, B) *is spanned by a cactus.*

We refer the reader to Ref.[4] for more details on dilations and cacti graphs as it is not in the scope of this dissertation.

As the problem was defined in graph theoretic terms, in 2011, Liu et.al [5] were able to find a geometric solution to efficiently find the driver nodes in a directed network and proved that they were the unmatched nodes in a maximum cardinality matching. Their second result was to establish an analytical expression for the fraction $f_d = n_d/n$ that depends on the degree distribution of the network.

3.3.2 Exact controllability

Despite the elegance of the contribution of Liu et.al [5], it only applies to directed and relatively sparse networks. Indeed, if a network is dense or contains self-loops all nodes can be matched and the method predicts that the network can be controlled from any single node. The reasoning holds for undirected networks since one can consider them as directed networks with twice as many links. This limitation motivated Yuan et.al [36] to develop a method valid for all cases: directed, undirected, with or without self-loops. For that, they based their method on the PBH criterion (3.2.1iii) and develop an algebraic algorithm to find the driver nodes. It works for more cases but has a higher complexity.

3.3.3 Gramian-based controllability

As previous studies focused on theoretical approaches to select driver nodes, Jie Sun and Adilson E. Motter [12] were the first to simulate trajectories and inspect practically the precision of the control. They computed the input signals that minimize the energy as in theorem 3.2.2 and evaluated the distance of the simulated final state to the desired one. Their main result is that even for networks that are theoretically controllable regarding the Kalman criterion, the control fails in practice if the number of drivers is not sufficient (fraction of 0.2). The reason behind this is that the controllability Gramian $\mathcal{W}(t_f)$ is not well-conditioned in such cases. Following this contribution, a shift occurred toward a Gramian-based characterization of controllability.

In the following year, Pasqualetti et.al [37] adopted a series of controllability metrics based on the Gramian to suggest an effective driver placement algorithm for large networks. These measures were introduced for linear systems in 1972 [38] and designed to have physically meaningful interpretations:

Gramian-based controllability metrics

- **Average control energy: Tr($\mathcal{W}^{-1}$)** is the average energy needed for a driver set to steer the network toward $\|x_f\|$ =1. This measure is to be minimized.
- **Worst-case controllability:** $\lambda_{\mathbf{min}}(\mathcal{W})$ is the inverse of the worst-case energy needed for a driver set to steer the network toward $\|x_f\|$ =1. If we remark that $\mathcal{W}$ is symmetric by definition, and thus, positive definite than regarding theorem 3.2.1iv it is intuitive that this measure has to be positive and maximized.
- **Average controllability: Tr($\mathcal{W}$)** reflects the impulse response of the system and thus reflects globally the amount of transmitted energy. Originally, this measure was suggested for unstable systems since its computation is stable for singular Gramians [39].
- **Physical controllability:** $cond(\mathcal{W}) = \frac{\lambda_{\mathbf{max}}(\mathcal{W})}{\lambda_{\mathbf{min}}(\mathcal{W})}$ that reflects the conditioning of the problem of controlling the network with minimal energy. Since the computation of the input signal that minimizes energy necessitates the inversion of the Gramian, its condition number will reflect the degree of propagation of round-off errors. So this measure has to be minimized. This metric was exploited in [40].

[39]: Shaker et al. (2013), 'Optimal sensor and actuator location for unstable systems'

[40]: Wang et al. (2017), 'Physical controllability of complex networks'

In 2018, Lindmark & Altafini [41] studied these metrics for various topologies and showed that a good topological proxy for driver placement strategies was the ratio of the out-degree to the in-degree. They also confirmed that $\lambda_{\min}(\mathcal{W})$ and Tr($\mathcal{W}^{-1}$) are equivalent and both are more reliable than Tr($\mathcal{W}$).

[41]: Lindmark (2018), 'Minimum energy control for complex networks'

3.3.4 Target controllability

In 2014, Gao et.al [42] paved the way for the exploration of target control as it is very often too costly or unnecessary to control the entire network. They adapted the methodology used in ref.[5] to propose a geometric characterization of target control based on graph maximum matching.

[42]: Gao et al. (2014), 'Target control of complex networks'

[5]: Liu et al. (2011), 'Controllability of complex networks'

A series of papers, [43–46], followed to study target control from an energetic point of view. The controllability Gramian of the targeted system

$$\mathcal{W}^{o} = C\mathcal{W}C^{T} \tag{3.4}$$

is studied to derive optimal control and show that energy scales exponentially with the number of targeted nodes.

[43]: Klickstein et al. (2017), 'Energy scaling of targeted optimal control of complex networks'
[44]: Shirin et al. (2017), 'Optimal control of complex networks'
[45]: Klickstein (2020), 'Target Control of Networked Systems'
[46]: Klickstein et al. (2021), 'Controlling network ensembles'

Further, Bassignana et.al [47] showed the Kalman criterion fails in practice for many cases because the controllability matrix $\mathcal{W}$ is numerically rank-deficient. To overcome the ill-posedness of the problem they suggested a heuristic step-wise algorithm to characterize the controllability of single nodes regarding a given target.

[47]: Bassignana et al. (2021), 'Stepwise target controllability identifies dysregulations of macrophage networks in multiple sclerosis'

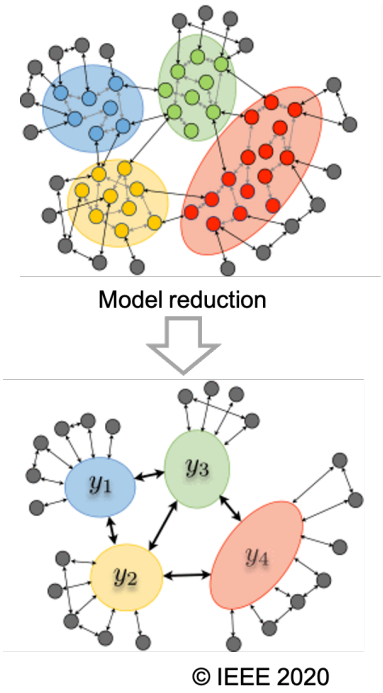

Figure 3.2: Figure adapted from [32, 33] **Average output controllability approach and model reduction**

[32]: Casadei et al. (2018), 'Controllability of Large-Scale Networks'
[33]: Casadei et al. (2020), 'Model Reduction Based Approximation of the Output Controllability Gramian in Large-Scale Networks'

3.3.5 Output controllability and model reduction

As the size of the considered networks increases, the control energy needed becomes unreasonably high and state transitions fail in practice, especially when the number of drivers is low. One solution is to consider the output controllability Gramian as in equation 3.4 instead. However, this definition still relies on the computation of the original Gramian. So Casadei et.al [32, 33] suggested to derive the Gramian and the control signals for a reduced model. They considered that grouping the nodes in clusters and controlling the average state of each cluster was a reasonable output to control. Then they reduced each cluster to one complex node and derived the topology of the new reduced network. Finally, they obtained reduced Gramians that were better conditioned and offered better control accuracy.

3.3.6 Conclusion

This dissertation lies specifically in the continuation and exploration of output controllability. We will suggest an alternative output that is informed from the topology of the network. Furthermore, we will adapt it to build a metric for characterizing the controllability of single driver nodes.

Low-dimensional network control: when output control meets Laplacian eigenmaps

4

The results presented in this section are part of the journal paper in preparation which is the main publication of this PhD project. This section presents the core idea and methodological contribution of this dissertation. We were inspired from the average output controllability approach introduced in Ref.[33] and from the usage of the Laplacian matrix in renormalization-group and coarse-graining techniques [48, 49]. We decided to combine both and that constitutes the originality of this work.

4.1 Methods

4.1.1 Network Laplacian and eigenmaps

We develop here the case of undirected networks (see Appendix for more details on Laplacians of directed networks).
The Laplacian matrix [50] is usually defined as

$$L = D - G. \tag{4.1}$$

where D is a diagonal matrix containing the degree sequence of the network. This is known as the combinatorial Laplacian which is the most basic definition. More sophisticated variants of the Laplacian exist but we decided to focus on the simplest definition here.

We expanded this definition to the Laplacian of a targeted subnetwork.
Remark: No prior literature was found regarding the Laplacian definition of a subnetwork.

Let us consider a given subset of $s \leq n$ target nodes whose states are Sx, where S is a $s \times n$ selection matrix with zeros and one element per line equal to one. The adjacency matrix of the target network is given by SGS^T and we denote D_S the diagonal matrix containing its degree sequence. The Laplacian matrix of the target network is

$$L_S = D_S - SGS^T. \tag{4.2}$$

We remark that if S is equal to the identity, than we find the original definition. The Laplacian can be decomposed in the spectral domain as

$$L_S = V\Lambda V^T. \tag{4.3}$$

where Λ is the diagonal matrix that contains the Laplacian eigenvalues $\lambda_1 = 0 \leq \lambda_2 ... \leq \lambda_p$ that can be interpreted as the spatial frequencies of the graph. The matrix V is orthonormal ($V^T = V^{-1}$) and its columns are the associated eigenvectors called "**eigenmaps**" [50]. An intrinsic characteristic of Laplacian eigenmaps is that they regroup the nodes of the network by similarity. Meaning, that distant nodes in the network will be projected far apart on each of the one-dimensional lines that

[50]: Chung (1997), *Spectral graph theory*

represent the eigenmaps. This property makes them a suitable projection for linear dimensionality reduction [48, 49, 51–53].

[48]: Gfeller et al. (2008), 'Spectral Coarse Graining and Synchronization in Oscillator Networks'
[49]: Villegas et al. (2023), 'Laplacian renormalization group for heterogeneous networks'
[51]: Rui et al. (2016), 'Dimensionality reduction of brain imaging data using graph signal processing'
[52]: Naseri et al. (2022), 'Converting high-dimensional complex networks to lower-dimensional ones preserving synchronization features'
[53]: Ghojogh et al. (2022), *Laplacian-Based Dimensionality Reduction Including Spectral Clustering, Laplacian Eigenmap, Locality Preserving Projection, Graph Embedding, and Diffusion Map*

Link between Laplacian eigenmaps and graph clustering

If the target network is connected, the first eigenvector is constant and can be seen as one average output. Moreover, if the network is composed of k disconnected components then the k first eigenmaps represent the averages of each component [50].

Thus, Laplacian eigenmaps have a natural link with clustering and can be seen as a generalized version of the cluster averages projection. In Graph Signal Processing, any signal z can be decomposed onto the basis of the Laplacian eigenmaps. It is called the Graph Fourier Transform (GFT) and is defined as

$$GFT : \tilde{z} = V^T.z \quad \text{and} \quad iGFT : z = V.\tilde{z} \tag{4.4}$$

$\tilde{z}$ contains the coefficients of the projection of z onto the eigenmaps basis. We show an example of signal decomposition onto the Laplacian eigenmaps in a small network in which $y^{\text{eig}} = GFT(Sx)$ (**Fig.4.1a**). Each eigenmap acts like a weighted sum of node states. They can be used as a projection basis to map high-dimensional data, or any state vector, defined on a network, onto a lower-dimensional space while preserving its underlying structure. Ultimately, closely connected nodes of the original network remain nearby in the lower dimensional space [53].

[53]: Ghojogh et al. (2022), *Laplacian-Based Dimensionality Reduction Including Spectral Clustering, Laplacian Eigenmap, Locality Preserving Projection, Graph Embedding, and Diffusion Map*

4.2 Output control of Laplacian eigenmaps

The idea behind our framework is that instead of controlling directly the states of the target nodes Sx to steer them toward a desired final state Sx_f of dimension s, we will steer their projections $y^{\text{eig}} = (H_r V^T S)x = C^{\text{eig}}x$ toward the desired final output ($y_f = C^{\text{eig}}x_f$) of dimension $r \leq s$ (**Fig.4.1b**). The $r \times s$ matrix $H_r = [e_{i_1}, e_{i_2}, ...e_{i_r}]^T$, selects r Laplacian eigenmaps and acts like a filter in the dual eigenspace. Its role can be seen as to reduce the s final constraints ($Sx(t_f) = Sx_f$), originally defined in the state space, to $r \leq s$ constraints defined in the dual eigenspace ($C^{\text{eig}}x(t_f) = H_r V^T Sx_f$). The resulting system is

$$\begin{aligned} \dot{x}(t) &= Ax(t) + Bu(t) \\ y^{\text{eig}}(t) &= C^{\text{eig}}x(t) \end{aligned} \tag{4.5}$$

In the following, we will refer to the output y^{eig} as the lower-dimensional eigenstate of the targeted network.

[54]: Cui et al. (2019), 'A Survey on Network Embedding'

Remark : Usually, when dealing with network embedding [54], we take $H_r = [I_r \ 0_{\text{s-r}}]$ so as to only keep the r first low spatial frequencies in consideration as they are the most representative of the network at the macro-scale. However, it is possible to select the matrix H_r differently in a task-dependent way. Indeed, in our case, the goal is to steer the network closer to a desired final state. That is why we decided to select the eigenmaps by descending order of magnitudes of the GFT of the

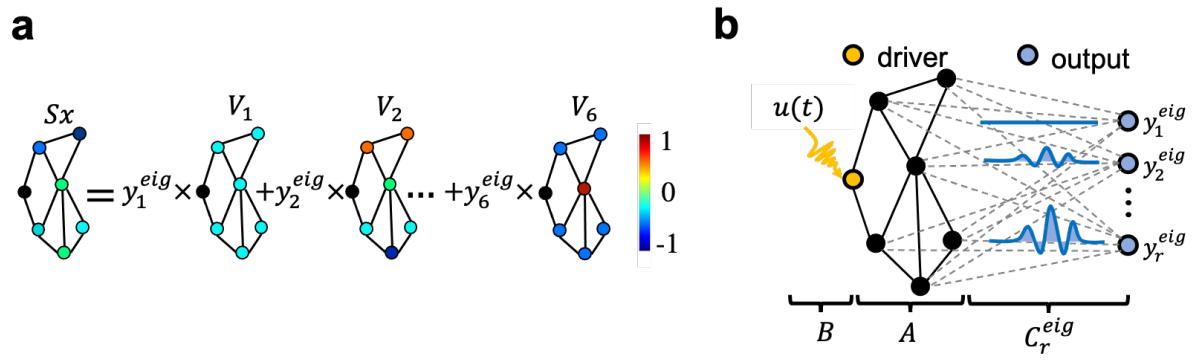

Figure 4.1: Output control of Laplacian eigenmaps: **a)** Spectral decomposition of the states Sx onto the 6 eigenmaps of a toy model network. **b)** Sketch of the controllability framework with Laplacian eigenmaps as output.

desired final $|\tilde{x}_f|_i$. This way we ensure maximum representativeness of the desired final state.

4.2.1 The hierarchical modular small-world network model

All synthetic networks generated had $n = 256$ nodes and were created using the hierarchical modular small-world network model (HMSW) model [55] implemented in the BCT toolbox [56]. There are, thus, 8 hierarchical levels and we fixed a decay parameter of $d = 2.5$ resulting in a global average density of 3.5% (**Fig.4.2**). The choice of this model was also motivated by the fact that it is widely used in topological analysis of brain networks [55] since they are known to exhibit hierarchical modularity [57, 58].

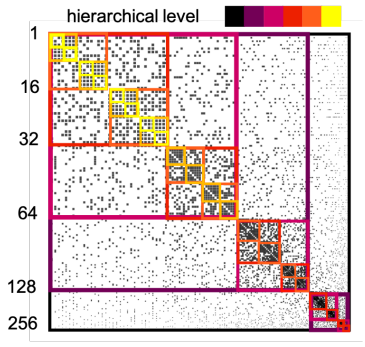

Figure 4.2: One realization of the hierarchical modular small-world network

Remark: This model was preferred to standard modular network models such as the stochastic block model (SBM) [59] or Girvan-Newman graph [60] because of its additional hierarchical aspect. Indeed, for standard modular networks, the topology is characterized by two meso-scales: the first emerges from the interactions of nodes within the same communities and the second comes from inter-communities' interactions. That is why authors in Ref. [61] observed two peaks, for the SBM model, when analyzing information diffusion through the range of Laplacian pathways whereas for the hierarchical networks there was a continuous ascending integration of information resulting in one peak at the biggest spatial lengths.

We hypothesized that the hierarchical aspect was more suited for our framework to have a continuous integration of information by individual eigenmaps across multiple spatial scales.

4.2.2 Network modeling and optimal control

All synthetic networks considered here are represented by their adjacency matrix G where the element $G_{i,j}$ is the weight of the link from node i to node j. No self-loops are considered so $G_{i,i} = 0$. The state matrices A are obtained as follows $A = G - \lambda_{max}(G)I$. Even though this step is not

[55]: Sporns (2006), 'Small-world connectivity, motif composition, and complexity of fractal neuronal connections'
[56]: Rubinov et al. (2010), 'Complex network measures of brain connectivity'

[57]: Meunier et al. (2010), 'Modular and Hierarchically Modular Organization of Brain Networks'
[58]: Ferrarini et al. (2009), 'Hierarchical functional modularity in the resting-state human brain'

[59]: Holland et al. (1983), 'Stochastic blockmodels'

[60]: Newman et al. (2004), 'Finding and evaluating community structure in networks'
[61]: Villegas et al. (2022), 'Laplacian paths in complex networks'

necessary for this section, we decided to stabilize the synthetic networks because we will translate the results to the controllability Gramian that is originally defined for stable systems.

To compute the input signal $u(t)$ and simulate the controlled trajectories, we solve the following minimization problem

$$\begin{aligned} \min_{u} \quad & J_\rho = (y_f - y(t_f))^T.(y_f - y(t_f)) + \rho \int_0^{t_f} u(t).u(t)^T \mathrm{dt} \\ \text{s.t.} \quad & x(0) = x_0 \; ; \; \dot{x}(t) = Ax(t) + Bu(t) \; ; \; y(t) = Cx(t) \end{aligned} \tag{4.6}$$

where ρ is a regularization parameter that permits to obtain results for ill-posed problems (See Appendix for the detailed calculus). The solution diverges for extreme values of ρ (**Fig.4.3**). In the following, we fix $\rho = 10^{-5}$ at the beginning of the local valley as a trade-off between energy and precision.

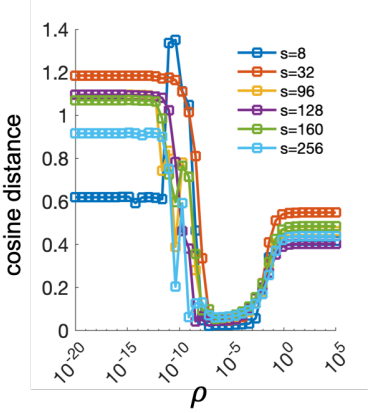

Figure 4.3: Effect of the regularization parameter ρ: We control an increasing number s of target nodes for different values of ρ. Low errors are achieved in the range $10^{-8} < \rho < 10^{-2}$. Outside that range, the errors show an unexpected behavior regarding the target size.

We evaluated the performance of each control action by measuring the cosine distance between the simulated and desired states or outputs at the terminal time t_f defined as:

$$\text{cosine distance } \delta = 1 - \frac{y(t_f).y_f}{\|y(t_f)\|\|y_f\|} \tag{4.7}$$

We selected this distance over the Euclidean one as it is bounded, compliant with high dimension [62], and interpretable. It is 0 for two colinear vectors, 1 if perpendicular, and 2 if colinear opposite.

Remark: We preferred this regularized control strategy over the classical minimum energy control in which the Gramian is inverted as in **theorem.3.2.2** because it is known that this second fails [12] for a low number of drivers and that is exactly the aspect we wanted to investigate. All the simulations were done in MATLAB and the code is made available at github.com/Inria-NERV/Network-Control

4.3 Results: Validation on synthetic networks

We show in this section the benefit of low-dimensional control using extensive simulations on synthetic networks.

4.3.1 Low-dimensional control of synthetic networks: a trade-off between precision and representativeness

To validate our framework, we tested it using the HMSW model. Examples are depicted in **Fig.4.4.a-c** where we show the coefficients of Laplacian eigenmaps. We generated 1000 realizations of the HMSW model of size n = 256 and sampled final desired states from $x_f \sim \mathcal{N}(\mu_f, \sigma_f^2)$. We set $x_0 = 0$ since controllability and reachability are equivalent for stable linear systems [41, 63]. First, we targeted the entire network using different driver sets n_d=1,8, and 64 (**Fig.4.4.d**). Drivers were picked as the most central nodes regarding betweenness centrality to ensure homogeneous distances to the rest of the nodes as it is a crucial parameter

[62]: Senoussaoui et al. (2014), 'A Study of the Cosine Distance-Based Mean Shift for Telephone Speech Diarization'

[41]: Lindmark (2018), 'Minimum energy control for complex networks'
[63]: Hallam (1981), 'David G. Luenberger'

for controllability and control [12, 64]. In each condition, we simulated the direct control of the states and that of the eigenmaps by varying their number r (**Fig.4.4.d-e**). Our first result is to highlight the trade-off between the number of drivers n_d and the output dimension r, or number of controlled eigenmaps. We show that for low values of output dimension r, we are able to precisely control the system and that a plateau is reached after $r > 5n_d$ (**Fig.4.4.d**). This controllability transition was already observed in the case of global controllability and is intrinsic to the control problem [12]. We also observe that controlling all of the $r = n$ eigenmaps is similar, in terms of control error, to controlling the states since it is equivalent to a coordinate transformation [65].

[12]: Sun et al. (2013), 'Controllability Transition and Nonlocality in Network Control'
[64]: Duan et al. (2022), 'Prevalence and scalable control of localized networks'

[65]: Georges (1995), 'The use of observability and controllability gramians or functions for optimal sensor and actuator location in finite-dimensional systems'

To simulate more realistic situations, we focused on the case of single-driver control. On average, reducing the number of eigenmaps improved the control precision in the eigenstate space but worsened the representativeness as measured by the cosine distance in the network state space $\delta_x = 1 - \frac{x(t_f).x_f}{\|x(t_f)\|\|x_f\|}$ (**Fig.4.4.e**). These last results indicated that optimal tradeoffs could be then explored considering unbiased indicators such as the total error, pointing out that the optimal number of components scales slowly with the network size. We used the built-in particle swarm optimization (PSO) algorithm of MATLAB to find the trade-off points r^*. Results suggested that the optimal trade-off point scales as $r^* \approx 0.2739\ n$ ($R^2 = 0.9891; p = 4.4961e^{-05}$) (**Fig.4.4.e**).

Lastly, we focused on the case where only subsets of the networks were targeted. An increasing number s, of target nodes, was selected and we

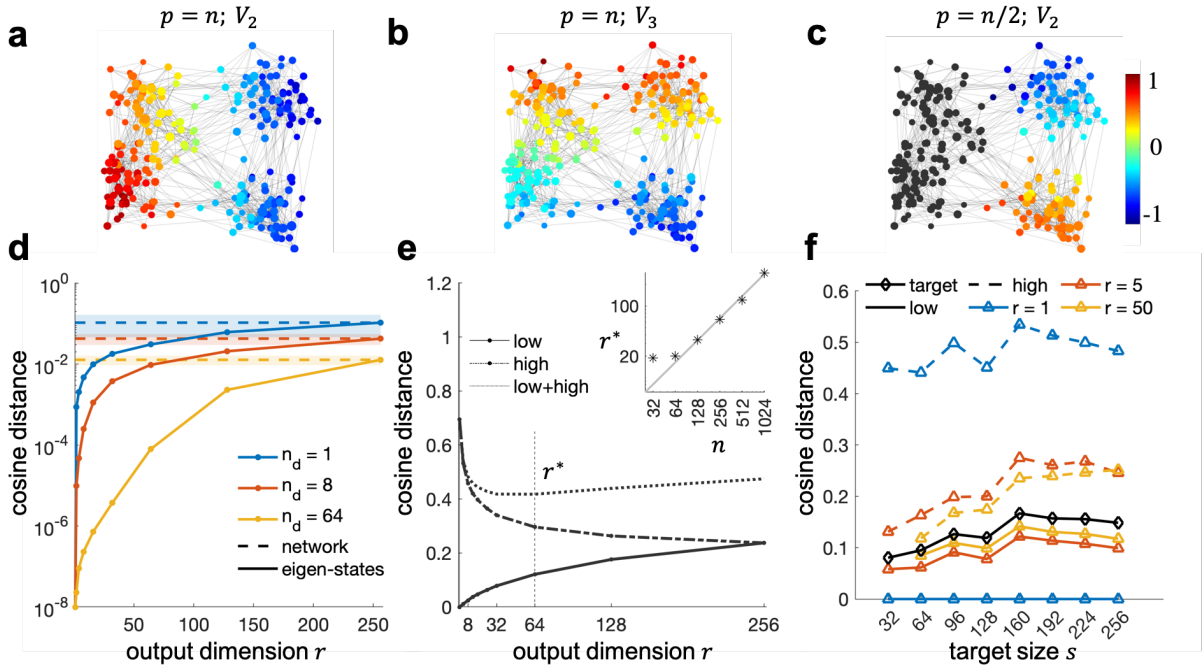

Figure 4.4: Output control of Laplacian eigenmaps: **a, b,** Second and third Laplacian eigenvectors, indicated by node color, of one realization of the HMSW network model. **c**, Second Laplacian eigenvector of a targeted subnetwork. **d**, Network average of cosine distance for 4 driver sets n_d=1,8, and 64. Solid lines correspond to the control of the eigenmaps and dashed lines to the control of the states. **e**, Network average of cosine distance for the low dimensional eigenstate and the high dimensional network state (see legend) when using single drivers. Their sum is taken as an objective metric to find a trade-off between precision and representativeness. Optimum points r^* are found by the Particle Swarm Optimization algorithm and shown in the inset for different network sizes. **f**, Network average of cosine distance when increasing the size p of the targeted network. The black line corresponds to the direct control of target states and the colored lines to the eigenmaps control.

computed the eigenmaps of the target Laplacian (**Fig.4.4.c**). We simulated the controlled trajectories using one single driver, the most central node in the target (results showed similar trends with peripheral drivers). We controlled the states of the target nodes ($r = s$) and their projections onto $r = 1$, 5, and 50 eigenmaps. Results showed that increasing the size of the targeted network does not affect the precision of the low-dimensional control but rather its representativeness (**Fig.4.4.f**).

4.3.2 Laplacian eigenmaps: a good network output?

However, even if the eigenmaps are theoretically a good candidate output for network control, is it suitable for different topologies, final states, and is it better than other outputs?

We took inspiration from this work [32, 33], in which the authors use the output controllability framework. However, our approaches are conceptually different. They define clusters and consider their average state in the goal of constructing a reduced model of the original network. In other terms, they build a coarse-grained version of the network and then study the properties of the reduced controllability Gramian. In our work, we do not build reduced models of the network dynamics and limit ourselves to the study of the output.

[32]: Casadei et al. (2018), 'Controllability of Large-Scale Networks'
[33]: Casadei et al. (2020), 'Model Reduction Based Approximation of the Output Controllability Gramian in Large-Scale Networks'

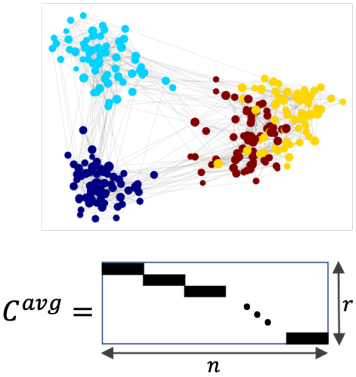

Figure 4.5: Average output control: The network is partitioned into r clusters. The lines of the output matrix C^{avg} define the clusters and contain the values $1/N_i$, where N_i is the number of nodes in the cluster i.

Average cluster state control:
Let us define the average state output. Whereas r, the output dimension previously corresponded to the number of controlled projection coefficients onto the most representative eigenmaps, now represents the number of clusters into which the network is partitioned. The states of the nodes of each cluster are averaged through the output matrix C^{avg} and we control the average output (**Fig.4.5**).

$$\begin{aligned} \dot{x}(t) &= Ax(t) + Bu(t) \\ y^{avg} &= C^{avg}x \end{aligned} \tag{4.8}$$

In order to compare the two output candidates, we analyzed, on top of the HMSW model, two classical synthetic network models: the Erdos-Reyni random graph model [2] and the Barabasi-Albert scale-free model [66]. In the case of the the HMSW model, the information about the clusters is known a priori. However, for the two others, the partition is random.

[2]: Paul Erdos et al. (1959), 'On random graphs I'

[66]: Barabási et al. (1999), 'Mean-field theory for scale-free random networks'

We generated 1k realizations of the network models and controlled and simulated the controlled trajectories for two different states: $\sigma_f = 0.1$ and $\sigma_f = 10^3$ (**Fig.4.6**).

Results showed that the final state rather than the underlying topology, was a crucial factor determining the performance of the output control. Indeed, error profiles seemed similar in the low dimension but drastically different in the high dimension. In the easy condition where the final state has low variance ($\sigma_f = 0.1$), the "Cluster average" strategy achieves better representativeness than the "Eigenmaps" regardless of the topology with the except for the single driver case. Additionally, the difference of representativeness between the two outputs seemed to depend on the topology, with biggest differences in the BA-SF model and the least in the HMSW one.

Taken together, these results suggested that it is difficult to say that one output is better than the other in the absolute. However, "eigenmaps" output could be preferred to better represent the network state over the "Cluster average" output for final states with large dispersion. This effect seemed to be emphasized as the number of drivers increased, and as the networks became less modular and smaller in terms of network diameter. Otherwise, for states with small dispersion, average output was more representative, except for scale-free networks. In all cases, the achieved precision of the low-dimensional output was consistently better for eigenmaps and this point remains without explanation.

Remark: Fig.4.6 displayed some odd non monotonic curves of the cosine distance. We do not have a clear and definite explanation for it. When using the classical minimum energy control which involves the Gramian inversion, we observed sharp but monotonic curves (not shown here). This effect is thus proper to the regularized control strategy we use here. Moreover, it seemed that the non-monotonic effect occurs at the point where $r = n_d$ (it is especially visible for $n_d = 8$).

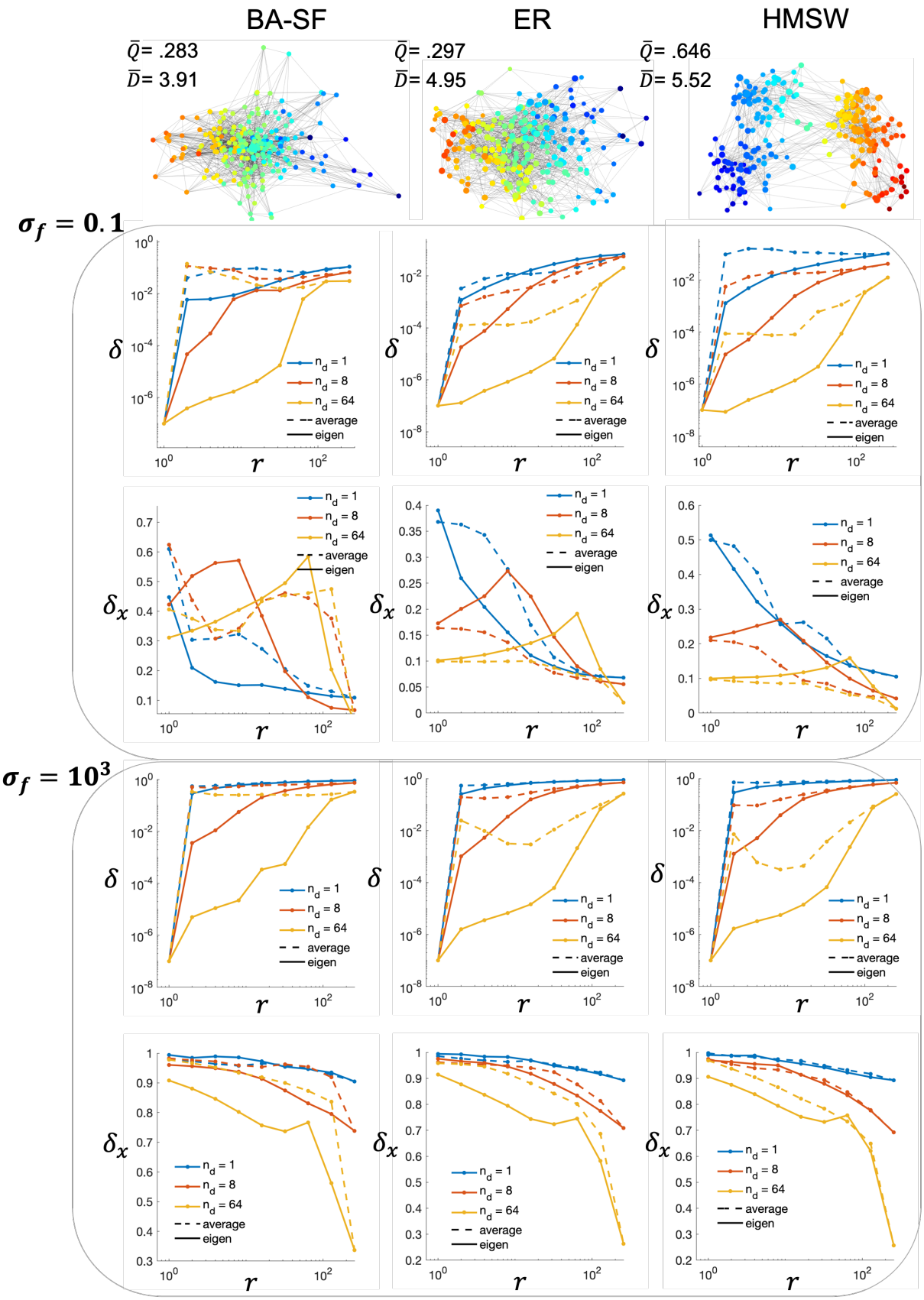

Figure 4.6: Effect of topology and final desired state: Network average (100k realizations) of cosine distance: δ in the low-dimensional output space and δ_x in the high-dimensional state space.

4.4 Application: A low-dimensional controllability metric

4.4.1 Projecting Gramians and accommodating dimension

Now that we demonstrated that eigenmaps projections constitute a precise output to control in the low-dimensional space and that it well represents the states in the high-dimensional space, we will show how we use it to define a new well-defined controllability metric.

Two controllability metrics were introduced in section **3.3**: **Average** and **worst-case controllability**. These are both extracted from the controllability Gramian of the system but describe it from two extremities of the dimensional prism. Average controllability is the sum of all the Gramian eigenvalues so it will be dominated by the very first modes because these latter usually have a range of several orders of magnitude. Worst-case controllability offers a "high dimensional" description of it by looking at the smallest eigenvalue but then, the dimension is too high, and computation errors occur. With our framework, we build output controllability Gramians that span a “continuum” of dimensions and permit us to reconcile dimensionality and complexity. We propose to project the single-driver controllability Gramians onto the first eigenmaps of the target network and to acquire its worst-case controllability.

For a given driver and a given set of target nodes selected by S, the classical target controllability Gramian is the $s \times s$ matrix $\mathcal{W}^S = S\mathcal{W}S^T$. We propose to project it onto the r first Laplacian eigenmaps of the targeted network:

Low-dimensional controllability metric $\lambda_{\min}(\mathcal{W}^{\text{eig}})$

$\mathcal{W}^{\text{eig}} = C^{\text{eig}}\mathcal{W}{C^{\text{eig}}}^T$, with $C^{\text{eig}} = H_r V^T S$, where $H_r = [I_r \ 0_{\text{s-r}}]$.
It corresponds to a low-dimensional version of the worst-case controllability.

This way, we measure the worst-case controllability, $\lambda_{\min}(\mathcal{W}^{\text{eig}})$, of a lower-dimensional Gramian of size $r \times r$ and we ensure it is well-scaled and positive.
Remark:

- We take $H_r = [I_r \ 0_{\text{s-r}}]$ here since there is no specific desired final state. We rather want to capture the global topological landscape of the targeted network that is better captured by the first eigenmaps which correspond to the low spatial frequencies or similarly high characteristic lengths [54].
- If the low-dimensional controllability metric is evaluated at its extremity, $r = s$, it is then equivalent to the worst-case controllability of the target network because of the similarity of the two Gramians, $\mathcal{W}^{\text{eig}} = V^T\mathcal{W}^S V = V^{-1}\mathcal{W}^S V$, and it is known that two similar matrices have the same spectrum.

[54]: Cui et al. (2019), ‘A Survey on Network Embedding’

4.4.2 Low-dimensional controllability: halfway between average and worst-case controllability

Let us now demonstrate our metric in small toy model network.
Worst-case controllability is supposed to be the most reliable metric when used to select the best driver nodes in a network [41, 67, 68]. However, the computation of the smallest eigenvalues is subject to round-off errors and numerical instabilities even for relatively small dimensions. On the other hand, Average controllability, even though computationally stable, does not capture the complexity of the network topology and is not informative enough [69]. We built our metric to combine the benefits of both metrics. Here is a showcase of its usage.

[41]: Lindmark (2018), 'Minimum energy control for complex networks'
[67]: Lindmark et al. (2019), 'Combining centrality measures for control energy reduction in network controllability problems'
[68]: Lindmark (2020), *Controllability of Complex Networks at Minimum Cost*
[69]: Tu et al. (2018), 'Warnings and Caveats in Brain Controllability'

We consider a directed toy model network (**Fig.4.7.a**) composed of 6 core target nodes (in black) to be controlled and 10 satellite potential drivers (colored nodes). It is clear that driver 1 is a source and driver 10 is a sink. We thus expect the considered metrics to capture that by assigning maximum value to driver 1 and minimum value to driver 10. However, even in this trivial case, average and worst-case controllability failed to rank them accurately. The target network is not strongly connected, so we used the symmetrized Laplacian definition and compute its eigenvectors, and used them to project the Gramians. We can see the resulting metrics in the table in **Fig.4.7.b-d**. Since some of the smallest Gramian eigenvalues are negative, we will consider their absolute value. Average controllability succeeded in identifying the worst driver (sink node 10) but not the best (source node 1). Inversely, worst-case controllability successfully identified the best driver 1 but not the worst driver 10. On the other hand, for $r \geq 3$, Low-dimensional controllability accurately identified both the source and the sink nodes. Additionally, driver 4 is also a "bad" driver by construction, and unlike our metric, the classical worst-case controllability is not able to capture it.
Moreover, the reason why average controllability selects node 5 as the best

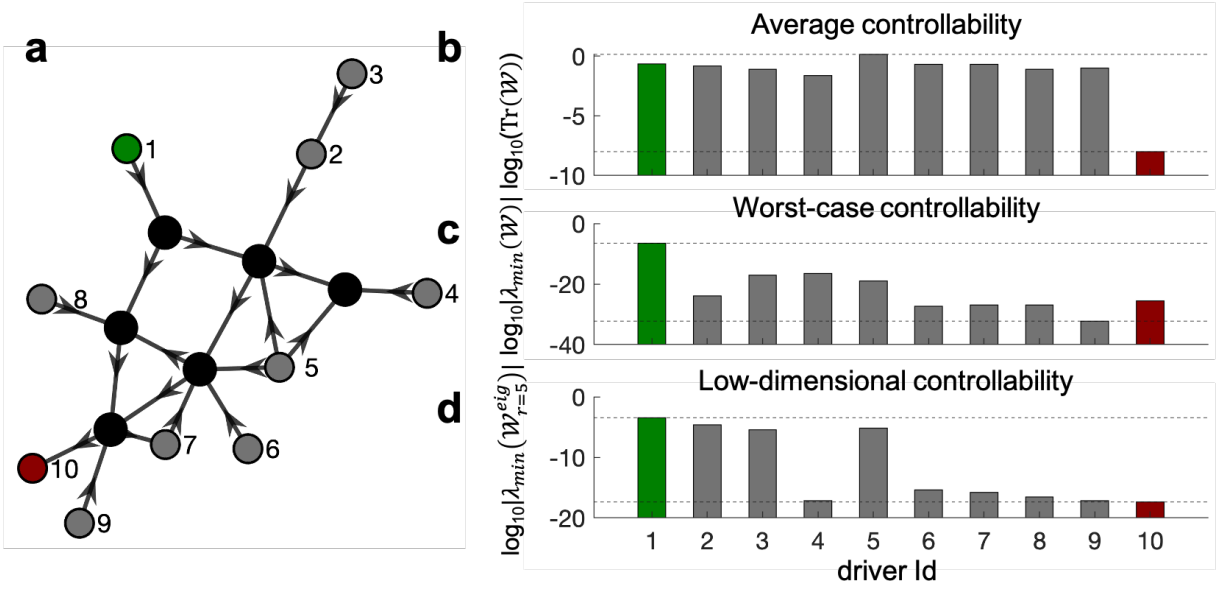

Figure 4.7: Low-dimensional controllability of a toy model: **a,** Toy model Network. target nodes are in black and the potential drivers are colored.**b, c, d** Magnitudes of the controllability metrics: Average, worst-case, and low-dimensional with $r = 5$.

driver is that it is the driver that has the biggest number of connections with the target set.

4.5 Discussion

We emphasize, firstly, that even though most real-world networked systems, such as the brain [70], have non-linear dynamics, linear systems theory can still infer valuable and relevant insights [71]. However, optimal control of network dynamics is not practically possible when just a few nodes can be driven simultaneously due to the ill-conditioning of the problem. The classical network controllability metrics also suffer from this limitation. This motivated us to reduce the dimension of the targeted networks by merging tools from linear output controllability theory with the informative power of the network Laplacian.

[70]: McKenna et al. (1994), 'The brain as a dynamic physical system'

[71]: Kim et al. (2020), 'Linear Dynamics and Control of Brain Networks'

4.5.1 Trade-offs in network and output control

Our framework allowed us to overcome the dimensionality-related limitations and the numerical round-off errors by encapsulating the mesoscopic topological information of the network in a low-dimensional space and will hopefully pave the way to broader applications. First, we demonstrated that output control of the network fails practically when the ratio of the number of drivers over the output dimension is below 0.2, extending previous results found in the case of global controllability [12]. At the same time, we showed that diminishing the number of controlled eigenmaps improved accuracy but also on the other hand, it diminishes the representativeness of the high dimensional network state. The Laplacian eigenvectors unravel the network's symmetries and organizational scales going from the largest spatial length to the smallest, even for complex and heterogeneous networks [49, 50, 61]. As we increase the number of eigenmaps r, the desired target state will be represented at finer and finer scales for all sorts of underlying topologies. However, we are limited in practice by the number of drivers and the conditioning of the problem. We suggested an objective way to choose the number of eigenmaps by considering the trade-off between the precision of the eigenstate control and the representativeness of the network state.

[12]: Sun et al. (2013), 'Controllability Transition and Nonlocality in Network Control'

[49]: Villegas et al. (2023), 'Laplacian renormalization group for heterogeneous networks'

[50]: Chung (1997), *Spectral graph theory*

[61]: Villegas et al. (2022), 'Laplacian paths in complex networks'

4.5.2 Laplacian eigenmaps: a good network output?

We listed several reasons for which we decided to use the Laplacian eigenmaps as the network output: Its informative power about diffusion [49, 61] and synchronization [72, 73] processes and its embedding power [54, 74].

We decided to confront it to another standard output, the average state output approach. Results indicated that the two approaches performed differently depending on the dispersion of the final state. Notably, for dispersed states, the eigenmaps were more representative of the network state than the cluster average. We hypothesized that the effect was due to the fact that we selectively chose to control the eigenmaps that are the most representative of the high dimensional state. Indeed, the used output

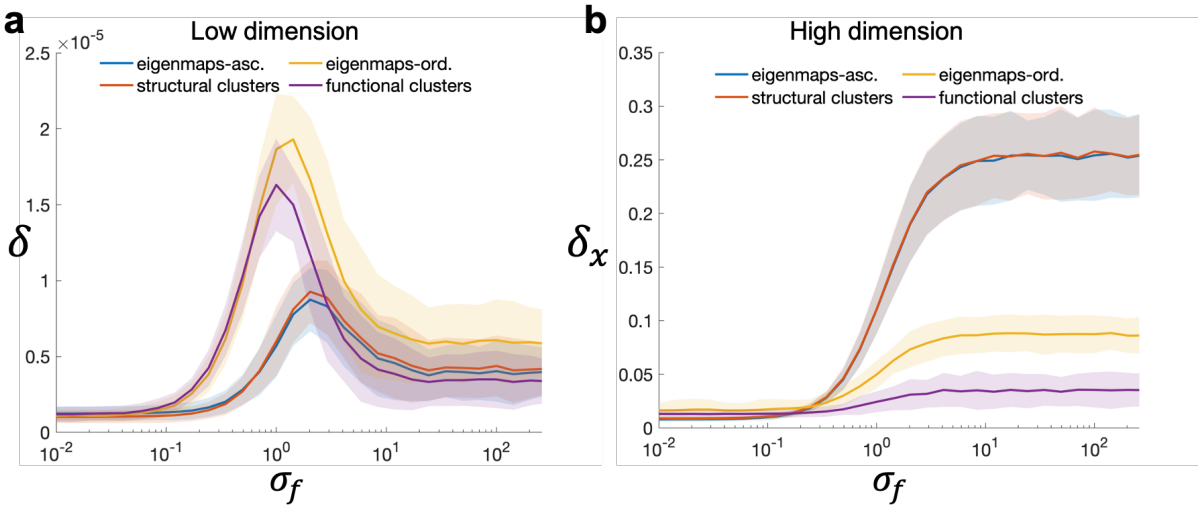

Figure 4.8: Laplacian eigenmaps as hybrid topologically and functionally informed output: **a, b,** Network average (100 realizations of the HMSW model, $n = 256$) of cosine distance in both the low and the high dimensions. We vary the dispersion σ_f of the final state. Its mean is fixed $\mu_f = 1$. We project the network state onto four different outputs of same dimension, $r = 64$ (see legend) and used all the nodes as drivers, $n_d = n$ as, the goal is to investigate the representativennes of the outputs. Eigenmaps-asc. are the r coefficients of the of the eigenstate corresponding to the r first (asc. stands for ascending order) Laplacian eigenvalues, whereas eigenmaps-ord. corresponds to the r most representative components (biggest magnitude). Regarding the clusters, "structural clusters" stands for the classical network clusters as defined previously. The "functional clusters" corresponds to the case where we only regroup the nodes regarding their desired final state. We simply ordered the values of x_f and then grouped them into r groups that we called "functional clusters".

is then informed of the desired state unlike the clusters which was just defined regarding the structure of the network. In order to confirm it we decided to compare four different outputs in terms of representativeness (**Fig.4.8**). First, intuitively we controlled the eigenmaps output without selection of the components but rather recruited them in their natural order that is by ascending order of the associated eigenvalues. This way we had a Laplacian output that was not informed of the final state but just reflects the topology. On the other hand, we decided to build an average state output which depended entirely on the final state. To do so, one aims at regrouping the nodes in r groups in a way that will best represent the final state. The task is easy and can be seen as a K-means procedure in one dimension for $K = r$. Then, the averaging output matrix was built in the same way, but just with a different partition.

Results showed that the output approaches acted differently regarding whether they are topologically informed ("eigenmaps-asc." and "structural clusters") or final state informed ("eigenmaps-ord." and "functional clusters"). In the low-dimensional output space, final state informed outputs captured the network state dispersion earlier than the topologically informed ones and achieved significantly better representativeness in the high-dimensional space. More importantly, we observed that "eigenmaps-asc." were equivalent to the "structural cluster" average and that the "functional clusters" achieved the highest representativeness.

Taken together, our results do not suggest the superiority of Laplacian eigenmaps over state-average. It rather demonstrated that eigenmaps constitute a hybrid and flexible method which captures the topology of the underlying network but can also be optimized to fit to specific network states.

4.5.3 Leveraging dimension for a more reliable metric

Building upon these findings, we used Laplacian eigenvectors to build low-dimensional output Gramians and suggested a new controllability metric. Indeed, classical controllability metrics have some pitfalls. Worst-case controllability is supposed to be the most reliable metric when used to select the best driver nodes in a network [41, 67, 68]. Although, the computation of the smallest eigenvalues of large ill-conditioned Gramians is subject to round-off errors. That is why, when examining the single driver worst-case controllability, $\lambda_{\min}(\mathcal{W})$, of entire brain networks, negative values appeared, and the overall distribution (2.5e-23 ± 4.8e-23) [9] was not statistically different from zero [69, 75] making this metric unusable to accurately measure global controllability [9]. On the other hand, average controllability, though computationally stable, is questioned regarding the fact that it is not disentangled from simpler network measures such as the node weighted-degree [69, 75, 76]. Originally it was suggested for unstable systems since its computation is stable for singular Gramians [39]. Our metric, on the other hand, by considering low-dimensional and better-conditioned Gramians, gives numerically stable results and reliable predictions.

[9]: Gu et al. (2015), 'Controllability of structural brain networks'

[69]: Tu et al. (2018), 'Warnings and Caveats in Brain Controllability'
[75]: Suweis et al. (2019), 'Brain controllability'
[76]: Stocker et al. (2023), 'Network controllability measures of subnetworks'

[39]: Shaker et al. (2013), 'Optimal sensor and actuator location for unstable systems'

4.6 Conclusion

In this section, we introduced the Laplacian matrix that is a classical tool in network science. The eigenmaps obtained by spectral decomposition of the Laplacian are known to encapsulate the structural properties of the network at multiple scales. We took advantage of the informative power of the eigenmaps and used them as the control output to reduce the network state to be controlled. We showed how reducing the output dimension, which is number of controlled eigenmaps, permits a more precise control, especially when a few driver nodes are controlled. Overall, a trade-off, in terms of number of components, can be found when we additionally consider the representativeness by the eigenstate of the high-dimensional network state.

Building upon this, we used the eigenmaps as a basis to project large controllability Gramians onto their lower-dimensional output versions. This permits to reliably calculate their smallest eigenvalues and ultimately obtain a reliable and representative controllability metric. We showed its benefit compared to the classical metrics Using a small toy-model directed network.

We show in the next section how we apply this new controllability metric to a large dataset of structural brain networks and how it permitted us to better characterize brain controllability.

Low-dimensional controllability of complex brain networks

5

5.1 Materials & Methods

5.1.1 The UK-biobank dataset

It is a large-scale database (more than 500k individuals) containing clinical, genetic, and imaging data (ukbiobank.ac.uk)[77]. We selected the individuals who had both T-1 weighted and diffusion MRI and had no known disease history. The resulting sample is composed of 6134 individuals. We rejected those who requested the withdrawal of their data. We also gathered basic clinical data like sex (3112 females), age (46-82 at the time of the MRI scans), and handedness (89% right-handed).

5.1.2 Neuroimaging data and structural connectome extraction

Downloaded imaging data are already corrected and preprocessed with the UK-biobank pipeline [78]. For the processing, we computed Tissue response and Fiber Orientation Distribution using multi-tissue and multi-shell algorithms in MRtrix3 [79]. T1 images were aligned to an extracted mean b0 volume via the FLIRT function in FSL [80]. We performed a 5-tissue type segmentation to compute the grey-white matter interface. These were then used in MRtrix3 to compute an anatomically constrained tractography with a cut-off of 0.1 and a density of 1M streamlines (**Fig.5.1.a,b**). A density of 1M streamlines was shown to be sufficient for reproducibility, especially in our case with more than 6k brains.

[77]: Sudlow et al. (2015), 'UK Biobank'

[78]: Alfaro-Almagro et al. (2018), 'Image processing and Quality Control for the first 10,000 brain imaging datasets from UK Biobank'

[79]: Tournier et al. (2019), 'MRtrix3'

[80]: Jenkinson et al. (2012), 'FSL'

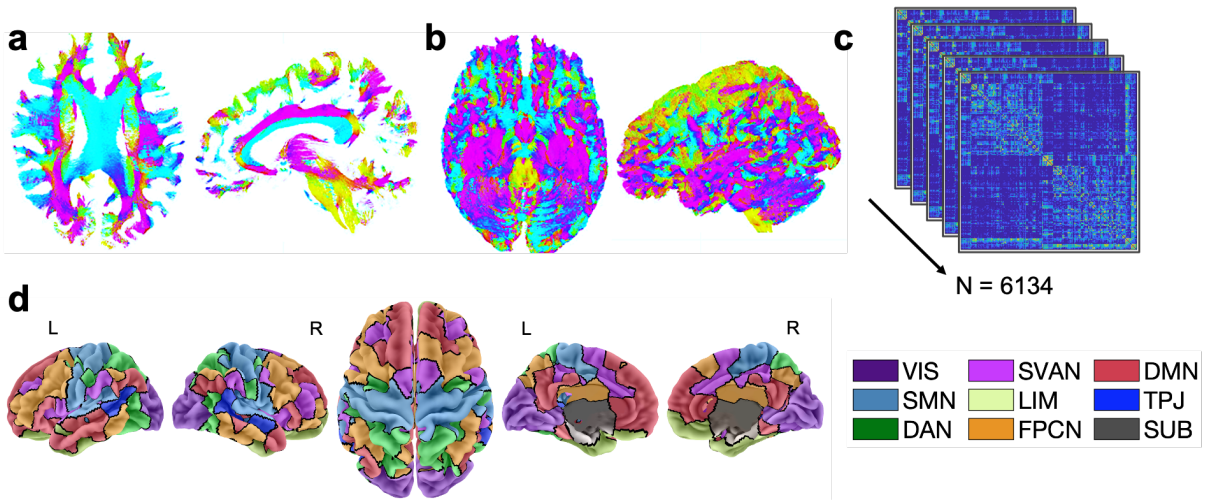

Figure 5.1: Assignment to 9 large-scale functional networks of the brain regions of Schaefer200 parcellation: VIS = Visual, SMN = Somatosensory network, DAN = Dorsal attention network, SVAN = Saliency and ventral attention network, LIM = Limbic network, FPCN = Frontoparietal control network, DMN = Default mode network, TPJ = Temporoparietal junction, SUB = Subcortical regions

For the parcellation, we decided to use, as in Ref.[11], the Schaefer atlas [81] of 200 cortical parcels because this resolution was shown to achieve high structural and functional representativeness[82]. Its regions are already mapped to the 17 large-scale networks identified in Ref.[83] that we regrouped in 8 as in Ref.[11]: VIS, SMN, DAN, SVAN, LIM, FPCN, DMN, TPJ (**Fig.5.1.d**). The cortical atlas is complemented by the 14 subcortical regions of the FreeSurfer segmentation that form the target network SUB. We refer the reader to the Appendix (**table.1**) for more details on the brain regions.

The parcellation was transferred to the subject space using the T1 linear co-registration and the UK-biobank warp field. It was finally dilated and masked to be used in MRtrix3 along the SIFT[84] for the connectome extraction. Fiber assignment was done with a radial search of 3mm and the resulting connectomes were symmetric with a zero diagonal (**Fig.5.1.c**). These parameters were optimized to extract precise connectomes while remaining relatively fast due to the high number of subjects (>6k).

All data are available upon request from the UK-biobank and the pipeline code is available at github.com/UKB-dwi-2-connectome.
The tractography pipeline was developed by Vincent Ledu. I participated as a counselor/supervisor and ultimately held the calculations for the whole cohort using the Paris Brain Institute computing facilities. The tractography pipeline lasted between 2 and 3 hours per subject using 1 cpu. In total, around $6134 \times 2.5 = 15k$ CPU hours of calculations were needed to extract the connectomes for this healthy cohort.

[11]: Menardi et al. (2022), 'Maximizing brain networks engagement via individualized connectome-wide target search'

[81]: Schaefer et al. (2018), 'Local-Global Parcellation of the Human Cerebral Cortex from Intrinsic Functional Connectivity MRI'

[82]: Luppi et al. (2021), 'Combining network topology and information theory to construct representative brain networks'

[83]: Thomas Yeo et al. (2011), 'The organization of the human cerebral cortex estimated by intrinsic functional connectivity'

[84]: Smith et al. (2015), 'The effects of SIFT on the reproducibility and biological accuracy of the structural connectome'

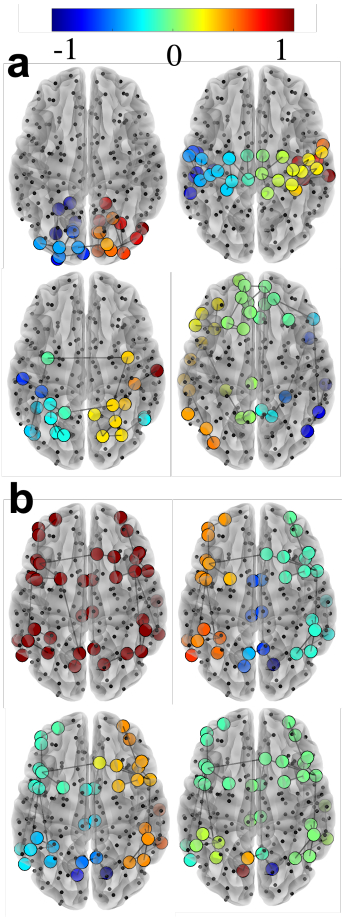

Figure 5.2: Brain subnetworks eigenmaps: a, 2nd eigenmap of: (top) VIS, SMN, and (bottom) DAN, and DMN networks. The second eigenmap divides the target network in two modules. **b,** 4 first eigenmaps of the FPCN network.

5.2 Understanding brain controllability at the nodal level

5.2.1 Leveraging dimensionality for better reliability: Gramian projections

We recall that the Gramian criterion 3.2.1-iv states that the system is controllable if and only if its Gramian is positive definite (all its eigenvalues are strictly positive) [37].

For each brain region considered as a single driver, the corresponding Gramian is computed and one can measure the worst-case controllability, $\lambda_{\min}(\mathcal{W})$ (see section 3.3.3). However, its computation suffers from numerical errors (see Discussion 4.5). Therefore, we suggested using the Laplacian-based output control framework to build a metric that combines reliability and computational stability.

We were specifically interested, as in a previous study [11], in characterizing the controllability of the 9 aforementioned large-scale networks (**Fig.5.1.d**). To do so, we computed the brain-specific and target-specific Laplacians and their eigenmaps (**Fig.5.2**). Then we projected the presumably ill-conditioned Gramians as explained ($\mathcal{W}^{\text{eig}} = C^{\text{eig}} \mathcal{W} {C^{\text{eig}}}^T$), and measured their smallest eigenvalues. We show how our metric scales with the number r of selected eigenmaps (**Fig.5.3**). It is clear that there is a limit, $r = 5$, after which the metric starts having negative values like the classical worst-case controllability (r = target size). This is coherent

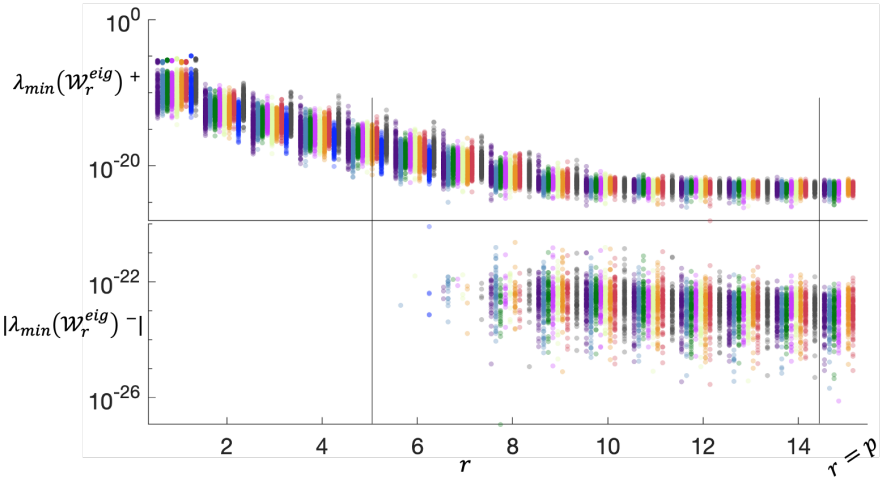

Figure 5.3: Brain subnetworks controllability values: The values are divided in their positive and negative parts for different values of the output dimension r

with results of previous section, with the controllability transition ratio of $(n_d/n < 0.2)$ [12], and with literature specific to brain controllability [69, 75, 76].

[69]: Tu et al. (2018), 'Warnings and Caveats in Brain Controllability'
[75]: Suweis et al. (2019), 'Brain controllability'
[76]: Stocker et al. (2023), 'Network controllability measures of subnetworks'

Subsequently, we will fix $r = 5$ in the rest of the analysis to ensure that the metric used is positive and that the Gramian criterion is respected for all single drivers.

We stress here that if the goal is just to select the best drivers than higher dimensions would have worked fine as well as the classical worst-case controllability since we see that there were consistently a portion of the drivers that had positive controllability values. However, we wanted to design our low-dimensional controllability metric in such a way we could compare all the drivers. This point is necessary for the next section.

5.2.2 Whole brain controllability and dependence to nodal weighted degree

In order to further illustrate how our metric is a good alternative to classical metrics, we analyzed the controllability of the entire network as it was done in previous studies [69, 75, 76]. Indeed, it is in such context that discrepancies of the classical metrics were observed, specifically the strong dependence between average controllability and the weighted degree also called strength. For each driver and each individual brain, we gathered average, worst-case, and our low-dimensional controllability of the entire network alongside with the nodal weighted degree (**Fig.5.4**). Results confirm conclusions of previous literature: Firstly, that average controllability is highly correlated on the weighted degree ($r = 0.88$), and secondly, that worst-case controllability is nearly zero [69, 75, 76].

Moreover, low-dimensional controllability is well scaled and lays halfway between them in terms of magnitude. But more importantly, like worst-case controllability, it is disentangled from the weighted degree (low correlation: $r = 0.241$).

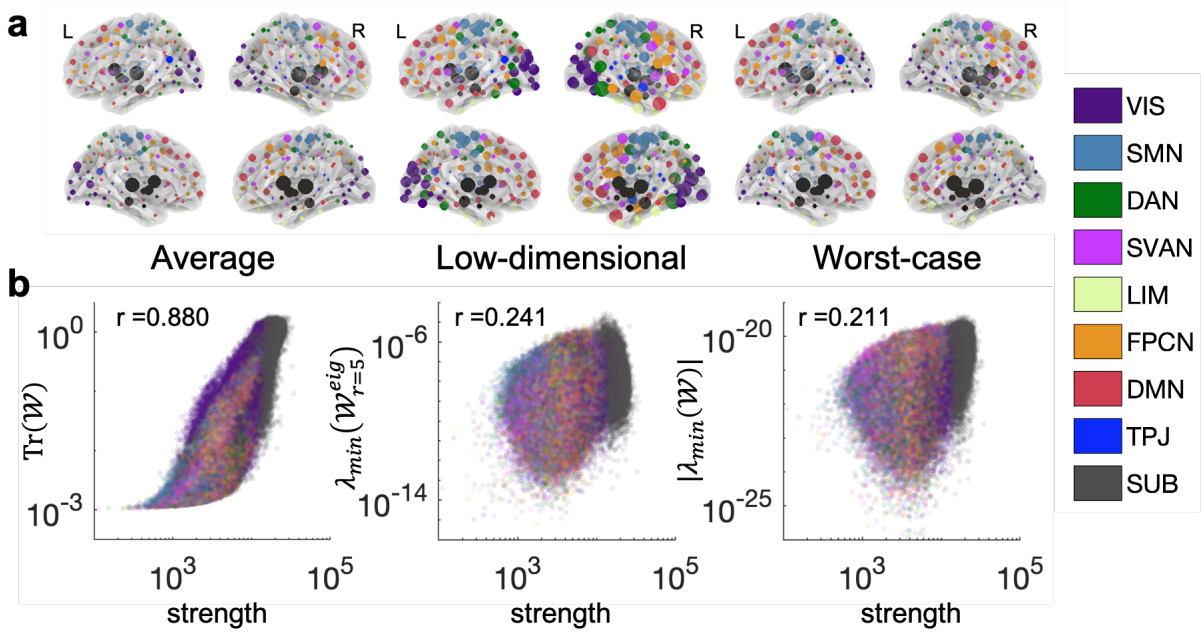

Figure 5.4: Low-dimensional controllability of whole brain networks: a, Group-level average of brain controllability. The whole-brain network is targeted and each node is taken as single driver. We measured average, low-dimensional ($r = 5$), and worst-case controllability and show their values by the node size. Node color represents the system to which brain regions belong. **b**, Scatter plots and Pearson correlation coefficients for nodal weighted degree and controllability values. One dot corresponds to one node among $n = 214$ from one of the $N = 6134$ brain networks.

5.2.3 Controllability and lateralization of brain systems

[11]: Menardi et al. (2022), 'Maximizing brain networks engagement via individualized connectome-wide target search'

We measured the low-dimensional controllability of the 9 aforementioned networked systems and computed a group-level average over the 6134 healthy brains of the UK-biobank dataset. In all the cases, not surprisingly and as reported in Ref.[11], the best drivers were systematically inside the target and controllability values of the nodes inside were in general two orders of magnitude bigger than those outside the target (**Fig.5.5.a**).

As a further opportunity to test our metric we analyzed its lateralization properties since most of brain systems have well characterized tendencies to be predominant in one of the two hemispheres. **Remark:** We made the hypothesis that the corresponding brain regions should have larger controllability in the predominant hemisphere in order to support the additional functional activity and cognitive load.

To do so, we quantified a lateralization index, $LI(z) = \frac{z^R - z^L}{z^R + z^L}$, of controllability for each of the 9 networks, by only considering the drivers inside the targets. Since the networks can be already asymmetrically distributed across the right and left hemispheres, z^R and z^L are the mean controllability values in each hemisphere. Results are shown in (**Fig.5.5.b**) when using low-dimensional ($r = 5$), and classical worst-case controllability ($r = p$). In 5 out of 9 networks, the two metrics were contradictory. The lateralization effect was larger for the low-dimensional controllability metric and was disentangled from the intrinsic asymmetry of brain systems distribution in right and left hemispheres represented here by the number of nodes (**Fig.5.5.b**). Moreover, worst-case controllability was almost systematically lateralized toward the left hemisphere which

could be due to a structural bias in the metric or in its dependence on the connectomes topology.

These results confirm the discrepancy of the classical approach since our method is in line with the literature. Indeed, it is accepted that the VIS, DAN, LIM, and TPJ present a rightward dominance whereas the SMN, FPCN, and the DMN have a leftward dominance [85–89].

Effect of gender, handedness, and age

For the categorical variables (sex and handedness), we conducted a 2 a 2-way ANOVA test for each subnetwork lateralization and corrected the p-values for multiple testing using the Benjamini & Hochberg procedure for controlling the false discovery rate (FDR) [90]. As for the age we computed Spearman's correlation coefficient (**Table** 5.1).

Results showed that only only one association was significant ($p = 0.0047$): the lateralization of the **visual** system controllability grouped by **sex**. The controllability of the visual system by its own drivers was more lateralized toward the right hemisphere for the male subjects than for the females.

Regarding the age, all correlation coefficients were negligible ($\rho_S < 0.3$) and in majority negative (less lateralized as age increases) except for DAN, SVAN, and SUB systems that were positive. Even though negligible, the TPJ had by far the highest correlation ($\rho_S = -0.1703$).

[85]: Agcaoglu et al. (2015), 'Lateralization of Resting State Networks and Relationship to Age and Gender'
[86]: Janssen et al. (2011), 'Behavioral evidence for left-hemisphere specialization of motor planning'
[87]: Bartolomeo et al. (2019), 'Hemispheric lateralization of attention processes in the human brain'
[88]: Sack et al. (2012), 'Hemispheric Differences within the Fronto-Parietal Network Dynamics Underlying Spatial Imagery'
[89]: Devinsky (2000), 'Right Cerebral Hemisphere Dominance for a Sense of Corporeal and Emotional Self'

[90]: Benjamini et al. (1995), 'Controlling the False Discovery Rate'

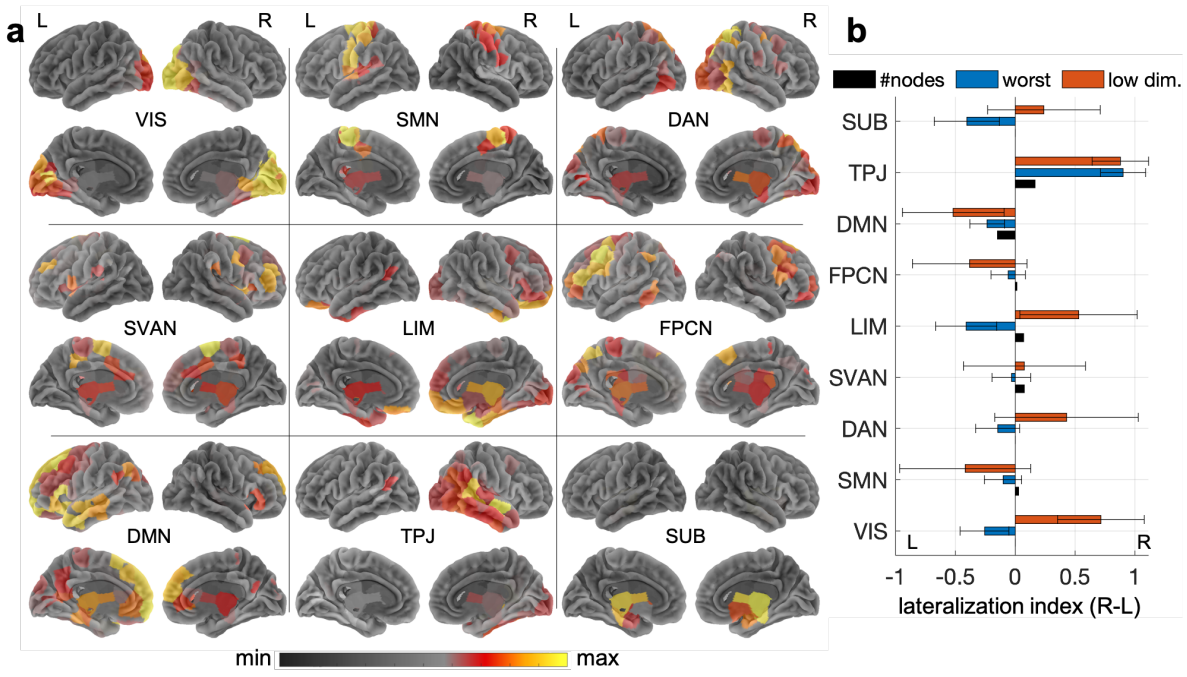

Figure 5.5: Low-dimensional controllability and lateralization of large-scale brain networks: a, Group-level average of single-driver low-dimensional controllability ($r = 5$) for each of all 9 target networks. **b**, Means and standard deviations of lateralization index, $LI(z) = \frac{z^R - z^L}{z^R + z^L}$, measured only on the drivers inside the targets for worst-case controllability ($r = p$) and low-dimensional controllability ($r = 5$) (see legend). As the networks are asymmetrical we also show the lateralization index for the number of nodes in right and left hemispheres. A lateralization index of 1 (or -1) would represent the extreme case of right (or left) lateralization.

Table 5.1: Adjusted p values from the 2-way ANOVA test for differences of the subnetwork controllability lateralization regarding sex and handedness, and ρ_S Spearman correlation coefficients with the age.

	2-way ANOVA: adj_p		Spearman ρ_S
	sex	handedness	age
VIS	0.0047	0.7720	-0.0337
SMN	0.2419	0.2419	-0.0193
DAN	0.9145	0.8577	0.0597
SVAN	0.2419	0.7720	0.0508
LIM	0.7720	0.7766	0.0076
FPCN	0.7768	0.2419	0.0070
DMN	0.7695	0.5929	-0.0223
TPJ	0.5644	0.7720	-0.1703
SUB	0.8577	0.9254	0.0168

5.2.4 Target brain controllability and distance metrics

These results were not merely due to the spatial proximity between the driver and the target but rather to the presence of shorter paths enabling a more efficient interaction. We correlated the previous low-dimensional controllability measures to the associated distance between single drivers and the targeted networks. We considered both spatial and network distances that were calculated respectively as the sum of the shortest paths and the euclidean distance to its composing nodes.

Pearson correlation tests were not significant ($R < 0.3$) for the spatial distance (**Fig.5.6**). On the other hand, results showed a high negative correlation between controllability and network distance indicating that the presence of shortest paths is of paramount importance for controllability. Similar conclusions were already held regarding the

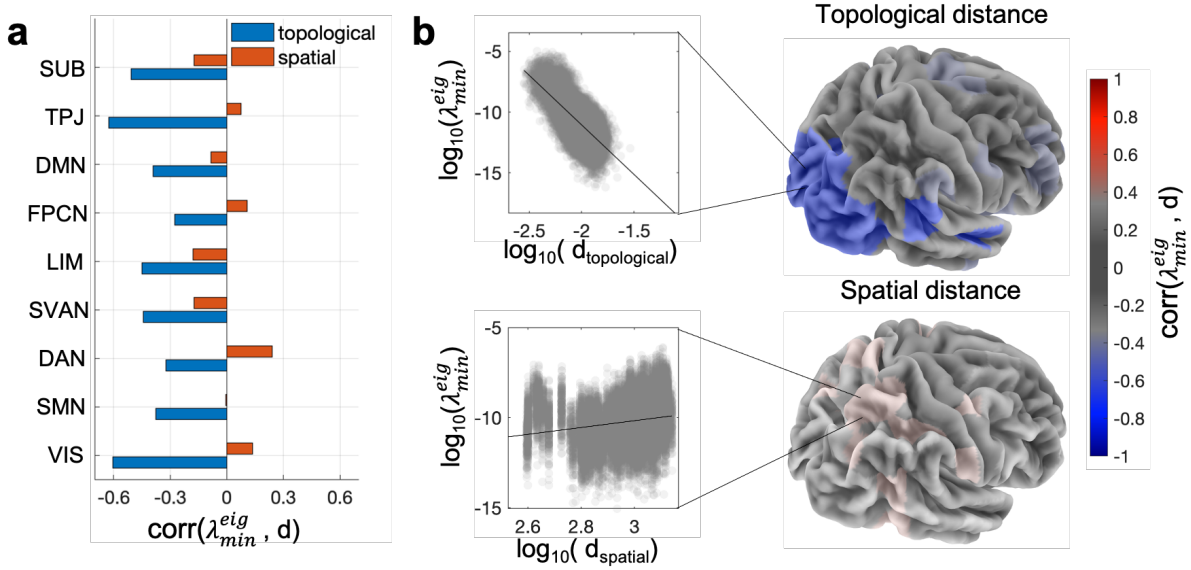

Figure 5.6: Correlation of low-dimensional controllability with simpler metrics: **a**, Pearson correlation between low-dimensional controllability and distances between drivers and targeted networks. We considered the distance to the targeted network as the sum of the distances to its nodes. Topological (blue) refers to the network distance and spatial (red) to the Euclidean distance. **b**, Visualization of the correlation coefficients and scatter plots for the most significant ones: the Visual network regarding topological distance and the DAN regarding spatial distance.

dependence of controllability to network distance [12] and other metrics like information distance and showed the importance of locality in network control [64].

[12]: Sun et al. (2013), 'Controllability Transition and Nonlocality in Network Control'

[64]: Duan et al. (2022), 'Prevalence and scalable control of localized networks'

5.2.5 Stimulation sites for Large-scale networks activation

From the perspective of future potential brain stimulation, we here refine the results by only keeping the best pairs of drivers and comparing them to the literature. It is important to remember that controllability is proper and different for each individual brain network and that there exists a large inter-subject variability. However, we were rather interested in testing if a group-level average over a large dataset of healthy individuals would highlight the traditional stimulation sites.

Recently, Menardi and colleagues [11] conducted an extensive in silico study in search of the drivers that maximize the engagement of these same large-scale networks (except the temporoparietal junction TPJ). Our results are not comparable since they considered a customized simulation-based metric for their selection. However, they also dressed a list of the traditional sites employed in transcranial magnetic stimulation for each large-scale network. We selected here the pairs of best drivers in the group-level average (**Fig.5.7**). So even if each structural connectome is unique and the best sites can thus differ, we expect some overlap between the group-level average and the traditional sites. Regarding the visual network, our result suggested the best driver is in the extra-striate superior cortex. In accordance with the literature, the second-best is in the striate calcarine cortex. For the SMN, our best-predicted driver was also a traditional site (primary cortex M1). Similarly, when targeting the

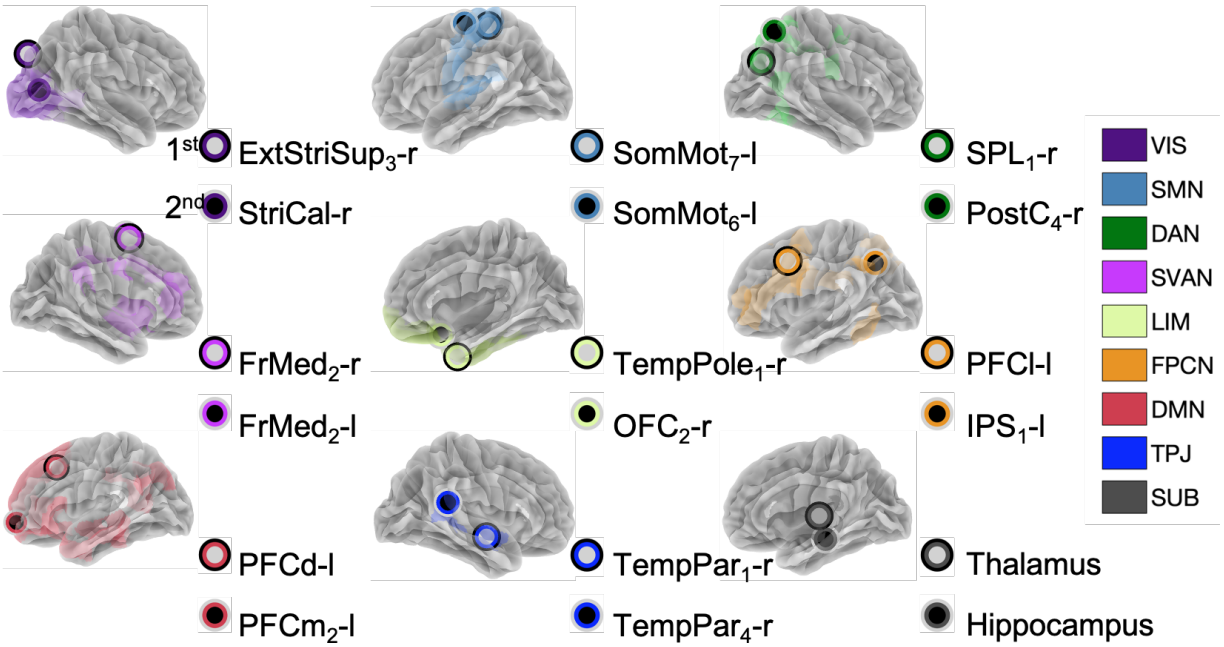

Figure 5.7: Pairs of best drivers according to the low-dimensional controllability metric ($r = 5$) for each of the aforementioned large-scale networks. Selected best drivers had the 2 highest controllability in the group-level average. Parcel names correspond to the Schaefer200 atlas. Abbreviations: ExtStriSup = extra-striate superior; StriCal = striate calcarine; SomMot = somatomotor; SPL = superior parietal lobule; PostC = post central; FrMed = frontal medial; TempPole = temporal pole; OFC = orbital frontal cortex; PFCl = lateral prefrontal cortex; IPS = intraparietal sulcus; PFCd = dorsal prefrontal cortex; PFCm = medial prefrontal cortex; TempPar = temporal parietal.

DAN, our method also spotted a traditional site, the superior parietal lobule (SPL). No overlap was found for the SVAN and the LIM network. As for the FPCN, our best-driver prediction, the prefrontal cortex (PFC) is also known as a traditional site. Our second-best prediction for the DMN, the medial prefrontal cortex is a traditional stimulation site as well. Finally, for the TPJ, no traditional site is known because of inter-individual variation in location and structure and the low number of studies [91].

[91]: Donaldson et al. (2015), 'Noninvasive stimulation of the temporoparietal junction'

5.2.6 Conclusion

In the previous section, we simulated state transition between fixed initial and final states using a regularized control strategy. However, here, our goal was to characterize the controllability of single nodes in a general sense. That is why we used metrics based on the controllability Gramian which is known to summarize the energetic landscape of the network state space.

We applied classical metrics: Average and worst-case controllability, and our low-dimensional version of the worst-case controllability to a large dataset of structural brain connectivity networks. The dataset is relatively large (N>6k) and for that reason, we assumed that small errors resulting from the construction of individual structural connectomes would cancel out when looking at group-level average results. We first explained that we fixed the dimension of smaller Laplacian-based output Gramians to $r = 5$ beyond which the metric started to be ill-posed since it gave negative values for some drivers like worst-case controllability. Then we showed by measuring whole-brain controllability that our metric was not as dependent on the node strength as average controllability. For these two reasons, our metric can be qualified as being a trade-off between the stability of average controllability and the representativeness of the worst-case controllability.

We took advantage of the well-known lateralization properties of large-scale functional brain networks to check the validity of our metric. We measured a lateralization index for each network and each subject and the group-level results were in line with literature, unlike worst-case controllability. we also showed that low-dimensional controllability was negatively correlated with network distance rather than spatial distance, especially for the visual system and temporoparietal junction. Finally, low-dimensional controllability is subject-specific but at the group-level average, it pointed out plausible drivers that were overlapping with traditional stimulation sites used in TMS.

Integrating brain controllability at the system level

6

Until this point of the dissertation, we were only interested in the controllability of a fixed network or a subnetwork by different nodes taken as single drivers. It is well-known that the "dual" problem of controllability is observability which refers to the ability of observing, estimating, or reconstructing the states x from the output y. However, let us not consider here the "dual" problem, but one that could be qualified as "reciprocal". For a given fixed driver node, how well can different targeted networks be controlled by it?

6.1 Theoretical considerations: controllability and target size

Indeed, if we fix one node $\mathcal{D}$ as single driver and measure its controllability for two different target sets S_1 and S_2, are the obtained values comparable? Can we say that S_1 can be better controlled from $\mathcal{D}$ than S_2 or inversely?

This question cannot be answered trivially. Indeed, as other parameters such as the number of drivers n_d, or the terminal time t_f, the size s of the targeted network (noted p in **Fig.6.1**) is also a crucial scaling parameter of the control energy obtained by the Gramian [43]. Indeed, the worst-case controllability is basically the inverse of the maximum control energy. Moreover, **Fig.6.1** shows that the scaling becomes sharper as one decreases the number of drivers.

Therefore, regarding our initial question it is legitimate to consider that the worst-case controllability measures of target sets S_1 and S_2 of different sizes $s_1 \neq s_2$ are not comparable. In other terms, the controllability measure is mostly dominated by the target size. This is no longer an issue when using our framework since all the targets are projected onto a lower-dimensional space of same dimension $r = 5$. Ultimately, it is as if our low-dimensional controllability metric could serve as a normalized measure. Of course, this only holds when the target network size is larger than the output dimension $s > r$.

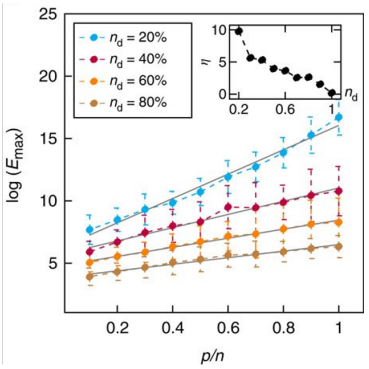

Figure 6.1: Effect of target size on controllability: Figure and legend adapted from [43] under the Creative Commons' license: "The plot shows how the log of the maximum control energy changes with target node fraction, p/n. The number of drivers n_d is varied for networks with the following properties: $n = 500$; $\gamma_{in} = \gamma_{out} = 3.0$; $k_{av} = 5.0$. "

[43]: Klickstein et al. (2017), 'Energy scaling of targeted optimal control of complex networks'

Significance statement

The fact that Gramian controllability metrics are mostly dominated by the number of drivers n_d and the target set size s is the main limitation preventing the study of mutual controllability properties of heterogeneous networks.

By considering low-dimensional projections of single-driver Gramians we suppress this effect and we can, for the first time, study the mutual influence of brain functional systems from a controllability perspective.

6.2 System-level controllability in the human brain and cognitive control

[92]: Wang et al. (2017), 'Brain network eigenmodes provide a robust and compact representation of the structural connectome in health and disease'
[93]: Gollo (), 'Mapping how local perturbations influence systems-level brain dynamics'

It is important to remember that these controllability results are derived from a group average and differ at the individual level. However, the macro-organization of the brain in functional systems that support cognition is relatively stable in healthy connectomes [92, 93] and mapping their mutual influence in terms of controllability is still an open question in neuroscience.

To fill this qualitative knowledge gap, we regrouped the results of the previous section and averaged them over the systems. This produces, for each subject, a meta graph in which a link i to j represents the controllability of the target system j by the drivers of the system i (**Fig.6.2**). We do not show the SUB network here for visualization purposes as it was a giant hub and we were more interested in cortico-cortical interactions.

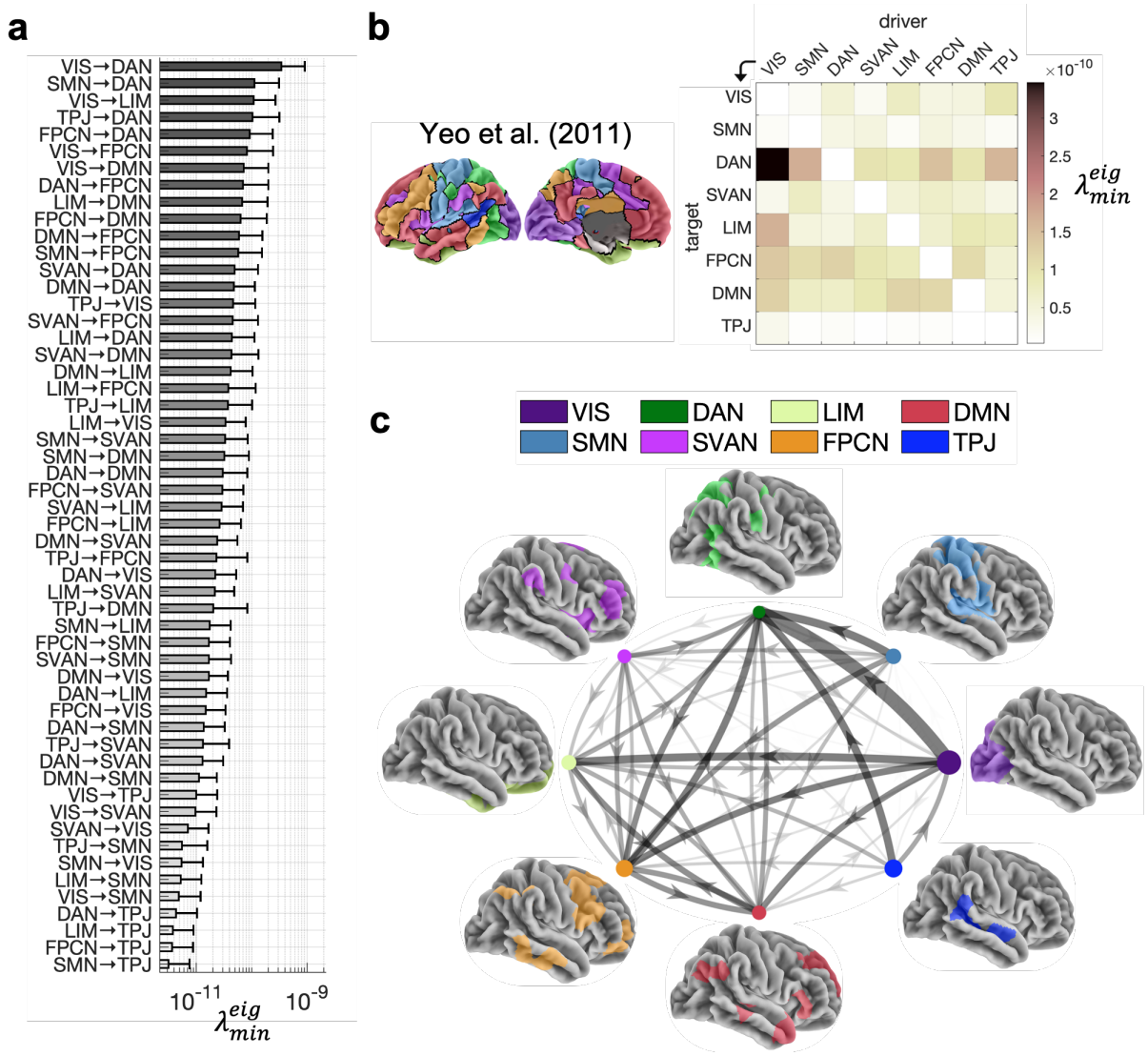

Figure 6.2: Group-level average and standard deviation of brain systems controllability. **a,** Mean and standard deviation of the meta-links of system-level controllability. **b, c,** Adjacency matrix and network visualization of the mean meta-graph. Self-loops are omitted here for clarity.

Among the largest links, the DAN was best controlled in descending order by the visual network, the somatosensory network, and the temporoparietal junction (**Fig.6.1.a**). This result could imply that the brain wiring facilitates the integration of primary stimuli and their relay to the attentional network DAN for further processing. The DAN, in turn, controls best the FPCN and the DMN that interact together during higher order cognitive tasks like language or motor control [94–98]. This supports the hypothesis that network controllability theory can be informative of cognitive control [99].

[94]: Uddin et al. (2008), 'Functional connectivity of default mode network components'
[95]: Maillet et al. (2019), 'Large-scale network interactions involved in dividing attention between the external environment and internal thoughts to pursue two distinct goals'
[96]: Raichle et al. (2001), 'A default mode of brain function'
[97]: Parks et al. (2013), 'Brain Connectivity and Visual Attention'
[98]: Corbetta et al. (2002), 'Control of goal-directed and stimulus-driven attention in the brain'

The mutual controllability between the visual network and the DAN was highly asymmetrical in favor of the visual system driving the DAN (**Fig.6.1.b.c**). The DAN is engaged when humans direct their attention in a visual scene. Such process is called "top-down control". On the other hand, the visual system influences the DAN in return when a sharp or odd stimulus occurs to relocate attention in the visual scene. Such a process is called "bottom-up" control. The results suggested that the "bottom-up" control is more facilitated by the brain's structural wiring than the "top-down" control. This is consistent with conclusions from Ref.[100] that showed that the increase in effective connectivity between the DAN and the VIS was higher during imagery than during visual perception. Seen from a control perspective, a higher coupling means higher activity and energy consumption, and that converges towards our observation. Moreover, this structural asymmetry could also be related to the hypothesis that the mammalian brain evolved to efficiently respond to danger and threat for survival. From this point of view, "bottom-up" communication has to be efficient for quick response to threats whereas "top-down" control is a process that happens a posteriori to integrate the bottom-up signals and implement conditioning and memory [101, 102].

[99]: Medaglia et al. (2017), 'Brain and cognitive reserve'

[100]: Dijkstra et al. (2017), 'Distinct Top-down and Bottom-up Brain Connectivity During Visual Perception and Imagery'

[101]: Pardi et al. (2023), 'Probing top-down information in neocortical layer 1'
[102]: Schroeder et al. (2023), 'Inhibitory top-down projections from zona incerta mediate neocortical memory'

Remark: We observe two poles in (**Fig.6.2.c**). The first one, on the right, is composed of the VIS, SMN, and TPJ. These three networks are engaged in the processing of primary stimuli and information. They all send information to the DAN, which acts as a control tower for dividing attention. On the other hand, three other networks: the FPCN, the DMN, and the LIM networks seemed to be densely connected. These networks are engaged in higher-order tasks like decision-making, language, imagination, and emotional processing [96].

[96]: Raichle et al. (2001), 'A default mode of brain function'

Remark: Sex-related differences in controllability Lastly, in almost every meta-link between systems, we observed significantly higher controllability values for males. We did not however, find a definite topological substrate for it. The main difference that we observed between male and female connectomes was in the number of tracts. Females had an average denser connectomes ($\text{tot.tracts}^{\text{female}} = 7.3672e+05 > \text{tot.tracts}^{\text{male}} = 7.2955e+05$, $p < 10^{-12}$). That corresponds to a relative difference of almost 1%. This effect is mostly due to the inter-hemispheric connections that were from far more abundant in females ($\text{RL-tracts}^{\text{female}} = 3.0438e+04 > \text{RL-tracts}^{\text{male}} = 2.6462e+04$, relative difference of almost 15%, $p < 10^{-126}$). We did not conduct further analysis to explain this sex-related difference.

6.3 Inferring neural control directionality from undirected structural connectomes

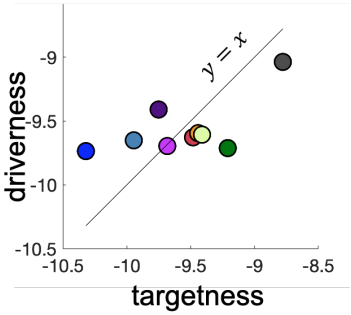

Figure 6.3: Scatter plot of average driverness and targetness of brain systems

From the results of the previous section, we observed certain tendencies (**Fig.6.1.a**). For example, the visual system was a recurrent driver in the largest meta-links. Similarly, the SMN and TPJ, were recurrent targets in the weakest meta-links. In order to capture the phenomenon, we decided to analyze the in and out weighted degree of the controllability meta-graph (**Fig.6.3**).

System-level driverness and targetness

For a given controllability meta-graph, we can define

- **Driverness:** as the sum of outgoing controllability meta-links.
- **Targetness:** as the sum of ingoing controllability meta-links.
- **Total contribution=** driverness + targetness (out+in).
- **driver-target asymmetry=** driverness - targetness (out-in).

We computed these metrics for each of the $N = 6134$ subjects. Results showed a substantial heterogeneity in the overall controllability profiles of the systems. In terms of total controllability (out+in), the subcortical system (SUB) acted as a major hub capable of controlling and being controlled as compared to the other systems. The saliency and ventral attention network (SVAN) was instead the least involved in the overall controllability dynamics (**Fig.6.4.b**). By looking at the controllability unbalance (out-in), the temporoparietal junction TPJ, as well as the primary visual (VIS) and sensorimotor (SMN) systems, exhibited a significantly higher tendency to control rather than being controlled, while the opposite tendency occurred for the other cognitive-related systems (e.g., the frontoparietal control network FPCN, the default mode network DMN, and dorsal attention network DAN) (**Fig.6.4.c**).

Neuroanatomical and functional interpretation

These results are highly consistent with functional and cognitive roles associated with these large-scale functional brain networks. Indeed, the visual system and the somatosensory areas had the highest driving propensities since they are the gates to the world that receive and relay external stimuli (**Fig.6.4.c**). They were followed by the TPJ which is known to be a hub of integration and processing of both internal and external sensory information to then relay it to attentional networks [103]. The TPJ and the SVAN interact together when odd stimuli are received like loud noises or surprising events and can interrupt ongoing tasks [98].

These notes convey a neuroanatomical interpretation and explanation for how the structural connectome topology facilitates the driving tendency of these systems. Similarly, the FPCN, DMN, and DAN had a propensity to be controlled easily and act as target networks. The DAN acts as a cognitive switch, or as the brain's lenses that works in cooperation with other networks and directs or divides the mind's attention [95]. In other terms, it is constantly solicited by other networks which explains its higher targetness. The FPCN and DMN were also classified as "target" systems. These systems constitute the main brain control networks. They

[103]: Abu-Akel et al. (2011), 'Neuroanatomical and neurochemical bases of theory of mind'

[98]: Corbetta et al. (2002), 'Control of goal-directed and stimulus-driven attention in the brain'

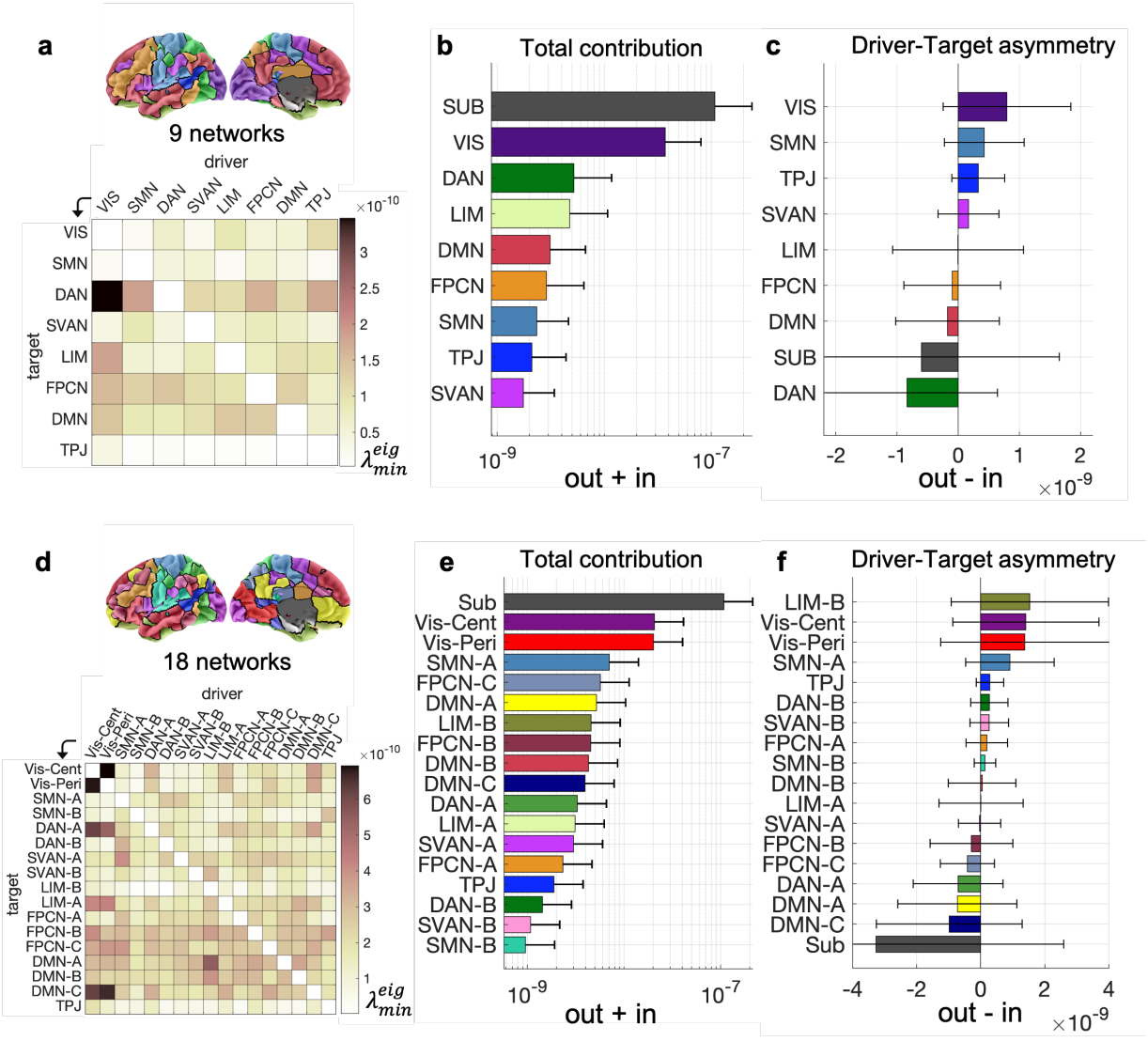

Figure 6.4: a, (top) Parcellation into 9 large-scale networks defined in [83], (bottom) group-level average controllability meta-graph. **b, c** , Mean and standard deviation of the total contribution and the driver-target asymmetry. They respectively correspond to the sum and difference of driverness and targetness for each system. **d, e, f,** same as **a, b, c,** reproduced with a finer parcellation into 18 networks also defined in [83].

counterbalance each other between rest and goal-oriented tasks [95, 96]. Even if they are both responsible for higher-order cognitive tasks, they engage differently though. The FPCN integrates external and internal information for rational or rule-based tasks. It is called the "external mind". However, the DMN is engaged in semantic processing, internal thoughts, and imagination and cooperated with the limbic (LIM) system for emotional processing [95, 96]. These considerations are in line with the results since we observe that the FPCN, DMN, and LIM networks form a cluster in the average controllability meta-graph (**Fig.6.2.c**). Specifically, we observe that the limbic (LIM) system strongly controls the DMN (8th meta-link) confirming their cooperation for emotional processing as well as an equal mutual controllability between DMN and FPCN. The fact that these networks were classified as "targets" is in line with their function since they integrate information coming from the rest of the networks to reflect, take decisions and imagine.

[95]: Maillet et al. (2019), 'Large-scale network interactions involved in dividing attention between the external environment and internal thoughts to pursue two distinct goals'
[96]: Raichle et al. (2001), 'A default mode of brain function'

Effect of gender, handedness, and age

As for the lateralization of controllability, we investigated the potential effects of sex, handedness, and age on the total contribution. We used the same analysis: 2-way ANOVA, corrected for FDR, for sex and handedness, and Spearman's correlation for age (**Table** 6.1).

Gender had a surprisingly significant effect in almost all the subnetworks except DAN, SVAN, and SUB. Total controllability of brain subsystems was higher in the male population.

No effect was found for the handedness even though the smallest p-value is associated with the SMN. But the effect is negligible (non adjusted p-value, $p = 0.2277$).

Regarding age, All correlations were negligible ($\rho_S < 0.3$) and negative except for VIS and LIM. As for the lateralization properties, the controllability of the TPJ was the most correlated to age ($\rho_S = 0.1497$).

Results showed that overall men had higher controllability values than women, handedness had no effect, and that there was a loss of controllability in most aged subjects.

Table 6.1: Adjusted p values from the 2-way ANOVA test for differences of the subnetwork total contribution regarding sex and handedness, and ρ_S Spearman correlation coefficients with the age.

	2-way ANOVA: adj_p		Spearman ρ_S
	sex	handedness	age
VIS	0.0004	0.9984	0.0485
SMN	0.0044	0.4554	-0.0708
DAN	0.0152	0.9984	-0.0575
SVAN	0.8270	0.7313	-0.0785
LIM	0.0028	0.9984	0.0070
FPCN	0.0032	0.7313	-0.0398
DMN	0.0022	0.9984	-0.0693
TPJ	0.0065	0.7313	-0.1497
SUB	0.3934	0.9984	-0.0592

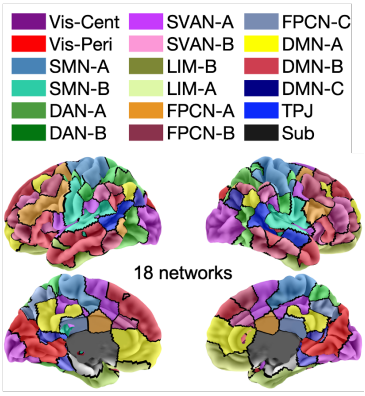

Figure 6.5: 4 views of the parcellation into 18 functional networks

Retest with a finer parcellation

Obviously, these conclusions depend on the way we define the network systems. In order to retest the results, we conducted the same analysis using a finer parcellation into 18 networks (17 cortical networks defined in [83] + SUB). Basically, each of the previously defined functional large-scale networks is in turn subdivided into 2 or 3 subnetworks.

Results were highly consistent with the first analysis (**Fig.6.4.d,e,f**). We still observed strong meta-links from the VIS networks driving the DAN-A. The subcortical regions, the visual system, and the motor regions were still the most contributing networks, followed by LIM, DMN, and FPCN in the middle, and SVAN and TPJ were the least contributing ones (**Fig.6.4.e**). Regarding the driver-target asymmetry, results were also similar for the most driving networks (VIS and SMN) but less evident for the target systems, even though DMN and FPCN were still in majority tending to act as "targets".

6.4 Comparison to network communication model

Results showed that brain large-scale networks could be characterized by their targetness and driverness. These notions can be bridged to the concept of send-receive communication asymmetry proposed by a recent study in which they captured whether a subsystem tends to send or receive information [104]. Indeed, our results, as a previous controllability study [105], showed that the SMN was a hard system to control, and It was also the system with the highest propensity to send information [104] (**Fig.6.6.b**). In addition, the DAN, LIM, FPCN, and DMN tended to be receivers in the same way our results suggested they were better targets (**Fig.6.4.c**).

In summary, the driver-target asymmetry, which captured to what extent large-scale functional networks could control or be controlled, seemed in line with conclusions drawn from a network communication model that classified them as senders and receivers [104]. This comparison confirms that even though network control theory and communication models are conceptually distinct, they are intertwined and more efforts should be done to integrate them in order to study brain networks dynamics [106].

[104]: Seguin et al. (2019), 'Inferring neural signalling directionality from undirected structural connectomes'

[105]: Bassignana et al. (2022), 'The impact of aging on human brain network target controllability'

[106]: Srivastava et al. (2020), 'Models of communication and control for brain networks'

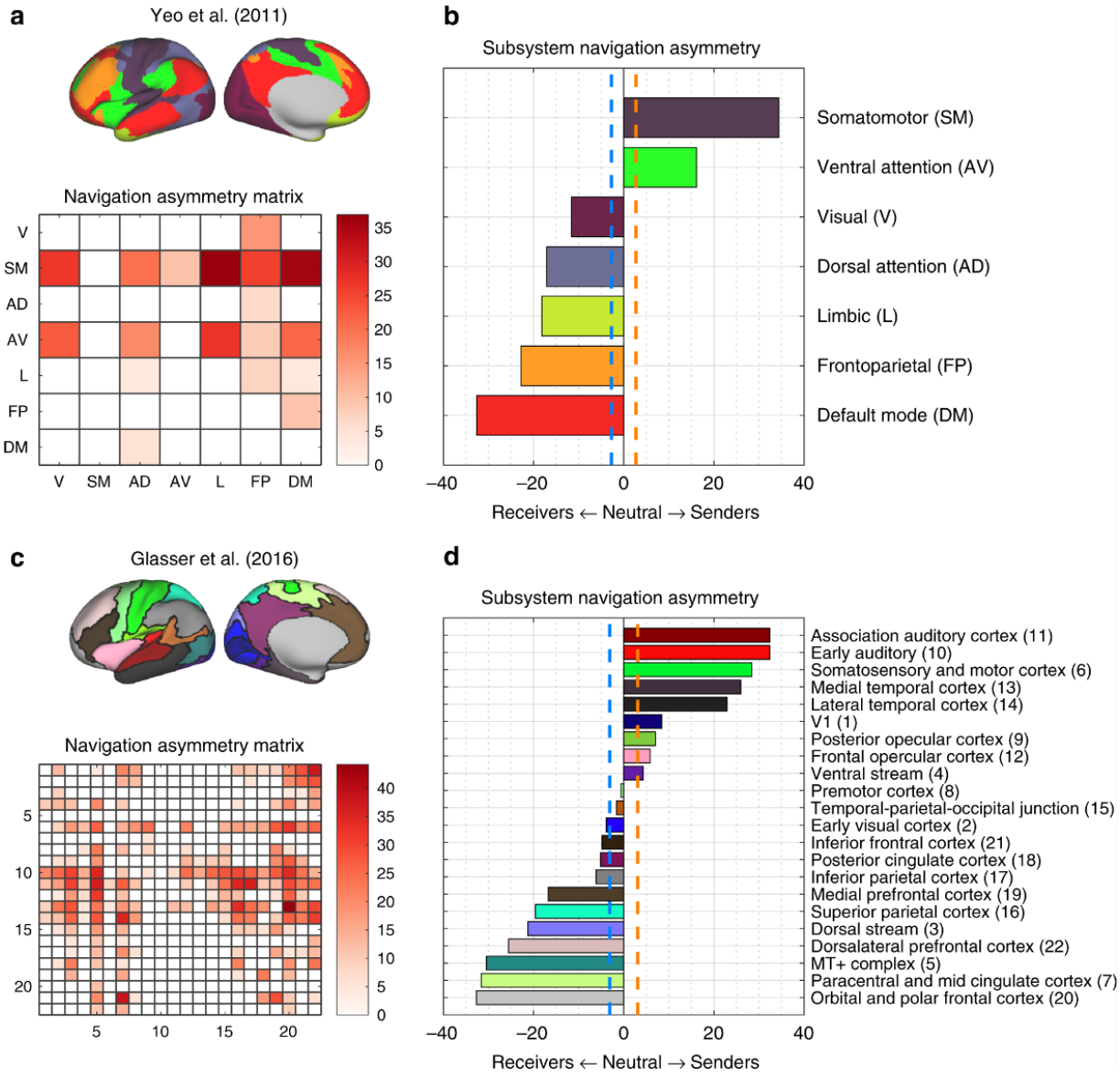

Figure 6.6: Figure and caption reproduced from [104] under the license Creative Commons. "Send-receive asymmetry of cortical subsystems under navigation ($N = 360$at 15% connection density). **a,** Projection of $M = 7$ distributed resting-state networks onto the cortical surface (top) and send-receive asymmetry matrix under navigation (bottom). A matrix element $A(i, j) > 0$ denotes that communication occurs more efficiently from i to j than from j to i. Send-receive asymmetry values that did not survive multiple comparison correction were suppressed and appear as white cells. For ease of visualization and without loss of information (since $A(i, j) = A(j, i)$), negative values were omitted. **b,** Resting-state networks ranked by propensity to send (top) or receive (bottom) information. Dashed vertical lines indicate a significant bias towards outgoing (orange) and incoming (blue) communication efficiency. **c, d** Same as **a, b**, but for $M = 22$ spatially contiguous cortical subsystems. Numbers listed next to module names identify corresponding rows and columns in the asymmetry matrix"

6.5 Conclusion: overview on the application of low-dimensional controllability to structural connectomes and originality of the results

After introducing our framework of low-dimensional controllability and validation with synthetic networks and a directed toy model, we applied it to brain structural connectivity data.

Our results were organized in two folds. The first is the direct application of low-dimensional controllability with single drivers and the interpretation of the results. we demonstrated why we fixed the dimension of the low-dimensional Laplacian eigenspaces to $r = 5$ after which the metric starts behaving poorly. We then computed the controllability of every single driver for 9 functionally relevant large-scale networks. Since these networks have well-known lateralization properties, we quantified a lateralization index of the controllability of each network by its composing nodes. Results showed that the lateralization of low-dimensional controllability was in line with experimental results.

The second fold of our results was to integrate the controllability of single drivers at the system-level. The main assumption we made here was that the controllability of a targeted network by a group of other nodes could be approximated by the mean controllability of those nodes as taken as single drivers. And this was only possible because of two aspects of our framework. The first is that our metric of low-dimensional controllability is well-defined and positive for all single drivers so that we can regroup them in systems. Secondly, our metric was derived from projected controllability Gramians of single drivers, that shared the same output dimension, or number of used eigenmaps, $r = 5$. By doing so we eliminated both effects of the target set size and the number of nodes and could characterize, in isolation, the controllability of heterogeneous networks. Thus, we could integrate the controllability at the level of functional brain subsystems and interpret our results from a cognitive point of view. Notably, we constructed a meta-graph of system-level controllability and observed that the visual system had a particularly high capacity to drive most systems. From a cognitive perspective, our results reflected most evident pathways such as the transfer of information from the sensory-related areas: VIS, SMN, and TPJ to the DAN which in turn could easily control and be controlled by the cognitive control networks: the FPCN and the DMN.

Ultimately, we analyzed the roles played by each functional network in the controllability meta-graph in terms of out-going and in-going degree which we called driverness and targetness. Results suggested that primary functional networks tended to be drivers whereas higher-order networks like FPCN and DMN tended to act as targets. Our conclusions were highly consistent with those of a previous study derived from a network communication model. This last point was highly promising regarding the integration of network control theory and communication models, paving the way for future work in that direction.

Hemispheric differences and competition for centrality in brain networks

7

This section covers another study, which was conducted as a side project, and which does not relate directly to network controllability.

Study motivation and outline

The project emerged from a collaboration with two neuroscientists: Paolo Bartolomeo and Brigitte Charlotte Kaufmann who work on white matter fiber systems and were interested in hemispheric dominance and lateralization of brain subsystems. The main question is whether there is one brain hemisphere that dominates the other in terms of network centrality. That is why we decided to apply the framework of Eigenvector centrality competition and share our results with them for further discussion and interpretation and prepare a publication. We studied hemispheric differences at multiple levels: the level of the hemispheres, the cognitive subsystems, and the individual brain parcels.

Even though it is not directly related to controllability, the study of brain hemispheric differences of other network metrics can help understand the topological substrate that leads to the lateralization of controllability. We also analyzed more in detail the differences related to gender since it had a significant effect on controllability.

7.1 Context: Competition for centrality between the right and the left hemispheres in the human brain

In 1861, Paul Broca showed that the language center in the brain is located in the left hemisphere and the specific area was named after him. The principle of functional lateralization was then well-established thanks to functional connectivity studies [107, 108]. Other cognitive functions like attentional processes depend on how the activity is distributed across the right and left hemispheres and the physiological substrates of this balance are still weakly known. Thus, the two hemispheres can be modeled as two agents that cooperate and compete to handle the cognitive load.

Building upon this hypothesis, authors of Ref.[109] used eigenvector centrality (EC) to analyze EEG-based functional brain connectivity networks to capture the role and centrality of right and left hemispheres modeled as two cooperating agents which compete for centrality. They, notably showed that inter-hemispheric connections play an important role in the degree of centrality asymmetry between the two hemispheres.

The mathematical foundation of this framework was introduced to model to understand the dynamics in play in networks of networks (NoN) where subnetworks are considered as agents that interact through

[107]: Gotts et al. (2013), 'Two distinct forms of functional lateralization in the human brain'
[108]: Karolis et al. (2019), 'The architecture of functional lateralisation and its relationship to callosal connectivity in the human brain'
[109]: Martínez et al. (2018), 'Role of inter-hemispheric connections in functional brain networks'

the underlying topology like cliques in social networks [110]. The case of 2 sub-networks detailed: the dominance of one over the other results from the inner topology of each one and the degree of inequality is then regulated by the connector nodes. It has been shown semi-empirically that a central-central (C-C) connection strategy results in most balancing configurations (reducing the two networks centrality gap), whereas a peripheral-peripheral (P-P) strategy leads to the most inequitable centrality distribution [109, 110].

[110]: Aguirre et al. (2013), 'Successful strategies for competing networks'

7.2 Materials & Methods

We used the same data from the previous chapter on controllability: 6134 healthy individuals of the UK-biobank. We define in this section the network centrality that we used and explain the modeling choices that were made.

7.2.1 Symmetrical and multi-scale brain parcellation

We used structural connectomes but projected into a different brain parcellation. We decided to use the Lausanne2008 atlas [111] for two reasons. The first is that it is a symmetrical atlas which is a crucial aspect since the goal is to study hemispheric connectivity differences. The second, is that it permits to obtain a mapping of brain connectivity at 5 different scales (**Fig.7.1**). We thought that this aspect was indeed valuable in terms of robustness since one can compare the results at different scales and test their stability. The Schaefer atlas [81] used previously is also multi-scale. It has 10 different scales (from 100 to 1k nodes) but it is not symmetrical. Later on, in 2023, the same authors released a symmetrical version with homotopic regions [112] but it was already too late for us to include it in our pipeline. However, it could be interesting to use this latter in future work.

[111]: Cammoun et al. (2012), 'Mapping the human connectome at multiple scales with diffusion spectrum MRI'

[81]: Schaefer et al. (2018), 'Local-Global Parcellation of the Human Cerebral Cortex from Intrinsic Functional Connectivity MRI'

[112]: Yan et al. (2023), *Homotopic local-global parcellation of the human cerebral cortex from resting-state functional connectivity*

The multi-scale Lausanne2008 parcellation is symmetrical (in terms of number of nodes per hemisphere) for all scales except the 3^{rd}. Indeed,

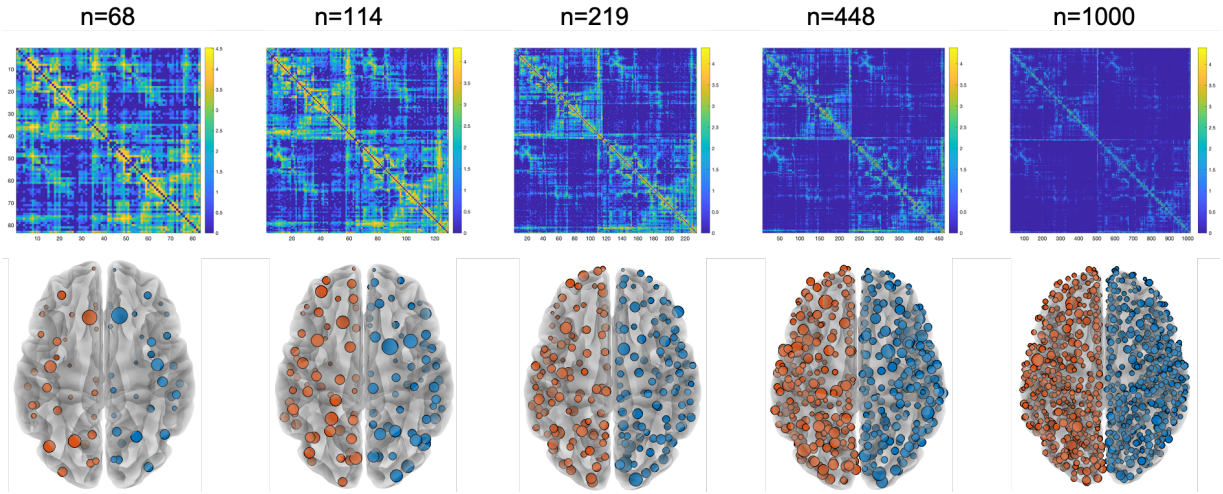

Figure 7.1: The multi-scale Lausanne2008 brain parcellation: (top) Adjacency matrices. (bottom) Node size represents the strength.

$n = 219$ is odd and the right hemisphere has one more node than the left. The first scale corresponds to the Desikan-Killyani atlas with 34 homotopic brain regions (see Appendix: **Table.2**) [113]. All scales are complemented with the brain stem and 14 homotopic subcortical structure which act as relays for the white matter fibers and are not accounted in the analysis of hemispheric differences.

[113]: Desikan et al. (2006), 'An automated labeling system for subdividing the human cerebral cortex on MRI scans into gyral based regions of interest'

7.2.2 Definition of fiber systems of interest: hemispheric dominance at the system level

The goal of this sub-project is to study hemispheric differences. We will answer the question in a multi-level fashion. The first two levels are evident: the first is the hemisphere level and the second is the nodal level. Since it is known that cognition is supported by inter-connected regions that form distinct networks with specific roles, we decided to incorporate a mesoscopic level corresponding to the subsystems. However, contrary to the previous sections where we focused on interconnected gray matter regions, for this study we were particularly interested in the white matter fiber structures. Specifically, we focused on two fiber systems: The Superior Longitudinal Fasciculus (SLF) and the Arcuate Fasciculus (AF) (**Fig.7.2**).

These two fiber systems were chosen because there is a large consensus about their function and lateralization properties. SLF is composed of three distinct bundles: SLF-I, SLF-II, SLF-III that are part of the longitudinal association fiber system, which lays connections between the frontal lobe and other areas of the ipsilateral hemisphere. It is known to regulate the focus of attention in spatial orientation and to be right-lateralized [114]. On the other hand, the AF is a three-branch pathway: the long (AF-long), anterior (AF-ant.), and posterior (AF-post.) segments, that support the processing and integration of auditory stimuli [115] but also integrate motor regions and language regions like Broca's and Wernicke's areas to support speech [116]. Notably, a left-ward asymmetry was reported for linguistic information processing and a rightward asymmetry for musical ones [115, 116].

[114]: Janelle et al. (2022), 'Superior Longitudinal Fasciculus'

[115]: Vaquero et al. (2021), 'Arcuate fasciculus architecture is associated with individual differences in pre-attentive detection of unpredicted music changes'

[116]: Hickok et al. (2007), 'The cortical organization of speech processing'

7.2.3 Identification of network nodes that are part of fiber systems

The credit for this specific part goes to Brigitte Charlotte Kaufmann. As stated before, the departing point of this side project is the white matter rather than the gray matter. Mostly because our collaborators, Paolo Bartolomeo and Brigitte Charlotte Kaufmann, are experts in the white matter fiber structures, their segmentation, and functions.

For each scale, we used Tractotron to identify the parcels that are connected by means of the respective white-matter fiber tracts. To do so, the cortical parcels were co-registered to the MNI152 template using FSL [117]. They are then mapped onto the tractography reconstructions of white matter pathways obtained from a group of healthy controls [118] using Tractotron and the BCBtoolkit [119] (`http://www.toolkit.bcblab.com/`). Tractotron provides the probability of connection, i.e. the probability

[117]: Smith et al. (2004), 'Advances in functional and structural MR image analysis and implementation as FSL'

[118]: Rojkova et al. (2016), 'Atlasing the frontal lobe connections and their variability due to age and education'

[119]: Alves et al. (2019), 'An improved neuroanatomical model of the default-mode network reconciles previous neuroimaging and neuropathological findings'

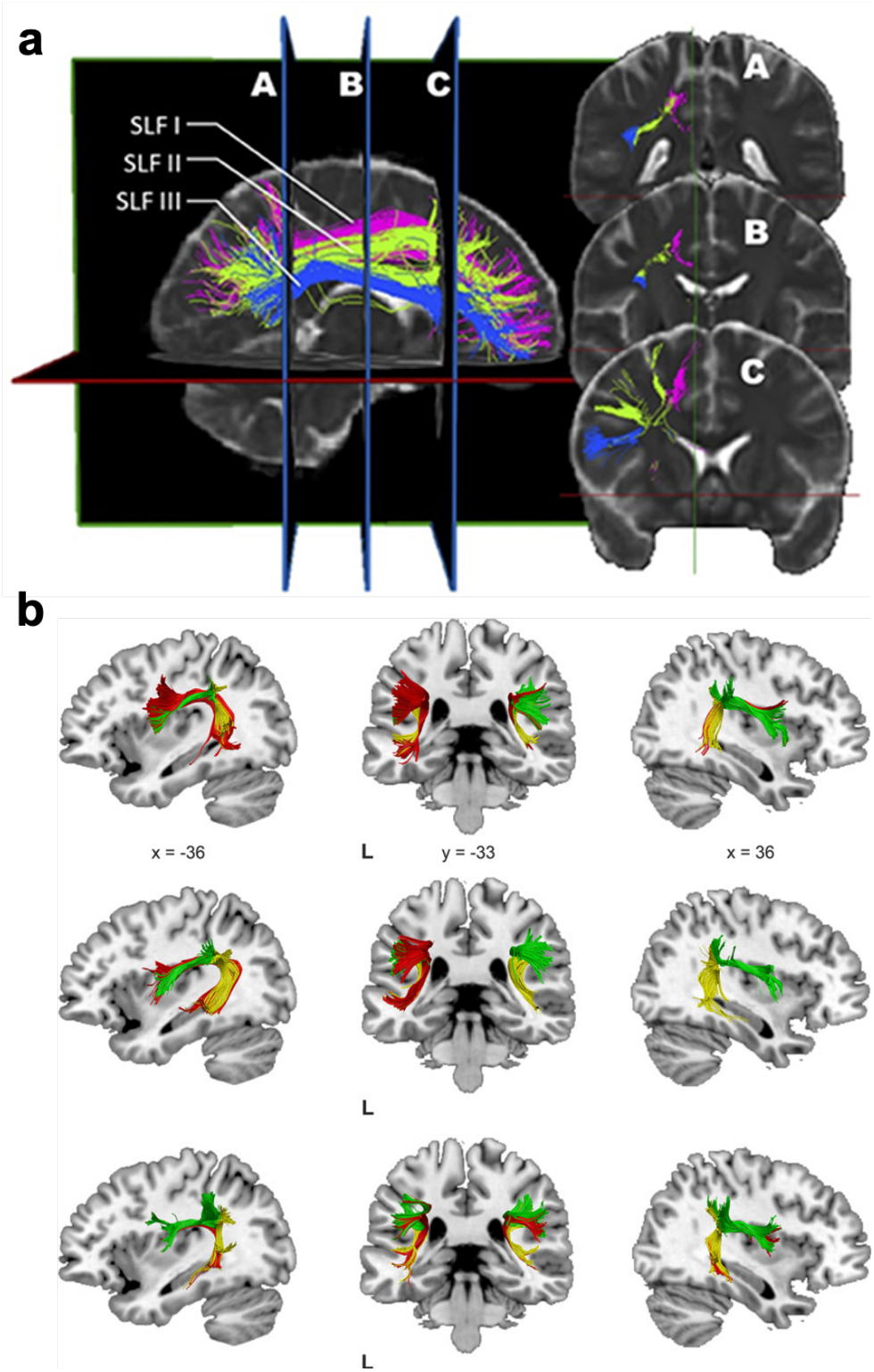

Figure 7.2: a, Figure and caption reproduced from [114] under the Creative Commons Attribution License (CC BY): "In vivo fiber tractography of the right SLF I (pink), SLF II (green), and SLF III (blue). A three-dimensional reconstruction of the three segments of the SLF is displayed at the left of the figure. The coronal sections of it (A, B, and C) are represented on the right. The dorso-ventral as well as medio-lateral localization of each sub-segment can be visualized on the coronal planes." **b,** Figure and caption reproduced from [115] under the Creative Commons Attribution-NonCommercial-No Derivatives License (CC BY NC ND): "Arcuate fasciculus dissection examples. Dissections of three participants are displayed on top of a T1-weighted template. MNI coordinates are provided. Red fibers correspond to the Long or direct segment, green fibers are the Anterior segment, and yellow fibers belong to the Posterior segment". Abbreviations: L, left hemisphere."

of a parcel being part of a white-matter tract [120]. All parcels with a probability of >50% were considered to belong to a white-matter tract, i.e. above a probability of 50% a parcel is more likely to belong than not belonging to a white-matter tract.

[120]: Thiebaut de Schotten et al. (2014), 'Damage to white matter pathways in subacute and chronic spatial neglect'

7.2.4 Comparison of the two hemispheres with global measures

Since our goal is to compare the brain hemispheres at multiple levels, we decided to compute two global measures for the two subnetworks taken separately and only considering their own topologies.

Global efficiency:
It informs on the efficiency of information exchange. It is computed as the average of the inverse shortest path length, and is inversely related to the characteristic path length [121].

[121]: Latora et al. (2001), 'Efficient Behavior of Small-World Networks'

$$E = \frac{1}{n(n-1)} \sum_{i \neq j} \frac{1}{d_{ij}}, \tag{7.1}$$

where d_{ij} contains the shortest distance between nodes i and j. We computed it using the "efficiency_wei" function of the BCT toolbox [56].

Modularity:
This metric quantifies to what extent the network is wired in a way that maximizes the within-group edges while minimizing the between-group edges [122]. We also computed it with the BCT toolbox [56] with the function "modularity_und".

[122]: Newman (2006), 'Finding community structure in networks using the eigenvectors of matrices'

see refs.[121, 122] for the formulas and details.

7.2.5 Network centrality: which metric for studying hemispheric differences?

Let us focus on the case of undirected networks and define the centralities that will be considered in this section. We note A the adjacency matrix of the network where A_{ij} contains the weight of the link between nodes i and j. The following definitions and **Fig.7.3** are picked from Ref.[123].

[123]: Rodrigues (2019), 'Network Centrality'

Degree centrality / Strength:
Degree centrality, or weighted degree (in weighted networks) also called strength is the simplest measure of node importance. It is defined as the sum of the weighted links attached to a node. It is obtained by summing over the rows or columns of A.

$$s_i = \sum_{j=1}^{n} A_{ij} \tag{7.2}$$

where n is the number of nodes in the network. The strength is intuitive but is a local measure that only captures the direct neighborhood of a node.

Eigenvector centrality:
Unlike degree centrality, eigenvector centrality (EC), which is the scope of

this section, is a global metric that takes the entire network into account. It is defined in terms of the neighborhood of each node. It assumes that a node is important if it is linked to other important nodes. If x denotes the eigenvector centrality then the importance of a node i is

$$x_i = \frac{1}{\lambda} \sum_{k=1}^{n} A_{k,i} x_k, \tag{7.3}$$

where $\lambda \neq 0$ is a constant. This equation can be rewritten in matrix form:

$$\lambda x = Ax. \tag{7.4}$$

The "importance" of node i is then defined by the left-hand eigenvector of the adjacency matrix A associated with the eigenvalue λ. That is why this measure is called eigenvector centrality. λ is chosen as the largest eigenvalue of A (see Ref.[123] for definitions and details about the other centralities shown in **Fig.7.3**. we can appreciate how nodes with same degree have different EC (**Fig.7.3**.a,e). Also, for degree centrality, most "important" nodes were located in the periphery of the network which is not the case anymore when considering EC.

More importantly, from the 6 metrics displayed in **Fig.7.3**, EC is the only one that clearly highlighted a difference between the two modules composing the toy model network. It was shown for functional brain networks that each centrality measure captures different aspects of the connectivity [124]. For the specific goal of quantifying network competition, EC seemed the most appropriate [109, 110].

[124]: Zuo et al. (2012), 'Network centrality in the human functional connectome'

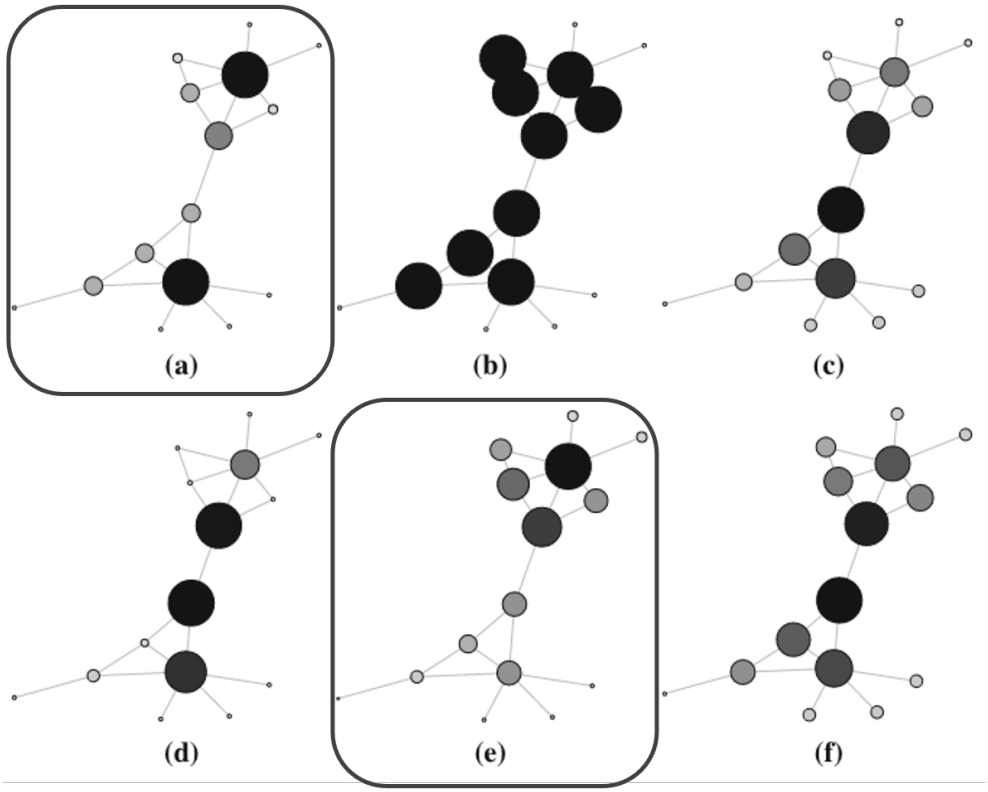

Figure 7.3: Figure reproduced from [123] with permission of the rights holder, Springer Nature: Comparison of centrality measures: **a,** degree centrality. **b,** k-core. **c,** closeness centrality. **d,** betweenness centrality **e,** eigenvector centrality. **f,** accessibility. The size and darkness of each node are proportional to its centrality measure.

7.2.6 Localization effect and Nonbacktracking centrality

The EC is designed to be distinctively different from degree/strength when there are some high-degree nodes connected to many low-degree others. Therefore, it will not be distinctively different from the degree in regular graphs or in core-periphery structures in which high-degree nodes tend to be connected to each other.

On the other hand, in some cases, EC can behave completely differently from strength and be driven by the presence of extreme connectivity patterns. Such an effect was first observed by authors of Ref.[125] when the presence of a giant hub was completely driving the behavior of the metric (**Fig.7.4**.a). The effect was called localization. It is not desirable to quantify the "importance" of the nodes and is due to the ping-pong network walks between the hub and its direct neighbors.

In order to avoid localization, the authors introduced an alternative to the EC which they called the "Nonbacktracking centrality" (NBT). To calculate it one has to introduce the Hashimoto or nonbacktracking matrix B [126]. It is a $2m \times 2m$ matrix, where m is the number of links where each row and each column correspond to the directed link $i \to j$. The matrix element $B_{k\to l,i\to j}$ is equal to one if edge $i \to j$ points into the same vertex that edge $k \to l$ points out of and edges $i \to j$ and $k \to l$ are not pointing in opposite directions between the same pair of vertices, and zero otherwise. If we note v the leading eigenvector of B, then the NBT of a node j is defined as:

$$x_j = \sum_i A_{ij} v_{i\to j} \tag{7.5}$$

The NBT centrality proposed by Ref.[125] rectifies the problem, giving values similar to the standard eigenvector centrality in cases where the latter is well behaved, but avoiding localization in cases where the standard measure fails (**Fig.7.4**.b).

We tested it with the brain networks and we observed the same result (**Fig.7.5**). In order to approximate the proportion of connectomes for

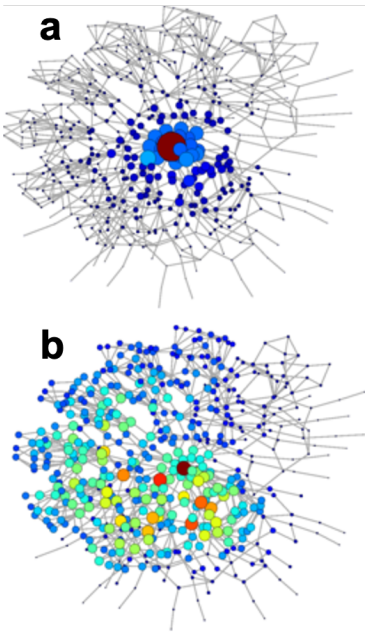

Figure 7.4: Figure reproduced from [125] with permission of the rights holder, American Physical Society **: Localization of eigenvector centrality**. **a,** Eigenvector centrality. **a,** Nonbackrtacking centrality

[125]: Martin et al. (2014), 'Localization and centrality in networks'

[126]: Hashimoto (1989), 'Zeta Functions of Finite Graphs and Representations of p-Adic Groups'

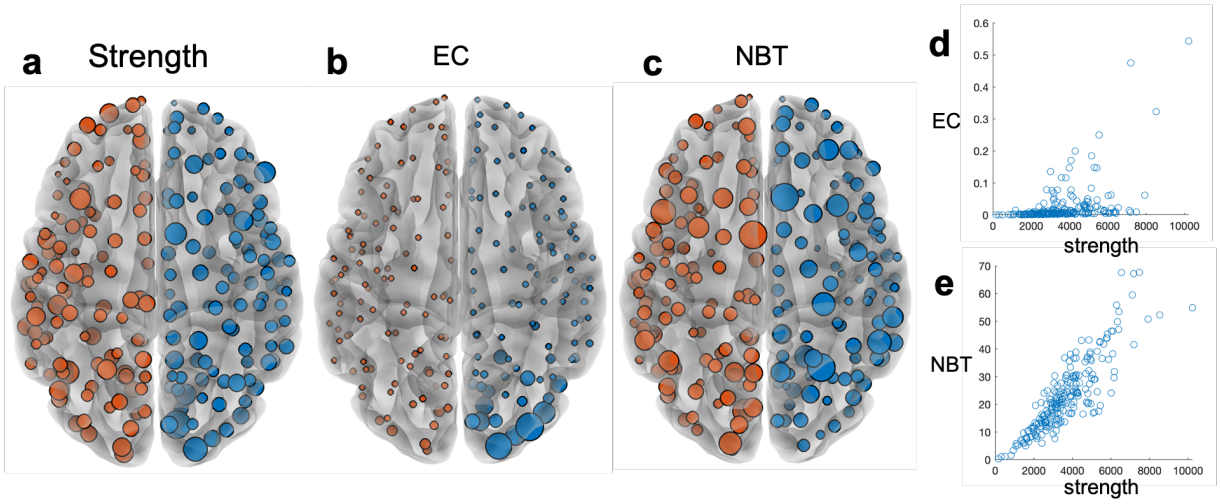

Figure 7.5: a, b, c Strength, EC, and NBT represented by node size for one representative connectome, at scale $n = 219$, for which EC is localized. **d, e** Scatter plots of the two centralities with the strength.

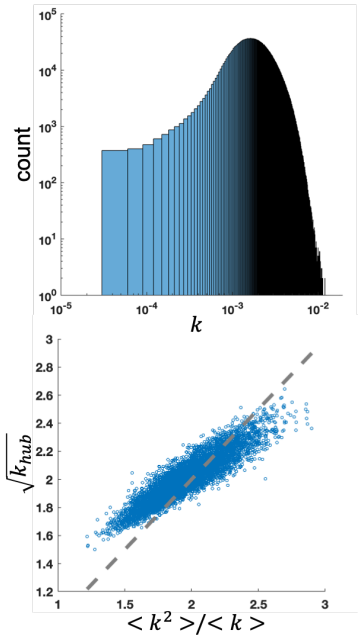

Figure 7.6: Criterion to detect localization explained in [125]. (top) Degree distribution of all the 6k connectomes. (bottom) Scatter plot of the dispersion index of the strength and the square root of the hub strength.

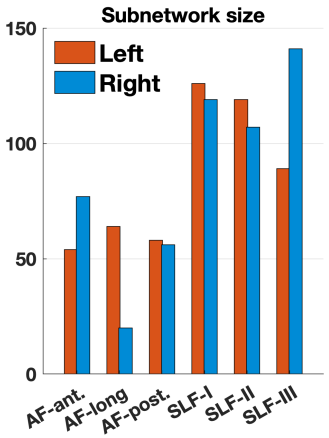

Figure 7.7: Size of the different fiber systems in left and right hemispheres for the scale 5. We count the number of nodes that have a probability higher than 50% to be traversed by the corresponding fiber system.

which EC is localized, we used the criterion introduced in [125] for power-law networks. This criterion fixes a localization threshold that works for power-law networks that are large enough. If $\sqrt{k_{hub}} > \frac{<k^2>}{<k>}$, then the leading eigenvector of A will be dominated by the hub. Brain structural networks do not exactly follow a power-law (**Fig.7.6**) but they are sparse (especially in higher scales here) and that highly accentuates localization as well [125]. Nonetheless, we used the criterion and estimated that, already for the smallest scale, EC would be localized for **67.92%** of the connectomes (**Fig.7.6**).

Strictly speaking, the competition between subnetworks, was established with EC [110] and was successfully applied to EEG-based functional connectivity networks [109]. However, we showed that EC failed in practice when applied to the structural data because of the localization effect. The main difference is the sparsity of structural connectomes compared to functional ones. On the other hand, NBT is supposed to behave like EC but we make the hypothesis that it is suitable to apply the competition framework. Taking all these considerations into account we decided to use NBT rather than EC even if it is strongly correlated with the strength ($r = 0.8683$, $p = 5.3834e - 68$) (**Fig.7.5.e**).

7.2.7 Using network null-models to rectify hemispheric asymmetry

As stated before, even though the Lausanne2008 atlas is composed of homotopic regions, there is still some asymmetries to take into account. The first one is at the hemisphere level, for the scale $n = 219$, the right hemisphere has one more node. The second asymmetry is at the system level since the fibers of interest have different volumes and shapes, and thus, did not connect the same number of nodes in the right and left hemispheres (**Fig.7.7**). The third level, the parcel level, also involves asymmetries at the higher scales. Each homotopic parcel of the Desikan-Killyani atlas (scale $n = 68$) is subdivided in a certain number of nodes in higher scales that is not equal in right and left hemispheres.

To rectify these asymmetries, we decided null-models. By generating 100 surrogate networks, for each connectome, we can derive surrogate metrics. Ultimately, we normalize the brain metrics by the averages of the surrogate metrics. This procedure solves all the aforementioned asymmetries.

Choice of the null-model

We tested two null-models based on links shuffling: the first conserves the strength sequence of the nodes while the second only conserves the degree sequence. They were computed respectively using functions "null_model_und_sign" and "randmio_und_connected" of the BCT toolbox [56]. As strength and NBT are very highly correlated (**Fig.7.5.e**), the null-model preserving strength was too constraining in the sense that NBT of the surrogate networks was almost the as the NBT of the original brain networks (**Fig.7.8.d,e,f**). Using it as null-model would completely cancel out the topological features of each individual connectome. That is why we chose to normalize the results by the surrogate metrics obtained from the degree preserving null-model (**Fig.7.8.g,h,i**).

7.2.8 Effect of sex, handedness, and age

As in the controllability section, we used n-way ANOVA and Spearman correlation coefficient. Although, since all Spearman correlations were negligible, we decided to test the effect of the age differently with an additional factor which we noted age-4. We regrouped the participants in 4 categories in function of the percentiles of the age distribution to have equal groups (-1/4-tile, median, 3/4-tile). This additional factor was added to the sex and handedness and we carried a 3-way ANOVA.

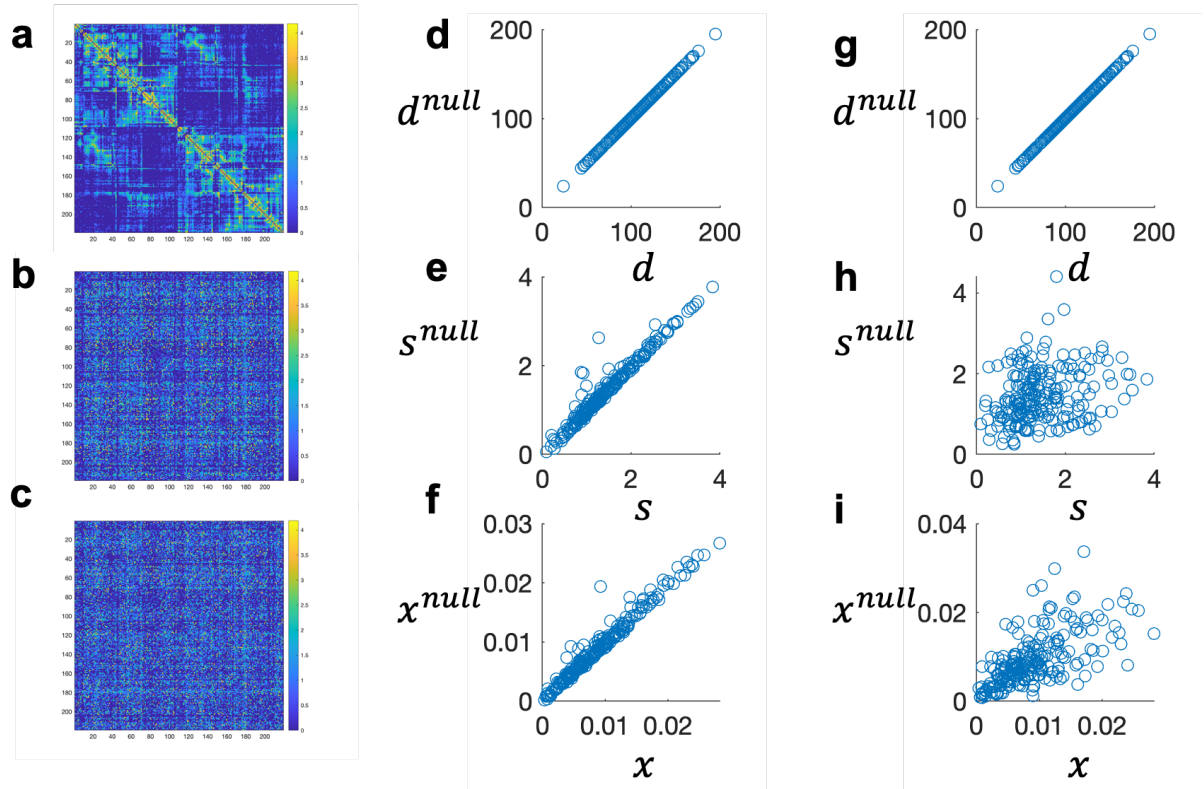

Figure 7.8: Effect of the null models on the strength and NBT: **a,** Adjacency matrix of a representative connectome at scale $n = 219$. **b, c** realizations of the null-models preserving strength and degree respectively. **d, e, f,** Scatter plots of the degree, strength, and NBT of the original network and the null-model preserving strength. **g, h, i,** same as **d, e, f,** with the null-model preserving degree.

7.3 Results

For all scales and all participants, we measured local measures, strength and NBT centralities using the entire network. Then we disconnected the two hemispheres and measured separately their global efficiency and modularity. Alongside we carried the same calculations for 100 realizations of the degree-preserving null-model. Finally, we normalized all metrics by their homologous average in the surrogate networks. Results were analyzed at the three levels introduced earlier going from the most general (or macro) to the most specific (or micro)

7.3.1 Structural brain asymmetry at the hemispheric level

Results showed that all metrics were slightly lateralized (lateralization index < 2%). Firstly, lateralization of the global measures were in line with literature: the right hemisphere was on average more efficient [127] whereas the left one had higher modularity [128] (**Fig.7.9.c,d,e**). We also observed that brain networks became less efficient than random networks when increasing network sampling resolution (**Table.7.1**). However, modularity of brain networks was consistently higher than random networks and monotonically increased when considering higher scales.

[127]: Iturria-Medina et al. (2011), 'Brain Hemispheric Structural Efficiency and Interconnectivity Rightward Asymmetry in Human and Nonhuman Primates'
[128]: Jajcay et al. (2022), 'Brain Functional Connectivity Asymmetry'

Secondly, strength and NBT presented a clear leftward asymmetry except for scale 3 (**Fig.7.9.a,b,e**). This exception is maybe due to the fact that it is the only scale for which the number of nodes was not equal in right and left hemispheres. This result is consistent with the literature since it was already demonstrated using diffusion tensor imaging that the left

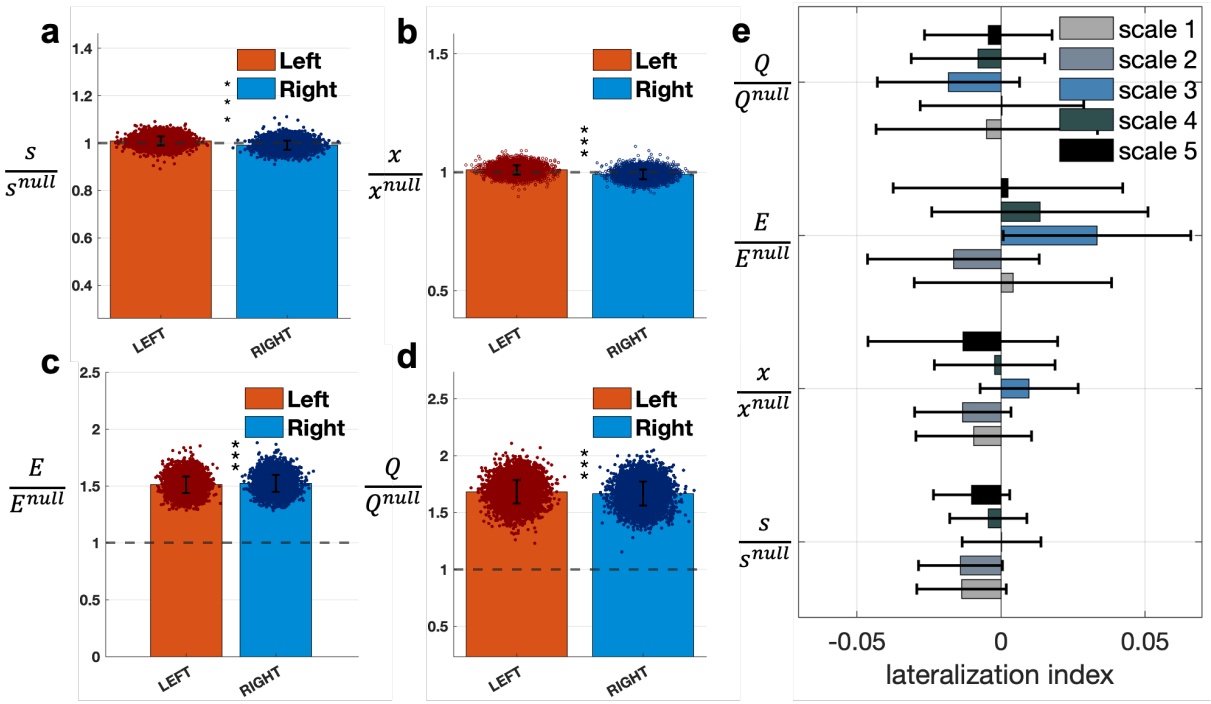

Figure 7.9: Structural brain asymmetries at the hemisphere level: **a, b** Strength and NBT centralities. Metrics are normalized using surrogate networks than aggreagated by summing over hemispheres. **e** Summary of lateralization indices for the 4 metrics in all the 5 scales.

hemisphere showed a higher density and connectivity of white matter tracts [129].

[129]: Schijven et al. (2023), 'Large-scale analysis of structural brain asymmetries in schizophrenia via the ENIGMA consortium'

Table 7.1: Group-level average of normalized efficiency and modularity for left and right brain hemispheres separated.

	Efficiency $\frac{E}{E^{null}}$		**Modularity** $\frac{Q}{Q^{null}}$	
	LEFT	**RIGHT**	**LEFT**	**RIGHT**
scale 1	1.5108	1.5234	1.6827	1.6662
scale 2	1.3700	1.3256	2.3867	2.3887
scale 3	1.1426	1.2216	2.9883	2.8812
scale 4	1.0277	1.0560	3.5434	3.4874
scale 5	0.8970	0.9015	4.2009	4.1648

Effect of gender

No significant association was observed for sex at the hemispheric level.

Effect of handedness

On the other hand, the 3-way ANOVA showed a significant effect of handedness on NBT for scale 5. Aggregated NBT had more pronounced leftward lateralization in right-handed participants. This effect could be due to the motor regions (to be discussed later).

Effect of age

For all metrics, the effect of age was negligible in both ways: ANOVA and Spearman ($|\rho_S| < 0.1$). Nevertheless, all negative correlation coefficients indicated that NBT centrality was lateralization was shifting leftward in older participants.

Table 7.2: Adjusted p-values of the 3-way ANOVA of NBT lateralization. They are complemented by the Spearman correlation coefficients between the NBT lateralization and age.

	3-way ANOVA: adj_p			**Spearman** ρ_S
	sex	**handedness**	**age-4**	**age**
scale 1	1.5574	3.2034	2.7418	-0.0264
scale 2	1.5574	0.9872	1.5574	-0.0551
scale 3	2.7418	1.5574	1.5574	-0.0811
scale 4	2.7418	0.0548	2.7418	-0.0754
scale 5	1.3663	0.0100	2.7418	-0.0459

7.3.2 Structural brain asymmetry at the fiber system level

Similarly to the previous section, we integrated here the normalized NBT centrality at the level of 6 fiber systems: Af-ant., Af-long., Af-post., SLF-I, SLF-II, and SLF-III.

Results showed that SLF pathways presented a rightward asymmetry in majority whereas AF segments were more dominant in the left hemisphere (**Fig.7.10.a**). However, results were not consistent across scales for AF-long and SLF-II.

Effect of gender, handedness, and age

An effect of sex was observed for the SLF-II. (**Table.7.10.b**). Males had fibers that accumulated more centrality in the right hemisphere than the females.

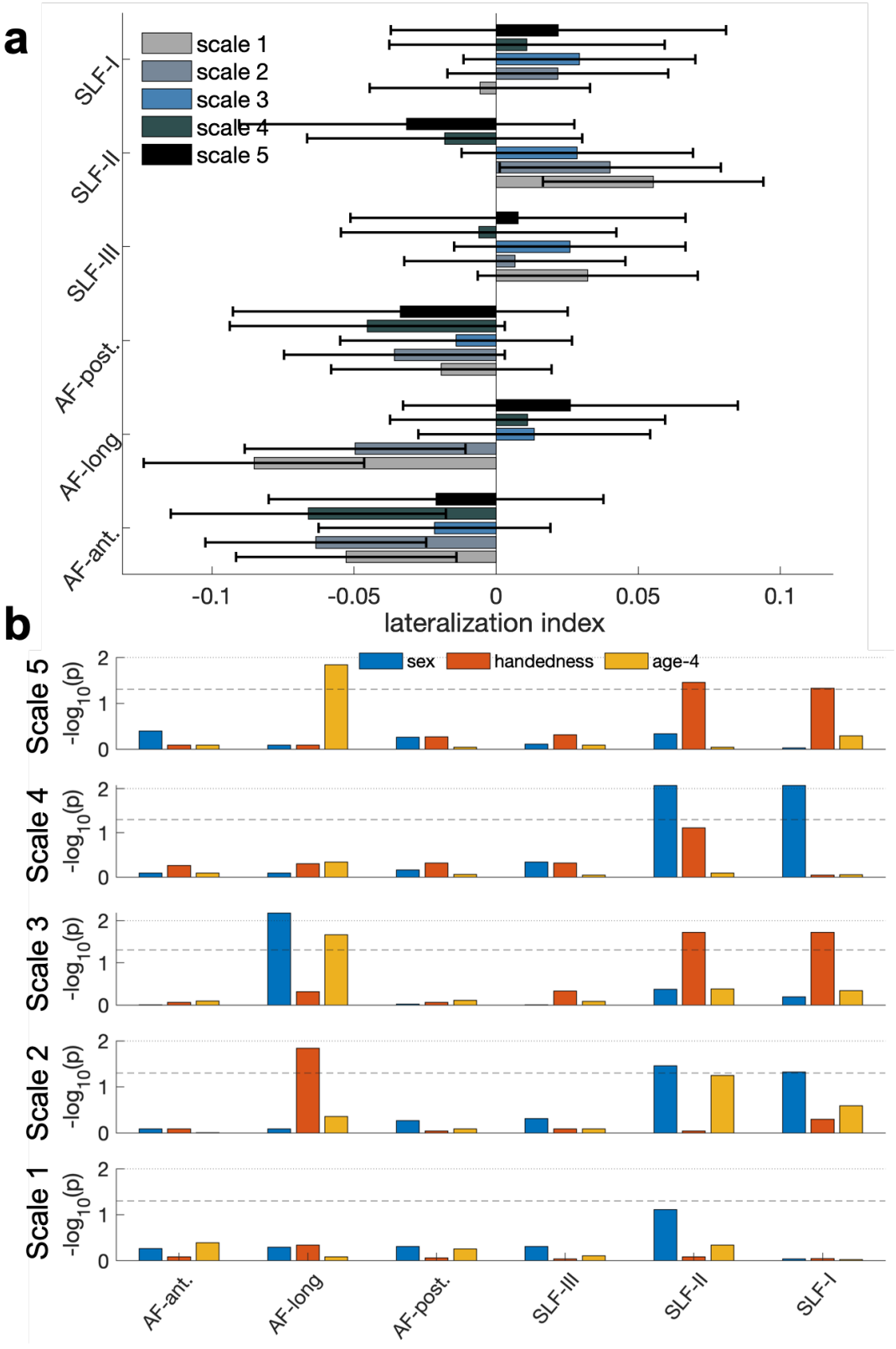

Figure 7.10: Structural brain asymmetries at the fiber systems level: **a,** Summary of lateralization indices for the NBT centrality for the 6 fiber systems in all the 5 scales.. **b,** Results of the 2-way ANOVA of NBT centrality lateralization grouped by sex and handedness for all 5 scales. P-values are adjusted using the false discovery rate procedure introduced in [90]. Horizental lines represent the significance levels 0.05 and 0.01.

3-way ANOVA analysis revealed associations between handedness and lateralization of centrality in SLF-I and SLF-II (**Fig.7.10.b**). lateralization of NBT centrality was higher for left-handed participants meaning that it was more lateralized to the right.

As previously, no significant effect was observed for the age using Spearman correlation (**Table.7.3**). And the results of the ANOVA regarding age were not consistent across scales.

Table 7.3: Spearman correlation coefficients between age and lateralization of aggregated normalized NBT centrality.

	Spearman ρ_S					
	AF-ant.	**AF-long**	**AF-post.**	**SLF-I**	**SLF-II**	**SLF-III**
scale 1	-0.0303	-0.0865	-0.0473	-0.0177	0.0180	0.0145
scale 2	-0.0132	-0.0112	-0.0148	-0.0086	0.0250	0.0250
scale 3	0.0191	-0.0384	0.0084	0.0011	0.0433	0.0296
scale 4	-0.0432	-0.0482	-0.0148	-0.0270	0.0372	0.0244
scale 5	-0.0387	-0.0925	-0.0304	-0.0118	0.0200	0.0234

7.3.3 Structural brain asymmetry at the node level

We now inspect lateralization properties of the NBT centrality at the smallest level of the study: the level of the brain parcels that correspond to the nodes of the 1st scale (Desikan-Killyani parcellation (**Table 2**)).

Overall, lateralization of most of brain parcels was stable and consistent across the different scales. We took into account the degree of lateralization and consistency across scales to order them (**Fig.7.11**).

Among the most left lateralized regions we can list: the bank of the Superior Temporal sulcus, the lateral orbitofrontal cortex, the entorhinal cortex, the cuneus, the pericalcarine, the supramarginal gyrus, and the superior temporal sulcus.

The most right-lateralized regions in terms of NBT centrality were: the frontal pole, the rostral middle frontal, the precuneus, the fusiform, the lingual, and the precentral gyri.

Effect of gender, handedness, and age

After adjusting for multiple testing none of the associations were significant except for the effect of sex on the lateralization of the superior temporal sulcus and the effect of handedness on the precentral gyrus. However, some associations were more significant than the rest.

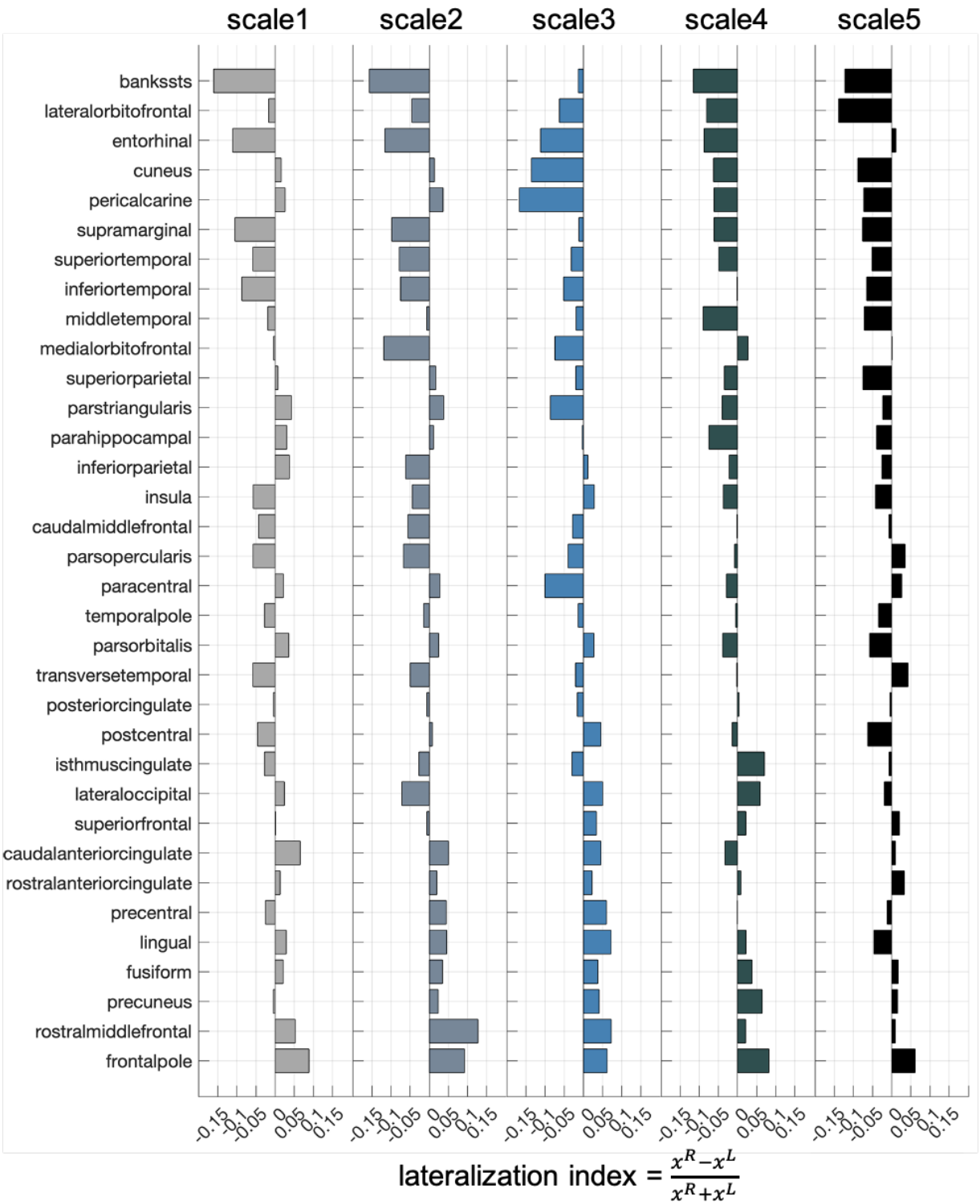

Figure 7.11: Structural brain asymmetries at the parcel level: Group-level average of lateralization indices. For scale 1 the calculation is trivial. for higher scales z^R and z^L represent the average value across the sub-parcels.

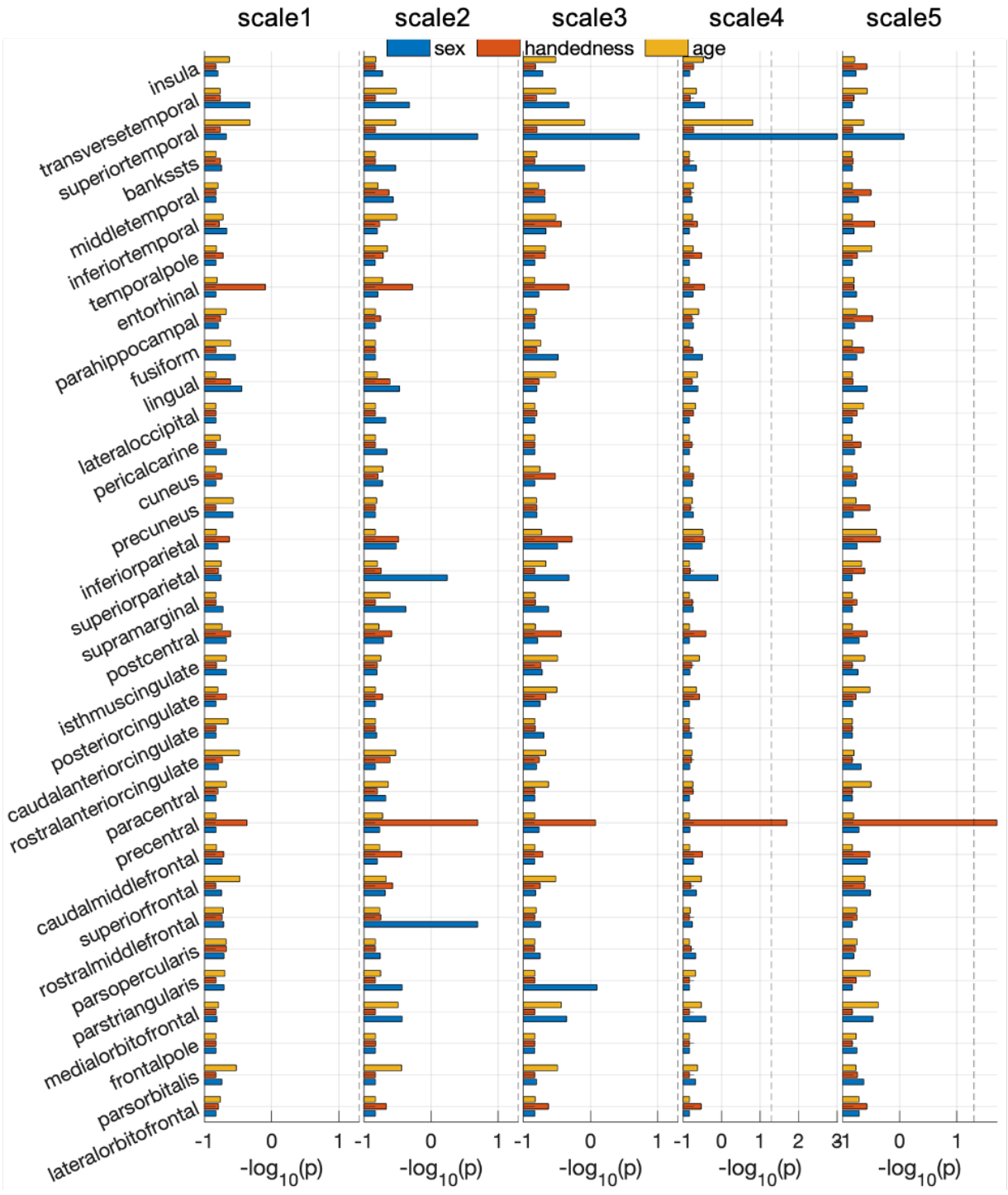

Figure 7.12: Effects of sex, handedness, and age on structural brain asymmetries at the parcel level with NBT centrality.

7.4 Discussion

Node centrality reflects its functional role?

We decided to use nonbacktracking (NBT) centrality as a proxy for Eigenvector centrality (EC) because this second failed in practice because of the localization effect. Moreover, these two metrics were preferred to the classic strength centrality because by construction EC and NBT take into account the neighboring of a node and encapsulate a dynamic component that is simply not grasped by the strength. However, as discussed later on, strength showed age-related changes that were not present when analyzing NBT.

Effect of network scale

We carried out a multi-resolution analysis of centrality in brain networks. Results were not always consistent across the scales sometimes showing opposite lateralization properties or different dependencies to the studied co-factors (sex, handedness, and age). We computed correlation coefficients of brain parcel centralities across the different scales (**Fig.7.13**). Correlation tests showed that close scales were more correlated between them. Results of scales 1 and 2 were similar and the same conclusion held for scales 4 and 5. Centrality obtained from scale 3 was less correlated with the rest. These considerations indicate that the resolution at which we sample the structural connectivity of brain networks has a significant effect on the results. For that reason, the analysis of connectivity at multiple scales should increase the robustness of our results since we retained the effects that were consistent in at least 3 scales over 5.

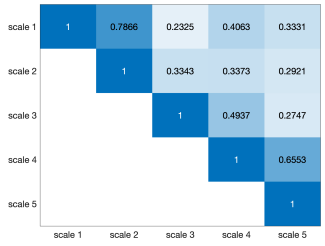

Figure 7.13: Effect of network scale: Pearson correlation coefficients of parcels centrality between scales.

Hemispheric differences in connectivity support cognitive specialization and lateralization

Overall, we observed higher lateralization indices at the individual parcel level than when considering the meso and macro levels of the fibers and hemispheres. This suggested that brain regions are differently specialized in the right and left hemispheres and support different functional processes. The same conclusion holds at the fiber systems level. When integrating the results at the whole brain level, the left hemisphere seemed more dominant, but this effect is mostly due to the fact that it is in general more densely connected which supports the idea that the left hemisphere is more engaged than the right in higher-order cognitive tasks like memory and language [129].

We also computed global measures: efficiency and modularity. The reason we did this was to have a sort of validity check since there exists literature on the subject. In Ref.[127], authors showed a higher efficiency for the right hemisphere in structural networks while Ref.[128] showed higher modularity of the left hemisphere but in functional networks. Our Results confirmed these findings in a large-scale dataset of structural connectomes.

ANOVA on 6k participants revealed effects of sex, handedness and age

Of course, each connectome is unique and has its own specificity and these are only group-level average tendencies. Notably, we observed that connectomes of right-handed participants were on average more biased to the left hemisphere. We confirmed later on by the inspection of

[129]: Schijven et al. (2023), 'Large-scale analysis of structural brain asymmetries in schizophrenia via the ENIGMA consortium'

[127]: Iturria-Medina et al. (2011), 'Brain Hemispheric Structural Efficiency and Interconnectivity Rightward Asymmetry in Human and Nonhuman Primates'

[128]: Jajcay et al. (2022), 'Brain Functional Connectivity Asymmetry'

lateralization of individual nodes that this effect was mostly due to the precentral gyrus.

At the mesoscopic level of the fiber systems, results also revealed an effect of sex. SLF-I, and SLF-II also showed a dependency on handedness which is certainly due to the fact that they both were connected to the precentral gyrus. But they also were dependent on sex, especially the SLF-II. This effect was probably due to the fact that the SLF-II included the superior temporal sulcus which was more biased to the left for males as highlighted by the node level analysis.

There was no significant effect for the age. However, by inspecting the same lateralization properties of the strength centrality we observed significant differences that were due to age (see **Appendix, Fig.1**). The superior temporal sulcus and the rostral anterior cingulate cortex were the most affected by age. The fact that strength centrality was more sensitive to age than NBT is not surprising. Indeed, as stated before, each centrality highlights different aspects of the connectome. Strength is more sensitive to local changes at the parcel level because NBT is defined by the neighboring of each node. Moreover, a previous study already came to the conclusion that strength was more affected by age than eigenvector centrality (here NBT) [124].

[124]: Zuo et al. (2012), 'Network centrality in the human functional connectome'

Nevertheless, the findings obtained from the lateralization of strength at the nodal level were in line with the literature. Pardo et.al [130] shows the most age-related metabolic dysfunctions and correlated with cognitive decline. Regarding the superior temporal sulcus (STS), two studies, one for deaf participants, and the other for participants attained from autism, showed age-related changes in the intrinsic function of this specific brain region. To our knowledge, no prior study showed the age-related changes in connectivity affecting the STS in healthy participants. Specifically, older participants had a bias toward the left hemisphere potentially indicating a stronger decline of the right STS. A previous study did report though, a significant left bias of cortical thickness and surface of the STS with increasing age in a large-scale meta-analysis including 17,141 healthy participants [131].

[130]: Pardo et al. (2020), 'Aging-Related Hypometabolism in the Anterior Cingulate Cortex of Cognitively Intact, Amyloid-Negative Seniors at Rest Mediates the Relationship between Age and Executive Function but Not Memory'

[131]: Kong et al. (2018), 'Mapping cortical brain asymmetry in 17,141 healthy individuals worldwide via the ENIGMA Consortium'

Comparison of structural connectivity with morphological features: cortical thickness and surface

We computed a lateralization index of strength and NBT centrality for each brain parcel of the Desikan-Killyani atlas. To our knowledge, most previous studies on connectivity lateralization studied functional networks or were focused on specific brain regions. Two studies performed a voxel-wise study of structural cortical asymmetries using morphological features: volume, thickness, and surface of brain parcels. One included 101 healthy participants [132] (**Fig.7.14.a,b,c**) while the other performed a meta-analysis on several datasets including 17,141 healthy participants [131] (**Fig.7.14.d,e**). The question of how cortical thickness and surface of gray matter relate to white fiber connectivity is an open question in neuroscience. When confronting our results with the conclusions of these studies, there seemed to be no link between strength/NBT and cortical thickness. However, striking similarities were observed with the cortical surface (**Fig.1**, **Fig.7.11**, **Fig.7.14.e**). Notably, the 8 most left lateralized regions for strength/NBT were also biased to the left for cortical surface. In the same way, the 9 most right-lateralized regions for strength/NBT,

[132]: Koelkebeck et al. (2014), 'The contribution of cortical thickness and surface area to gray matter asymmetries in the healthy human brain'

except the fusiform, were also biased to the right hemisphere for the cortical surface.

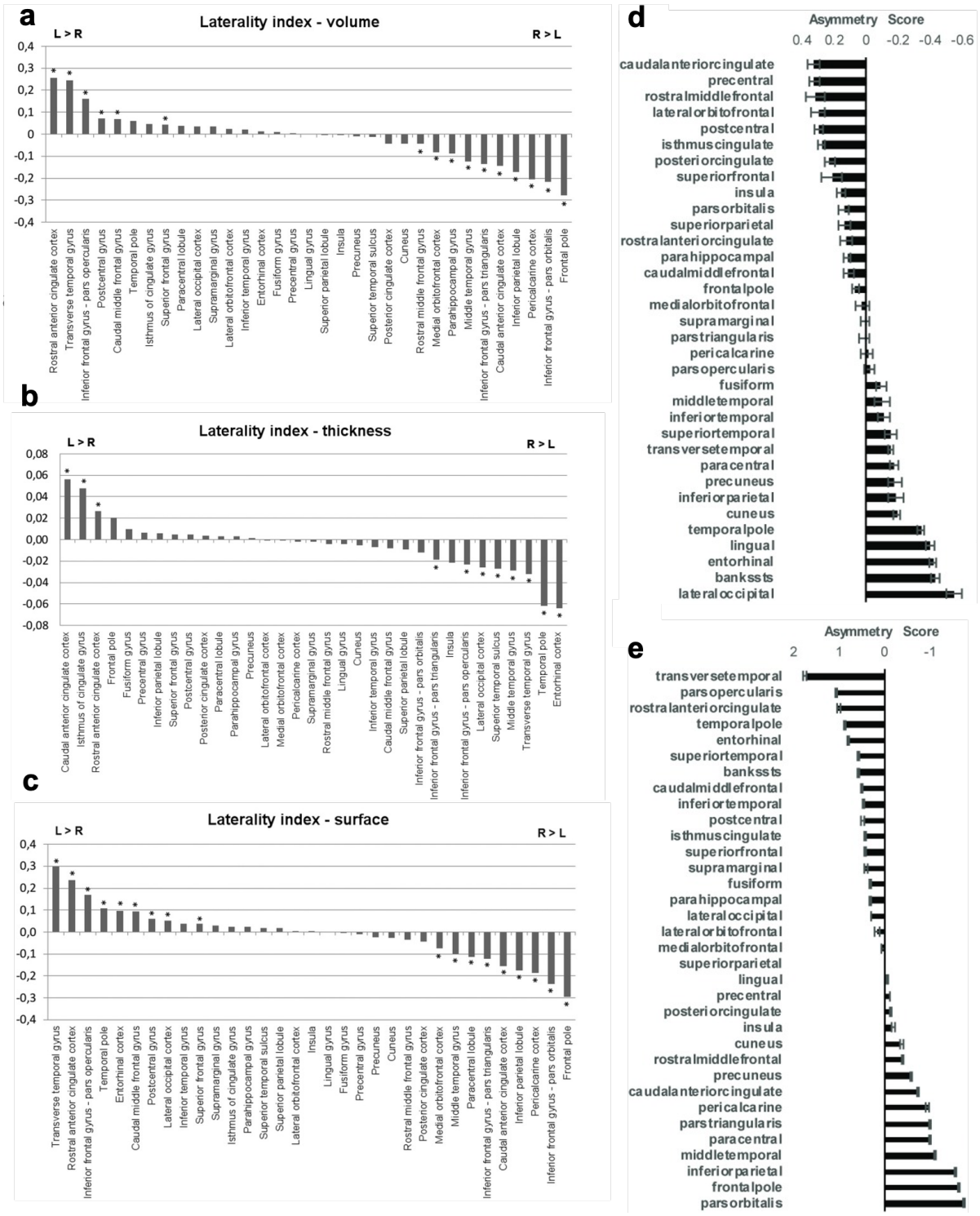

Figure 7.14: a,b,c) are reproduced from [132] with permission of the rights holder, John Wiley and Sons. d,e) are reproduced from [131] with permission from right holders, National Academy of Science. **Asymmetries of cortical volume, thickness, and surface**: Group-level average of lateralization indices for different morphological metrics.

7.5 Conclusion

We were interested to know in this section whether there was one brain hemisphere that was dominating the other from a structural perspective. We answered the question by analyzing an alternative to eigenvector centrality: Nonbacktracking centrality. We calculated it for more than 6k participants alongside strength centrality and efficiency and modularity of both hemispheres.

By integrating the results at the hemispheric level, it seemed that there was leftward bias of centrality that reflected the fact that the left hemisphere simply has a denser white matter architecture. The left hemisphere was also more modular while the right hemisphere had a higher efficiency. These findings are in line with current knowledge of the brain: the right hemisphere is the gate that perceives the outside world and is in charge of spatial attention while the left hemisphere is more engaged during introspection and supports higher-order tasks like language and imagination.

We integrated the results at the level of six fiber systems: the three pathways of the Superior Longitudinal Fasciculus (SLF) and the three pathways of the Arcuate Fasciculus (AF). Results showed that the SLF branches accumulated more centrality in the right hemisphere while AF did more in the left one. These findings were in line with the role of SLF in spatial attention processing which is known to be dominant in the right hemisphere. In the same way, AF tracts are known to support language and speech processing that is biased to the left hemisphere.

These lateralization properties emerged from the fact that individual homotopic brain parcels were asymmetrically connected, and thus had different centralities, in the left and right hemispheres since they serve different functions. We unraveled the effect of handedness on the centrality of the precentral gyrus that was more leftward biased for right-handed participants. We could see this effect at both the fiber and the hemisphere level. In addition, we showed that Superior Temporal Sulscus (STS) was one of the brain regions that changed the most according to sex and age. It was more lateralized to the left hemisphere for males than females. The analysis of strength lateralization showed a decline in connectivity of the right STS.

All in all, we confirmed that the left hemisphere is more interconnected, that the functional specialization of each hemisphere was reflected at the fiber system, and that this resulted from asymmetrical connectivity properties of homotopic regions.

8 Conclusions, limitations, and future directions

This piece of work summarizes the main deepened directions and results obtained during this PhD project. We take advantage here to describe the hidden part of the iceberg and explain the steps and reasonings that led us to this final work.

Outline of the motivations and directions

The research started with an intensive review of the literature of course, but also, since I come from engineering, by getting familiar with all known ways to select driver nodes in networks and trying out the available codes. We commuted graph maximum matchings, extracted spanning cacti, tried Kalman and PBH criteria, and calculated controllability Gramians. Overall, from this phase, we retained that maximum matchings and spanning cacti only work with directed and sparse networks and that Kalman, PBH, and Gramian-based metrics were obsolete even for medium-sized networks (n>20).

An important guiding motivation was that we were not only interested in selecting driver nodes in a network but actually controlling it, to steer it to a desired final state. This led us to exploit existing code from Jennifer Stiso, who recently obtained her Ph.D. in brain network dynamics and control under the supervision of Danielle Basset. The code was used to derive the optimal input that would steer the states of selected target nodes to a desired state. In other terms, it was the solution to the target control problem. We used that code in simple simulations with small toy models and chain networks and came to the conclusion that in general, one driver node could only control five target nodes with reasonable precision which was in line with previous literature. Another guiding motivation we had was that our goal was to deepen the framework of single-driver network controllability and control. For that reason, we decided to adopt the output control approach and got inspired by the work of Casadei et.al (2020) in which they aggregated the targeted network by clusters and controlled their average state. Stiso's code was obsolete at this point since it only controlled the states of target nodes. We built our own solution for the output control problem and made the code available.

Output control of the network eigenmaps: a hybrid solution

At that moment we were able to control any output of the considered networks but which one to choose. Casadei et.al (2020) decided to reduce the network to supernodes representing the average of the clusters which seemed intuitive and easily interpretable. We decided instead, to take advantage of the network Laplacian. Its eigenvectors, called eigenmaps, are a classical tool in network science that constitute a topologically informed basis to embed states or signals defined on the network. This way, our framework of network control had two building blocks: the first was the output control from control theory and the second was Laplacian eigenmaps from network science. We evaluated the control precision using our framework and came to the same conclusion that one single driver could only control five components, which were projections of the network state into five selected eigenmaps. We evaluated the representativeness of this reduction technique and compared it to supernodes representing the average states of predefined clusters in synthetic networks. Our method was better when used with few drivers and/or with very dispersed desired states. Furthermore, we used this rule of thumb of: "one driver for five controlled components" to build a metric for characterizing the controllability of targeted network eigenmaps by single drivers. Our metric proved more reliable than classical ones and could not only spot the best drivers but also provide a full ranking of the drivers' controllability. To summarize, if one asks if it is better to use the supernodes average approach or the Laplacian eigenmaps one, the answer would depend on the usage case. If the final state has a high dispersion, then it would be better captured by the eigenmaps. In states with low dispersion, eigenmaps were still more representative when only one driver was used. This advantage is merely due to the flexibility in the choice of the eigenmaps that best represent the final state. We also showed that choosing the supernodes to best fit the final state was the best solution in terms of representativeness. In general, when considering controllability metrics there is no specific final state to be fitted. We saw that in that case, the eigenmaps are equivalent to the supernodes in representativeness. However, one still has to define the

supernodes which means partitioning the network into five clusters. It is possible and, in that case, the two methods would be equivalent. Still partitioning algorithms could fail in practice if no clear structure exists. And a large part of the clustering techniques is already using the Laplacian. We showed with this piece of work that we can skip that part and directly use the eigenmaps as a projection basis for the output controllability Gramian.

Low-dimensional controllability of structural brain networks

Another strength of the project was the application of the method in a large dataset of healthy participants (N>6k) that would cancel out noise in the imaging data, or individual extreme variations. The choice of the Schaefer200 parcellation constituted another strength of the application since its regions were mapped to functionally relevant large-scale networks. We confirmed previous criticism of average controllability stating that it is too much dependent on node strength (r>0.8). We also confirmed that worst-case controllability was very small and negative for more than half of the nodes. Low-dimensional controllability was positive, scaled between 10-15 and 10-5, and was as correlated to strength as worst-case controllability. The analysis of the controllability of the 9 functional networks was in line with the literature in terms of lateralization properties and offered new insights into the least known networks. When aggregated at the group level, our results overlapped with traditional stimulation sites that are experimentally consensual.

One point that could be ameliorated here is concerning the analysis of lateralization properties of the considered functional networks in terms of controllability. The main hypothesis was that if a network is experimentally and functionally dominant in one brain hemisphere, is it reasonable to suppose that it should be more easily controllable from that same hemisphere? This is debatable. One argument in favor is the propensity of the brain to minimize the neural communication costs which would happen through the most controllable (lowest energy consumption). An argument against our hypothesis is that if previous studies observed increased BOLD signals or "activity" in the dominant hemisphere, then that would mean higher energy consumption and, thus lower controllability. Another point, that is debatable is the effect of the intrinsic asymmetry of the functional networks. As we explained, they were, for some, not composed of the same number of nodes in the right and left hemispheres which is why we considered the mean values to calculate the lateralization indices. Still, we could not quantify the effect of size asymmetry and disentangle it from the lateralization of controllability.

Integration of controllability at the subsystem level: comparing the incomparable

Mapping the mutual controllability of heterogeneous networks is tricky because of the dominating effects of the number of drivers and the size of the targets. Our framework enabled us to align the different functional brain networks because they were projected into similar output spaces of same dimension and quantify their controllability independently of their size. These implications were not part of the initial motivations for our work per se but more like a pleasant consequence that was realized a posteriori. We derived, for each subject, a directed meta-graph in which nodes were the functional systems and links represented the controllability of one system by another. Results showed that the systems differently acted as targets or drivers which was in line with their cognitive roles.

This part of our work constituted a novelty in the field. We validated the results by comparing them to the conclusions of a previous study that employed a different dynamical model: network communication. We observed a strikingly high similarity between the results. Systems classified as senders in the previous study tended to be drivers according to our results and the same was observed for receiver and target systems.

Limitations and future directions regarding the work on network controllability

The study of Laplacian eigenmaps proved as efficient as the supernode average approach to embed network states. However, the comparison of both could be deepened. Future work could focus on the analysis of interplays between topology, state, and reduction approaches. For example, we could try other ways of selecting the eigenmaps. Study different networks that span a continuum of topological features like starting from a small-world network and rewire it with increasing probability while analyzing its controllability properties with different approaches. Moreover, Casadei et.al (2020) used the supernodes to derive reduced models of the network dynamics and avoid computing large Gramians. Could Laplacian eigenmaps be used in such a way for model reduction?

Regarding the application to brain networks, this study focused on healthy participants. Now that the method proved relevant and insightful, the next step would be to apply it to non-healthy subjects. Potentially, the controllability meta-graphs of subjects attained by neurological diseases could contain alterations that are not visible from simple inspection of raw images or raw structural and functional networks.

Regarding the selection of individualized stimulation sites for transcranial magnetic stimulation (TMS), the applicability of the network control theory (NCT) is questionable and needs to be addressed with experiments. In addition, TMS can be used to activate or inhibit activity in a region. How does that translate in NCT? It is an open question. On that matter, structural connectivity networks used here and in most studies are built with fiber counts, fiber length, or width, all of which result in positive networks. However, it is accepted that neural communication includes both excitatory and inhibitory pathways. Future efforts could be made to rethink the ways brain network dynamics are modeled.

Moreover, we could not find a definite explanation for sex-related differences in controllability. When aggregating results at the system level, we observed that the connectomes of males were systematically more controllable. We inspected global sex differences at the global level in terms of the density of white matter fibers. Females had significantly more interhemispheric tracts than males. Could it be the reason that explains the difference in controllability or is it rather due to other topological differences? Finding the topological substrate for sex-related differences in controllability is an open question for future work.

Hemispheric asymmetries in brain connectivity and competition for centrality

This part aimed at applying the hemispheric competition framework which was successfully applied to functional EEG-based networks. It was conducted as a side project which took approximately 10% to 50% percent of my time depending on the period of the PhD. It was the first opportunity to collaborate with Brigitte and Paolo. In the beginning, the main question was whether the right or left hemisphere dominated in terms of centrality. The project was extended later to the study of fiber systems and parcel lateralization. We encountered some methodological challenges in the route.

This side project was way more rooted in network science frameworks. The solutions we decided to implement like normalizing the results using surrogate data obtained from network null-models is a classical technique in network science. The localization effect was another difficulty that we faced and was not awaited because structural brain networks are way sparser than functional networks. Our solution was to employ the Nonbacktracking centrality. As explained by the authors of ref. [125] other techniques exist to avoid this effect like adding a regularizing “teleportation” term as for PageRank centrality but we decided to stick with NBT because of its parameter-free aspect.

Regarding results, our conclusion highlighted a tendency of the left hemisphere to accumulate more centrality than the right one. The Superior Longitudinal Fasciculus was biased to the right hemisphere and the Arcuate Fasciculus was biased to the left. This conclusion was in line with their major cognitive roles in spatial attention and language processing. We finally showed that these effects were due to the asymmetric connectivity patterns of individual brain parcels. This asymmetry supports the fact that homotopic brain regions support different cognitive functions in the right and left hemispheres. The large number of participants (N>6k) enabled us to uncover the effects of gender and handedness in some specific regions like the precentral gyrus which was more leftward lateralized in right-handed participants and the superior temporal sulcus which was more leftward biased in males. Age did not have a significant effect on NBT centrality but further analysis showed its effect on strength centrality. Results notably spotted a potential age-related decline in the right superior temporal sulcus. Finally, from a comparison to previous studies on the lateralization of morphological parcel attributes, we concluded that the connectivity of a brain region was more related to its cortical surface rather than its thickness.

Limitations and future directions regarding the work on network centrality and hemispheric asymmetry

This first debatable point concerns the usage of the nonbacktracking centrality as a proxy for eigenvector centrality. Even though in theory NBT behaves as EC should without the effect of localization, we did not check this in practice. This is an open question for future efforts. Secondly, we did not calculate the total modularity and total efficiency of the networks, this would have been an opportunity to find more possible

explanations for the observed sex-related differences. In general, the last part of the dissertation seems unrelated to the first part. Which is normal since they are two distinct projects. But there could have been more interplay between both to have one unique guiding line through the whole dissertation.

Regarding the dataset, it was mostly composed of adults over 40 years old and that could have an effect on the results which was not discussed here.

One definite amelioration would be to use the newly designed multiscale schaefer parcellation with homotopic regions. It is composed of 10 different scales going from 100 nodes to 1000 nodes. This would double the robustness of the multiscale approach and the results.

Appendix

.1 Optimal control: input signal derivation

In the results section 4.3, we validated our framework for synthetic networks by simulating trajectories. We first, need to find the control input $u(t)$. To do so we solve the following optimization problem:

$$\begin{aligned} \min_{u} \quad & J_\rho = (y_f - y(t_f))^T.(y_f - y(t_f)) + \rho \int_0^{t_f} u(t).u(t)^T \mathrm{dt} \\ \text{s.t.} \quad & x(0) = x_0 \; ; \; \dot{x}(t) = Ax(t) + Bu(t) \; ; \; y(t) = Cx(t) \end{aligned} \tag{.1}$$

Overall, it is a minimization problem with soft constraints on the output. The term $\rho \int_0^{t_f} u(t).u(t)^T \mathrm{dt}$, called the scalar running cost function, minimizes the energy and the term:
$E(x(t_f)) = (y_f - y(t_f))^T.(y_f - y(t_f)) = (y_f - Cx(t_f))^T.(y_f - Cx(t_f))$,
called the scalar terminal cost function, is where we express the final constraint on the output.

The problem can be solved using Pontriyargin's maximum principle (see sections 5.1 and 5.2 of Ref.[133]) by introducing the Hamiltonian equation:

[133]: Kirk (2012), *Optimal Control Theory*

$$\mathscr{H}(x(t), v(t), u(t)) = \rho u(t)^T u(t) + v(t)^T (Ax(t) + Bu(t)), \tag{.2}$$

where $v(t)$ represents the vector of the adjoint states.
We know from the fundamentals of optimal control theory[134] that the optimal trajectory (x^*, v^*, u^*) is the solution to the following equations:

[134]: Anderson et al. (1990), *Optimal Control*

Adjoint equation:

$$\frac{\partial \mathscr{H}}{\partial x} = \dot{v}(t) = -A^T v(t) \tag{.3}$$

Stationary equation:

$$0 = \frac{\partial \mathscr{H}}{\partial u} = 2\rho u(t) + B^T v(t) \tag{.4}$$

Boundary condition:

$$v(t_f) = \frac{\partial E(x(t_f))}{\partial x(t_f)} = -2C^T (y_f - Cx(t_f)) \tag{.5}$$

The adjoint and stationary equations, .3 and .4, can be rewritten in condensed form:

$$\begin{bmatrix} \dot{x^*} \\ \dot{v^*} \end{bmatrix} = \begin{bmatrix} A & \frac{-BB^T}{2\rho} \\ 0 & -A^T \end{bmatrix} \begin{bmatrix} x^* \\ v^* \end{bmatrix} = H \begin{bmatrix} x^* \\ v^* \end{bmatrix} \tag{.6}$$

where H is the Hamiltonian matrix. Equation .6 can be solved as:

$$\begin{bmatrix} x^*(t) \\ v^*(t) \end{bmatrix} = e^{\mathrm{tH}} \begin{bmatrix} x^*(0) \\ v^*(0) \end{bmatrix} \tag{.7}$$

This way we have an expression for $v^*(t)$, and the problem is almost solved since $u^*(t) = -B^T v(t)/2\rho$. We still are left with the unknown $v^*(0)$, which can be found using the boundary conditions .5.
If we note $e^{\mathrm{tH}} = \begin{bmatrix} M_{11} & M_{12} \\ M_{21} & M_{22} \end{bmatrix}$, we have the three following boundary

constraints:

$$\begin{aligned} x^*(t_f) &= M_{11}x_0 + M_{12}v^*(0) \\ v^*(t_f) &= M_{21}x_0 + M_{22}v^*(0) \\ v^*(t_f) &= -2C^T(y_f - Cx^*(t_f)) \end{aligned} \tag{.8}$$

The first two equations come from Eq..7 and the third is the Hamiltonian boundary condition. We have three unknowns $v^*(0)$, $x^*(t_f)$, $v^*(t_f)$, and three equations. The calculus comes down to:

$$v^*(0) = (M_{22} - 2C^TCM_{12})^\dagger \left[(2C^TCM_{11} - M_{21})x_0 - 2C^Ty_f\right], \tag{.9}$$

where † denotes the pseudo-inverse of a matrix.

.1.1 Laplacian of directed networks

In general, the combinatorial Laplacian, $L = D - G$, of a directed network is asymmetrical and also depends on whether we consider the ingoing or outgoing degree. Therefore, its eigenvectors will not be real and would not be usable in our framework. This is why we used an alternative definition based on the Random walk operator4:

$$L = I - \frac{\Phi^{1/2}.P.\Phi^{-1/2} + \Phi^{-1/2}.P^T.\Phi^{1/2}}{2} \tag{.10}$$

where P is the transition probability matrix and Φ is the Perron vector of the network. We direct the reader to Ref.[135] for more details. An implementation is available in the GSPBOX: a MATLAB toolbox for graph signal processing [136]. This way the Laplacian is symmetric, its eigenvectors are real and we can use them in our framework. However, this definition is only valid for strongly connected and aperiodic networks. Thus, for directed networks that do not satisfy these conditions, one can simply compute the Laplacian of the symmetrized network as:

$$L = 1/2(D^+ + D^- - G - G^T) \tag{.11}$$

where, D^+ and D^- are respectively the outdegree and indegree. Even with some loss of information, this trivial approach will still recover the mesoscopic structural properties of the targeted networks, like the presence of clusters for instance. The next supplementary section shows how it can be used with our framework in a small toy model directed network.

[135]: Chung (2005), 'Laplacians and the Cheeger Inequality for Directed Graphs'

[136]: Perraudin et al. (2016), *GSPBOX*

.2 Lateralization of strength had a higher dependency to age than NBT centrality

Effect of sex
The pars triangularis, the posterior cingulate, the fusiform, the superior parietal, and the superior temporal cortici were differently lateralized in males and females with a rightward bias for males.

Effect of handedness
The lateral orbitofrontal and the precentral were more left-lateralized for right-handed participants.

Effect of age

The superior temporal sulcus and the rostral anterior cingulate cortex were the most correlated with age. Leftward lateralization was more pronounced in older participants.

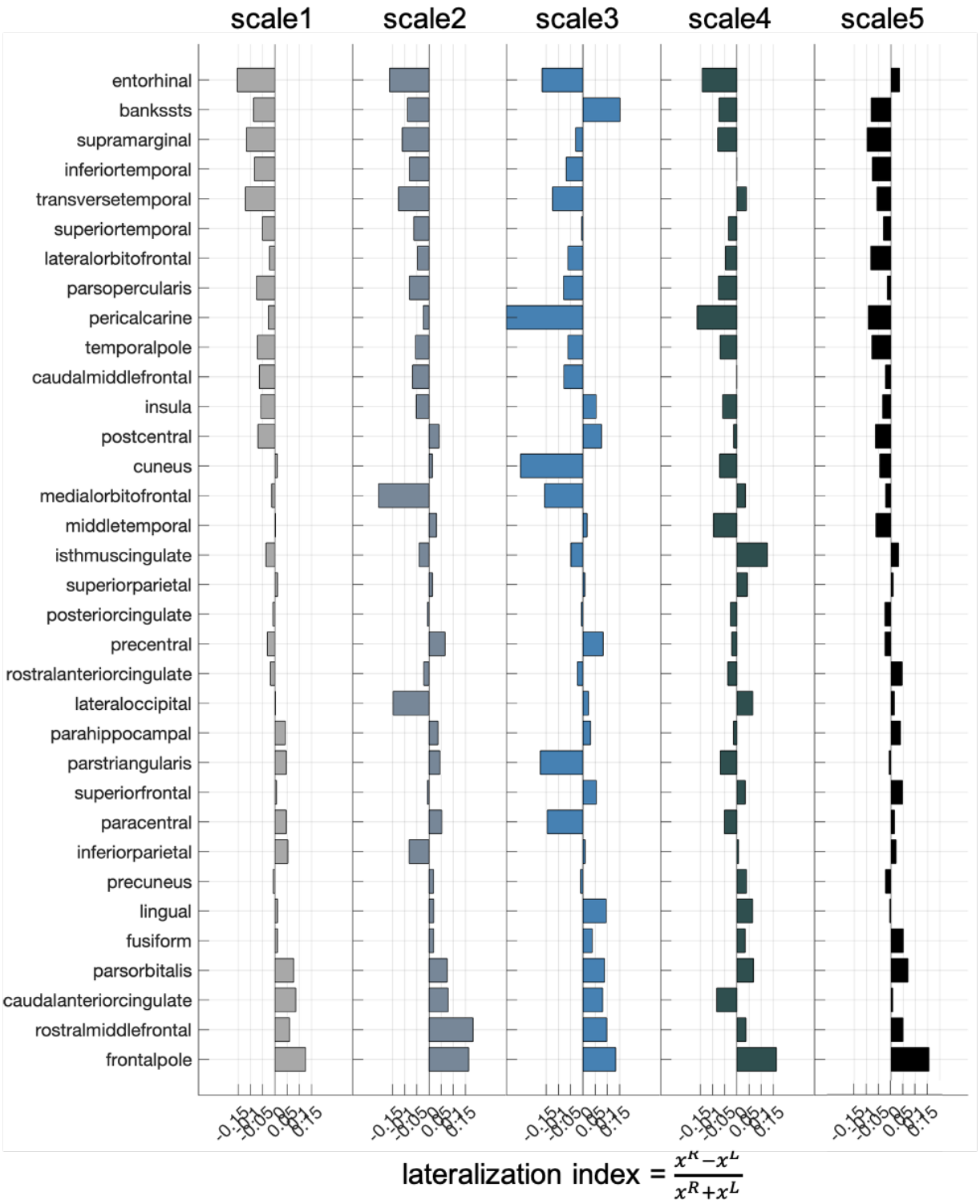

Figure 1: Structural brain asymmetries at the parcel level for the strength centrality: For scale 1 the calculation is trivial. for higher scales z^R and z^L represent the average value across the sub-parcels.

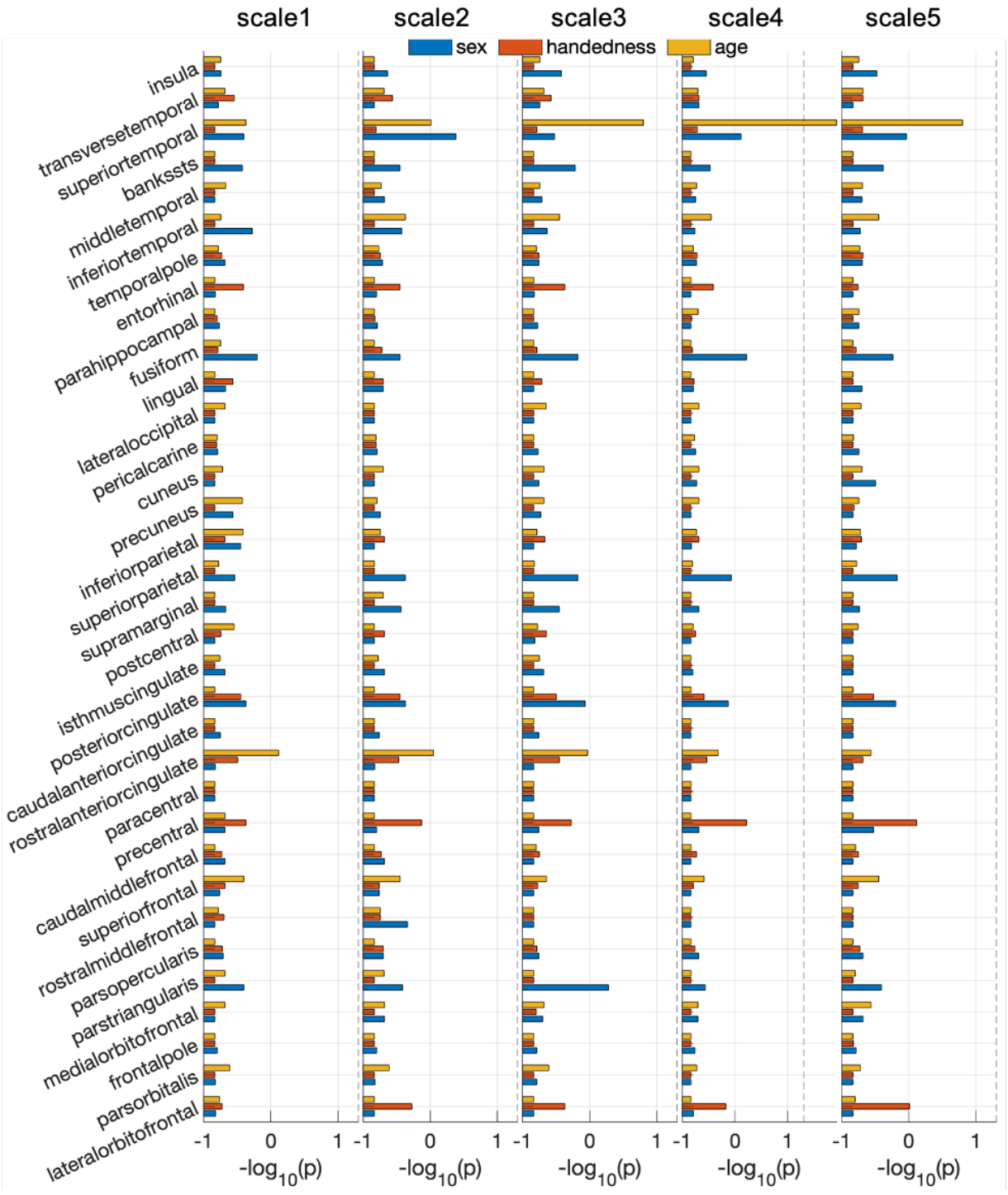

Figure 2: Effects of sex, handedness, and age on structural brain asymmetries at the parcel level with strength centrality.

.3 Schaefer parcellation details

Table 1: Labels of the schaefer200 parcellation. The first part of the label indicates the functional network the region belongs to.

ROI_label: left	ROI_label: right	Abbreviation	Full parcel Name
VisCent_ExStr_1	VisCent_ExStr_1	AntTemp	anterior temporal
VisCent_ExStr_2	VisCent_ExStr_2	Aud	auditory
VisCent_Striate_1	VisCent_Striate_1	Cent	central
VisCent_ExStr_3	VisCent_ExStr_3	Cinga	cingulate anterior
VisCent_ExStr_4	VisCent_ExStr_4	Cingm	mid-cingulate
VisCent_ExStr_5	VisCent_ExStr_5	Cingp	cingulate posterior
VisPeri_ExStrInf_1	VisPeri_ExStrInf_1	ExStr	extrastriate cortex
VisPeri_ExStrInf_2	VisPeri_ExStrInf_2	ExStrInf	extra-striate inferior
VisPeri_ExStrInf_3	VisPeri_StriCal_1	ExStrSup	extra-striate superior
VisPeri_StriCal_1	VisPeri_ExStrSup_1	FEF	frontal eye fields
VisPeri_ExStrSup_1	VisPeri_ExStrSup_2	FPole	frontal pole
VisPeri_ExStrSup_2	VisPeri_ExStrSup_3	FrMed	frontal medial
SomMotA_1	SomMotA_1	FrOper	frontal operculum
SomMotA_2	SomMotA_2	IFG	inferior frontal gyrus
SomMotA_3	SomMotA_3	Ins	insula
SomMotA_4	SomMotA_4	IPL	inferior parietal lobule
SomMotA_5	SomMotA_5	IPS	intraparietal sulcus
SomMotA_6	SomMotA_6	OFC	orbital frontal cortex
SomMotA_7	SomMotA_7	ParMed	parietal medial
SomMotA_8	SomMotA_8	ParOcc	parietal occipital
SomMotB_Aud_1	SomMotA_9	ParOper	parietal operculum
SomMotB_Aud_2	SomMotA_10	pCun	precuneus
SomMotB_S2_1	SomMotA_11	pCunPCC	precuneus posterior cingulate cortex
SomMotB_S2_2	SomMotB_Aud_1	PFCd	dorsal prefrontal cortex
SomMotB_Aud_3	SomMotB_Aud_2	PFCl	lateral prefrontal cortex
SomMotB_S2_3	SomMotB_S2_1	PFCld	lateral dorsal prefrontal cortex
SomMotB_Cent_1	SomMotB_S2_2	PFClv	lateral ventral prefrontal cortex
SomMotB_Cent_2	SomMotB_S2_3	PFCm	medial prefrontal cortex
DorsAttnA_TempOcc_1	SomMotB_S2_4	PFCmp	medial posterior prefrontal cortex
DorsAttnA_TempOcc_2	SomMotB_Cent_1	PFCv	ventral prefrontal cortex
DorsAttnA_ParOcc_1	DorsAttnA_TempOcc_1	PHC	parahippocampal cortex
DorsAttnA_SPL_1	DorsAttnA_ParOcc_1	PostC	post central
DorsAttnA_SPL_2	DorsAttnA_SPL_1	PrC	precentral
DorsAttnA_SPL_3	DorsAttnA_SPL_2	PrCd	precentral dorsal
DorsAttnB_PostC_1	DorsAttnA_SPL_3	PrCv	precentral ventral
DorsAttnB_PostC_2	DorsAttnA_SPL_4	RSC	retrosplenial cortex
DorsAttnB_PostC_3	DorsAttnB_PostC_1	Rsp	retrosplenial
DorsAttnB_PostC_4	DorsAttnB_PostC_2	S2	S2
DorsAttnB_FEF_1	DorsAttnB_PostC_3	SPL	superior parietal lobule
SalVentAttnA_ParOper_1	DorsAttnB_PostC_4	ST	superior temporal
SalVentAttnA_Ins_1	DorsAttnB_FEF_1	Striate	striate cortex
SalVentAttnA_FrOper_1	SalVentAttnA_ParOper_1	StriCal	striate calcarine
SalVentAttnA_FrOper_2	SalVentAttnA_PrC_1	Temp	temporal
SalVentAttnA_ParMed_1	SalVentAttnA_Ins_1	TempOcc	temporal occipital
SalVentAttnA_FrMed_1	SalVentAttnA_Ins_2	TempPar	temporal parietal
SalVentAttnA_FrMed_2	SalVentAttnA_FrOper_1	TempPole	temporal pole
SalVentAttnB_IPL_1	SalVentAttnA_FrMed_1		
SalVentAttnB_PFCl_1	SalVentAttnA_ParMed_1		
SalVentAttnB_Ins_1	SalVentAttnA_ParMed_2		
SalVentAttnB_PFCmp_1	SalVentAttnA_FrMed_2		
LimbicB_OFC_1	SalVentAttnB_IPL_1		
LimbicB_OFC_2	SalVentAttnB_PFClv_1		
LimbicA_TempPole_1	SalVentAttnB_PFCl_1		

Table 1 continued from previous page

ROI_label: left	ROI_label: right	Abbreviation	Full parcel Name
LimbicA_TempPole_2	SalVentAttnB_Ins_1		
LimbicA_TempPole_3	SalVentAttnB_Ins_2		
LimbicA_TempPole_4	SalVentAttnB_PFCmp_1		
ContA_Temp_1	LimbicB_OFC_1		
ContA_IPS_1	LimbicB_OFC_2		
ContA_IPS_2	LimbicB_OFC_3		
ContA_IPS_3	LimbicB_OFC_4		
ContA_PFCd_1	LimbicA_TempPole_1		
ContA_PFClv_1	LimbicA_TempPole_2		
ContA_PFCl_1	LimbicA_TempPole_3		
ContA_PFCl_2	LimbicA_TempPole_4		
ContA_PFCl_3	ContA_IPS_1		
ContA_Cingm_1	ContA_IPS_2		
ContB_Temp_1	ContA_PFCd_1		
ContB_IPL_1	ContA_PFCl_1		
ContB_PFCl_1	ContA_PFCl_2		
ContB_PFClv_1	ContA_Cingm_1		
ContB_PFClv_2	ContB_Temp_1		
ContC_pCun_1	ContB_Temp_2		
ContC_pCun_2	ContB_IPL_1		
ContC_Cingp_1	ContB_IPL_2		
DefaultA_IPL_1	ContB_PFCld_1		
DefaultA_PFCd_1	ContB_PFCld_2		
DefaultA_pCunPCC_1	ContB_PFClv_1		
DefaultA_pCunPCC_2	ContB_PFClv_2		
DefaultA_pCunPCC_3	ContB_PFCmp_1		
DefaultA_PFCm_1	ContB_PFCld_3		
DefaultA_PFCm_2	ContC_pCun_1		
DefaultA_PFCm_3	ContC_pCun_2		
DefaultB_Temp_1	ContC_Cingp_1		
DefaultB_Temp_2	DefaultA_IPL_1		
DefaultB_Temp_3	DefaultA_PFCd_1		
DefaultB_Temp_4	DefaultA_pCunPCC_1		
DefaultB_IPL_1	DefaultA_PFCm_1		
DefaultB_PFCd_1	DefaultA_PFCm_2		
DefaultB_PFCd_2	DefaultA_PFCm_3		
DefaultB_PFCd_3	DefaultB_Temp_1		
DefaultB_PFCd_4	DefaultB_AntTemp_1		
DefaultB_PFCv_1	DefaultB_PFCd_1		
DefaultB_PFCv_2	DefaultB_PFCv_1		
DefaultB_PFCv_3	DefaultC_IPL_1		
DefaultB_PFCv_4	DefaultC_Rsp_1		
DefaultC_IPL_1	DefaultC_PHC_1		
DefaultC_Rsp_1	TempPar_1		
DefaultC_PHC_1	TempPar_2		
TempPar_1	TempPar_3		
TempPar_2	TempPar_4		
Sub_thalamusproper	Sub_thalamusproper		
Sub_caudate	Sub_caudate		
Sub_putamen	Sub_putamen		
Sub_pallidum	Sub_pallidum		
Sub_hyppocampus	Sub_hyppocampus		
Sub_amygdala	Sub_amygdala		
Sub_accumbensarea	Sub_accumbensarea		

.4 Lausanne parcellation: details on the brain regions:

The following table is adapted from the Supplementary information provided in [9] (we refer the reader to the publication for details and references):" They assigned each of the 34 cortical regions to the following functional systems: the fronto-parietal, cingulo-opercular, dorsal attention, ventral attention, default mode, motor and somatosensory, auditory, and visual.

Table 2: Regions of the Desikan-Killyani atlas [113] and their functional network assignment.

Brain parcel	**Network assignment**
Lateral Orbitofrontal	Ventral Attention
Pars Orbitalis	Cingulo-Opercular
Frontal Pole	Fronto-parietal
Medial Orbitofrontal	Fronto-parietal
Pars Triangularis	Fronto-parietal
Pars Opercularis	Cingulo-Opercular
Rostral Middle Frontal	Cingulo-Opercular
Superior Frontal	Default Mode
Caudal Middle Frontal	Fronto-parietal
Precentral	Somatosensory
Paracentral	Somatosensory
Rostral Anterior Cingulate	Cingulo-Opercular
Caudal Anterior Cingulate	Cingulo-Opercular
Posterior Cingulate	Default Mode
Isthmus Cingulate	Default Mode
Post Central	Somatosensory
Supramarginal	Cingulo-Opercular
Superior Parietal	Dorsal Attention
Inferior Parietal	Fronto-parietal
Precuneus	Default Mode
Cuneus	Visual
Pericalcarine	Visual
Lateral Occipital	Visual
Lingual	Visual
Fusiform	Visual
Parahippocampal	Other
Entorhinal	Visual
Temporal Pole	Other
Inferior Temporal	Visual
Middle Temporal	Other
Bank of the Superior Temporal Sulcus	Auditory
Superior Temporal	Auditory
Transverse Temporal	Auditory
Insula	Fronto-parietal
Thalamus	Subcortical
Caudate	Subcortical
Putamen	Subcortical
Pallidum	Subcortical
Nucleus Accubens	Subcortical
Hyppocampus	Subcortical
Amygdala	Subcortical
Brainstem	Other

Bibliography

Here are the references in citation order.

[1] J.A. Bondy and U.S.R Murty. *Graph Theory*. 1st. Springer Publishing Company, Incorporated, 2008 (cited on page 1).

[2] Paul Erdos and Alfred Reyni. 'On random graphs I'. In: *Publ. math. debrecen* 6.290-297 (1959), p. 18 (cited on pages 1, 22).

[3] R. Kálmán. 'Contributions to the Theory of Optimal Control'. In: 1960. (Visited on 05/17/2023) (cited on pages 1, 11).

[4] Ching-Tai Lin. 'Structural controllability'. In: *IEEE Transactions on Automatic Control* 19.3 (June 1974). Conference Name: IEEE Transactions on Automatic Control, pp. 201–208. DOI: 10.1109/TAC.1974.1100557 (cited on pages 1, 11, 13, 14).

[5] Yang-Yu Liu, Jean-Jacques Slotine, and Albert-László Barabási. 'Controllability of complex networks'. en. In: *Nature* 473.7346 (May 2011), pp. 167–173. DOI: 10.1038/nature10011. (Visited on 10/14/2020) (cited on pages 1, 11, 14, 15).

[6] Tyler H. Summers, Fabrizio L. Cortesi, and John Lygeros. 'On Submodularity and Controllability in Complex Dynamical Networks'. In: *IEEE Transactions on Control of Network Systems* 3.1 (Mar. 2016). Conference Name: IEEE Transactions on Control of Network Systems, pp. 91–101. DOI: 10.1109/TCNS.2015.2453711 (cited on page 1).

[7] Marco Rinaldi. 'Controllability of transportation networks'. en. In: *Transportation Research Part B: Methodological* 118 (Dec. 2018), pp. 381–406. DOI: 10.1016/j.trb.2018.11.005. (Visited on 03/28/2023) (cited on page 1).

[8] Min Li et al. 'Control principles for complex biological networks'. In: *Briefings in Bioinformatics* 20.6 (Nov. 2019), pp. 2253–2266. DOI: 10.1093/bib/bby088. (Visited on 03/28/2023) (cited on page 1).

[9] Shi Gu et al. 'Controllability of structural brain networks'. en. In: *Nature Communications* 6.1 (Dec. 2015), p. 8414. DOI: 10.1038/ncomms9414. (Visited on 10/05/2020) (cited on pages 1, 2, 8, 29, 81).

[10] John D. Medaglia. 'Clarifying cognitive control and the controllable connectome'. en. In: *WIREs Cognitive Science* 10.1 (2019). _eprint: https://onlinelibrary.wiley.com/doi/pdf/10.1002/wcs.1471, e1471. DOI: 10.1002/wcs.1471. (Visited on 04/27/2023) (cited on pages 2, 8).

[11] Arianna Menardi et al. 'Maximizing brain networks engagement via individualized connectome-wide target search'. English. In: *Brain Stimulation: Basic, Translational, and Clinical Research in Neuromodulation* 15.6 (Nov. 2022). Publisher: Elsevier, pp. 1418–1431. DOI: 10.1016/j.brs.2022.09.011. (Visited on 01/20/2023) (cited on pages 2, 7, 32, 34, 37).

[12] Jie Sun and Adilson E. Motter. 'Controllability Transition and Nonlocality in Network Control'. In: *Physical Review Letters* 110.20 (May 2013). Publisher: American Physical Society, p. 208701. DOI: 10.1103/PhysRevLett.110.208701. (Visited on 09/29/2021) (cited on pages 2, 14, 20, 21, 27, 33, 37).

[13] Brian C. Kavanaugh et al. 'Neurocognitive Effects of Repetitive Transcranial Magnetic Stimulation With a 2-Coil Device in Treatment-Resistant Major Depressive Disorder'. eng. In: *The journal of ECT* 34.4 (Dec. 2018), pp. 258–265. DOI: 10.1097/YCT.0000000000000494 (cited on page 2).

[14] Danielle S Bassett and Olaf Sporns. 'Network neuroscience'. en. In: *Nature Neuroscience* 20.3 (Mar. 2017), pp. 353–364. DOI: 10.1038/nn.4502. (Visited on 10/05/2020) (cited on pages 5, 6).

[15] Morten L. Kringelbach et al. 'Translational principles of deep brain stimulation'. en. In: *Nature Reviews Neuroscience* 8.8 (Aug. 2007). Number: 8 Publisher: Nature Publishing Group, pp. 623–635. DOI: 10.1038/nrn2196. (Visited on 08/08/2023) (cited on page 6).

[16] Eran Dayan et al. 'Noninvasive brain stimulation: from physiology to network dynamics and back'. en. In: *Nature Neuroscience* 16.7 (July 2013). Number: 7 Publisher: Nature Publishing Group, pp. 838–844. DOI: 10.1038/nn.3422. (Visited on 08/08/2023) (cited on pages 6, 7).

[17] Rafael Polanía, Michael A. Nitsche, and Christian C. Ruff. 'Studying and modifying brain function with non-invasive brain stimulation'. en. In: *Nature Neuroscience* 21.2 (Feb. 2018). Number: 2 Publisher: Nature Publishing Group, pp. 174–187. DOI: 10.1038/s41593-017-0054-4. (Visited on 08/08/2023) (cited on page 7).

[18] Marie-Claire Smith and Cathy M. Stinear. 'Transcranial magnetic stimulation (TMS) in stroke: Ready for clinical practice?' eng. In: *Journal of Clinical Neuroscience: Official Journal of the Neurosurgical Society of Australasia* 31 (Sept. 2016), pp. 10–14. DOI: 10.1016/j.jocn.2016.01.034 (cited on page 7).

[19] John D. Medaglia et al. 'Language Tasks and the Network Control Role of the Left Inferior Frontal Gyrus'. eng. In: *eNeuro* 8.5 (2021), ENEURO.0382–20.2021. DOI: 10.1523/ENEURO.0382-20.2021 (cited on pages 7–9).

[20] Christopher W. Lynn and Danielle S. Bassett. 'The physics of brain network structure, function and control'. en. In: *Nature Reviews Physics* 1.5 (May 2019). Number: 5 Publisher: Nature Publishing Group, pp. 318–332. DOI: 10.1038/s42254-019-0040-8. (Visited on 08/08/2023) (cited on page 7).

[21] Jennifer Stiso et al. 'White Matter Network Architecture Guides Direct Electrical Stimulation through Optimal State Transitions'. en. In: *Cell Reports* 28.10 (Sept. 2019), 2554–2566.e7. DOI: 10.1016/j.celrep.2019.08.008. (Visited on 10/05/2020) (cited on pages 7, 13).

[22] Anjali Sivaramakrishnan, Lenore Tahara-Eckl, and Sangeetha Madhavan. 'Spatial localization and distribution of the TMS-related 'hotspot' of the tibialis anterior muscle representation in the healthy and post-stroke motor cortex'. In: *Neuroscience letters* 627 (Aug. 2016), pp. 30–35. DOI: 10.1016/j.neulet.2016.05.041. (Visited on 08/08/2023) (cited on page 7).

[23] Charles J. Lynch et al. 'Automated optimization of TMS coil placement for personalized functional network engagement'. en. In: *Neuron* 110.20 (Oct. 2022), 3263–3277.e4. DOI: 10.1016/j.neuron.2022.08.012. (Visited on 08/08/2023) (cited on page 7).

[24] Yoed N. Kenett et al. 'Driving the brain towards creativity and intelligence: A network control theory analysis'. In: *Neuropsychologia*. The neural bases of creativity and intelligence: common grounds and differences 118 (Sept. 2018), pp. 79–90. DOI: 10.1016/j.neuropsychologia.2018.01.001. (Visited on 09/20/2023) (cited on page 8).

[25] Eli J. Cornblath et al. 'Temporal sequences of brain activity at rest are constrained by white matter structure and modulated by cognitive demands'. en. In: *Communications Biology* 3.1 (May 2020). Number: 1 Publisher: Nature Publishing Group, pp. 1–12. DOI: 10.1038/s42003-020-0961-x. (Visited on 06/14/2021) (cited on page 8).

[26] Zaixu Cui et al. 'Optimization of energy state transition trajectory supports the development of executive function during youth'. en. In: *eLife* 9 (Mar. 2020), e53060. DOI: 10.7554/eLife.53060. (Visited on 10/05/2020) (cited on page 8).

[27] Won Hee Lee et al. 'Heritability and Cognitive Relevance of Structural Brain Controllability'. In: *Cerebral Cortex* 30.5 (May 2020), pp. 3044–3054. DOI: 10.1093/cercor/bhz293. (Visited on 11/09/2021) (cited on page 8).

[28] Urs Braun et al. 'Brain network dynamics during working memory are modulated by dopamine and diminished in schizophrenia'. en. In: *Nature Communications* 12.1 (June 2021). Number: 1 Publisher: Nature Publishing Group, p. 3478. DOI: 10.1038/s41467-021-23694-9. (Visited on 06/14/2021) (cited on page 9).

[29] Aswin Chari et al. 'Drug-resistant focal epilepsy in children is associated with increased modal controllability of the whole brain and epileptogenic regions'. en. In: *Communications Biology* 5.1 (Apr. 2022). Number: 1 Publisher: Nature Publishing Group, pp. 1–14. DOI: 10.1038/s42003-022-03342-8. (Visited on 06/15/2022) (cited on page 9).

[30] Brittany H. Scheid et al. 'Time-evolving controllability of effective connectivity networks during seizure progression'. en-GB. In: *Proceedings of the National Academy of Sciences of the United States of America* 118.5 (2021). Number: 5, undefined–undefined. DOI: 10.1073/pnas.2006436118. (Visited on 11/18/2021) (cited on page 9).

[31] R.E. Kalman. 'Lectures on Controllability and Observability'. en. In: *Controllability and Observability*. Ed. by E. Evangelisti. C.I.M.E. Summer Schools. Berlin, Heidelberg: Springer, 2011, pp. 1–149. DOI: 10.1007/978-3-642-11063-4_1. (Visited on 07/18/2023) (cited on page 12).

[32] Giacomo Casadei, Carlos Canuda-de-Wit, and Sandro Zampieri. 'Controllability of Large-Scale Networks: An Output Controllability Approach'. In: *2018 IEEE Conference on Decision and Control (CDC)*. ISSN: 2576-2370. Dec. 2018, pp. 5886–5891. DOI: 10.1109/CDC.2018.8619598 (cited on pages 13, 16, 22).

[33] Giacomo Casadei, Carlos Canudas-de-Wit, and Sandro Zampieri. 'Model Reduction Based Approximation of the Output Controllability Gramian in Large-Scale Networks'. In: *IEEE Transactions on Control of Network Systems* 7.4 (Dec. 2020). Conference Name: IEEE Transactions on Control of Network Systems, pp. 1778–1788. DOI: 10.1109/TCNS.2020.3000694 (cited on pages 13, 16, 17, 22).

[34] Teresa M. Karrer et al. 'A practical guide to methodological considerations in the controllability of structural brain networks'. en. In: *Journal of Neural Engineering* 17.2 (Apr. 2020). Publisher: IOP Publishing, p. 026031. DOI: 10.1088/1741-2552/ab6e8b. (Visited on 02/08/2023) (cited on page 13).

[35] E. B. Lee and L. Markus. *Foundations of optimal control theory*. The SIAM series in applied mathematics. New York: Wiley, 1967 (cited on page 13).

[36] Zhengzhong Yuan et al. 'Exact controllability of complex networks'. en. In: *Nature Communications* 4.1 (Dec. 2013), p. 2447. DOI: 10.1038/ncomms3447. (Visited on 10/30/2020) (cited on page 14).

[37] Fabio Pasqualetti, Sandro Zampieri, and Francesco Bullo. 'Controllability Metrics, Limitations and Algorithms for Complex Networks'. In: *IEEE Transactions on Control of Network Systems* 1.1 (Mar. 2014). Conference Name: IEEE Transactions on Control of Network Systems, pp. 40–52. DOI: 10.1109/TCNS.2014.2310254 (cited on pages 14, 32).

[38] P. C. Müller and H. I. Weber. 'Analysis and optimization of certain qualities of controllability and observability for linear dynamical systems'. en. In: *Automatica* 8.3 (May 1972), pp. 237–246. DOI: 10.1016/0005-1098(72)90044-1. (Visited on 11/02/2022) (cited on page 14).

[39] Hamid Reza Shaker and Maryamsadat Tahavori. 'Optimal sensor and actuator location for unstable systems'. en. In: *Journal of Vibration and Control* 19.12 (Sept. 2013). Publisher: SAGE Publications Ltd STM, pp. 1915–1920. DOI: 10.1177/1077546312451302. (Visited on 07/19/2023) (cited on pages 15, 29).

[40] Le-Zhi Wang et al. 'Physical controllability of complex networks'. en. In: *Scientific Reports* 7.1 (Jan. 2017). Number: 1 Publisher: Nature Publishing Group, p. 40198. DOI: 10.1038/srep40198. (Visited on 03/28/2023) (cited on page 15).

[41] Gustav Lindmark. 'Minimum energy control for complex networks'. en. In: *Scientific REPOrTS* (2018), p. 14 (cited on pages 15, 20, 26, 29).

[42] Jianxi Gao et al. 'Target control of complex networks'. en. In: *Nature Communications* 5.1 (Dec. 2014), p. 5415. DOI: 10.1038/ncomms6415. (Visited on 11/04/2021) (cited on page 15).

[43] Isaac Klickstein, Afroza Shirin, and Francesco Sorrentino. 'Energy scaling of targeted optimal control of complex networks'. en. In: *Nature Communications* 8.1 (Apr. 2017). Number: 1 Publisher: Nature Publishing Group, p. 15145. DOI: 10.1038/ncomms15145. (Visited on 03/28/2023) (cited on pages 15, 39).

[44] Afroza Shirin, Isaac S. Klickstein, and Francesco Sorrentino. 'Optimal control of complex networks: Balancing accuracy and energy of the control action'. en. In: *Chaos: An Interdisciplinary Journal of Nonlinear Science* 27.4 (Apr. 2017). Publisher: AIP Publishing LLCAIP Publishing, p. 041103. DOI: 10.1063/1.4979647. (Visited on 10/04/2021) (cited on page 15).

[45] Isaac Klickstein. 'Target Control of Networked Systems'. In: *Mechanical Engineering ETDs* (Apr. 2020) (cited on page 15).

[46] Isaac Klickstein and Francesco Sorrentino. 'Controlling network ensembles'. en. In: *Nature Communications* 12.1 (Dec. 2021), p. 1884. DOI: 10.1038/s41467-021-22172-6. (Visited on 10/05/2021) (cited on page 15).

[47] Giulia Bassignana et al. 'Stepwise target controllability identifies dysregulations of macrophage networks in multiple sclerosis'. en. In: *Network Neuroscience* 5.2 (May 2021), pp. 337–357. DOI: 10.1162/netn_a_00180. (Visited on 03/14/2022) (cited on page 15).

[48] David Gfeller and Paolo De Los Rios. 'Spectral Coarse Graining and Synchronization in Oscillator Networks'. In: *Physical Review Letters* 100.17 (May 2008). Publisher: American Physical Society, p. 174104. DOI: 10.1103/PhysRevLett.100.174104. (Visited on 10/19/2022) (cited on pages 17, 18).

[49] Pablo Villegas et al. 'Laplacian renormalization group for heterogeneous networks'. en. In: *Nature Physics* 19.3 (Mar. 2023). Number: 3 Publisher: Nature Publishing Group, pp. 445–450. DOI: 10.1038/s41567-022-01866-8. (Visited on 04/25/2023) (cited on pages 17, 18, 27).

[50] Fan R. K. Chung. *Spectral graph theory*. eng. Regional conference series in mathematics. OCLC: 35718609. Providence, R.I.: Published for the Conference Board of the mathematical sciences by the American Mathematical Society, 1997 (cited on pages 17, 18, 27).

[51] Liu Rui, Hossein Nejati, and Ngai-Man Cheung. 'Dimensionality reduction of brain imaging data using graph signal processing'. In: *2016 IEEE International Conference on Image Processing (ICIP)*. ISSN: 2381-8549. Sept. 2016, pp. 1329–1333. DOI: 10.1109/ICIP.2016.7532574 (cited on page 18).

[52] Nafise Naseri et al. 'Converting high-dimensional complex networks to lower-dimensional ones preserving synchronization features'. en. In: *Europhysics Letters* 140.2 (Oct. 2022). Publisher: EDP Sciences, IOP Publishing and Società Italiana di Fisica, p. 21001. DOI: 10.1209/0295-5075/ac98de. (Visited on 12/15/2022) (cited on page 18).

[53] Benyamin Ghojogh et al. *Laplacian-Based Dimensionality Reduction Including Spectral Clustering, Laplacian Eigenmap, Locality Preserving Projection, Graph Embedding, and Diffusion Map: Tutorial and Survey*. arXiv:2106.02154 [cs, stat]. Aug. 2022. DOI: 10.48550/arXiv.2106.02154. URL: http://arxiv.org/abs/2106.02154 (visited on 03/21/2023) (cited on page 18).

[54] Peng Cui et al. 'A Survey on Network Embedding'. In: *IEEE Transactions on Knowledge and Data Engineering* 31.5 (May 2019). Conference Name: IEEE Transactions on Knowledge and Data Engineering, pp. 833–852. DOI: 10.1109/TKDE.2018.2849727 (cited on pages 18, 25, 27).

[55] Olaf Sporns. 'Small-world connectivity, motif composition, and complexity of fractal neuronal connections'. en. In: *Biosystems*. Dedicated to the Memory of Ray Paton 85.1 (July 2006), pp. 55–64. DOI: 10.1016/j.biosystems.2006.02.008. (Visited on 03/07/2023) (cited on page 19).

[56] Mikail Rubinov and Olaf Sporns. 'Complex network measures of brain connectivity: Uses and interpretations'. en. In: *NeuroImage*. Computational Models of the Brain 52.3 (Sept. 2010), pp. 1059–1069. DOI: 10.1016/j.neuroimage.2009.10.003. (Visited on 03/07/2023) (cited on pages 19, 53, 56).

[57] David Meunier, Renaud Lambiotte, and Edward Bullmore. 'Modular and Hierarchically Modular Organization of Brain Networks'. In: *Frontiers in Neuroscience* 4 (2010). (Visited on 02/20/2023) (cited on page 19).

[58] Luca Ferrarini et al. 'Hierarchical functional modularity in the resting-state human brain'. en. In: *Human Brain Mapping* 30.7 (July 2009). Publisher: Wiley-Blackwell, p. 2220. DOI: 10.1002/hbm.20663. (Visited on 03/15/2023) (cited on page 19).

[59] Paul W. Holland, Kathryn Blackmond Laskey, and Samuel Leinhardt. 'Stochastic blockmodels: First steps'. en. In: *Social Networks* 5.2 (June 1983), pp. 109–137. DOI: 10.1016/0378-8733(83)90021-7. (Visited on 09/20/2022) (cited on page 19).

[60] M. E. J. Newman and M. Girvan. 'Finding and evaluating community structure in networks'. In: *Physical Review E* 69.2 (Feb. 2004). Publisher: American Physical Society, p. 026113. DOI: 10.1103/PhysRevE.69.026113. (Visited on 06/28/2022) (cited on page 19).

[61] Pablo Villegas et al. 'Laplacian paths in complex networks: Information core emerges from entropic transitions'. In: *Physical Review Research* 4.3 (Sept. 2022). Publisher: American Physical Society, p. 033196. DOI: 10.1103/PhysRevResearch.4.033196. (Visited on 10/19/2022) (cited on pages 19, 27).

[62] Mohammed Senoussaoui et al. 'A Study of the Cosine Distance-Based Mean Shift for Telephone Speech Diarization'. In: *IEEE/ACM Transactions on Audio, Speech, and Language Processing* 22.1 (Jan. 2014). Conference Name: IEEE/ACM Transactions on Audio, Speech, and Language Processing, pp. 217–227. DOI: 10.1109/TASLP.2013.2285474 (cited on page 20).

[63] Thomas G. Hallam. 'David G. Luenberger: Introduction to Dynamic Systems, Theory, Models, and Applications. New York: John Wiley & Sons, 1979, 446 pp'. en. In: *Behavioral Science* 26.4 (1981). _eprint: https://onlinelibrary.wiley.com/doi/pdf/10.1002/bs.3830260412, pp. 397–398. DOI: 10.1002/bs.3830260412. (Visited on 09/08/2023) (cited on page 20).

[64] Chao Duan, Takashi Nishikawa, and Adilson E. Motter. 'Prevalence and scalable control of localized networks'. In: *Proceedings of the National Academy of Sciences* 119.32 (Aug. 2022). Publisher: Proceedings of the National Academy of Sciences, e2122566119. DOI: 10.1073/pnas.2122566119. (Visited on 08/26/2022) (cited on pages 21, 37).

[65] D. Georges. 'The use of observability and controllability gramians or functions for optimal sensor and actuator location in finite-dimensional systems'. In: *Proceedings of 1995 34th IEEE Conference on Decision and Control* 4 (1995). Conference Name: 1995 34th IEEE Conference on Decision and Control ISBN: 9780780326859 Place: New Orleans, LA, USA Publisher: IEEE, pp. 3319–3324. DOI: 10.1109/CDC.1995.478999. (Visited on 08/05/2023) (cited on page 21).

[66] Albert-László Barabási, Réka Albert, and Hawoong Jeong. 'Mean-field theory for scale-free random networks'. In: *Physica A: Statistical Mechanics and its Applications* 272.1 (Oct. 1999), pp. 173–187. DOI: 10.1016/S0378-4371(99)00291-5. (Visited on 09/18/2023) (cited on page 22).

[67] Gustav Lindmark and Claudio Altafini. 'Combining centrality measures for control energy reduction in network controllability problems'. In: *2019 18th European Control Conference (ECC)*. June 2019, pp. 1518–1523. DOI: 10.23919/ECC.2019.8795867 (cited on pages 26, 29).

[68] Gustav Lindmark. *Controllability of Complex Networks at Minimum Cost*. en. Vol. 2074. Linköping Studies in Science and Technology. Dissertations. Linköping: Linköping University Electronic Press, June 2020. (Visited on 10/03/2022) (cited on pages 26, 29).

[69] Chengyi Tu et al. 'Warnings and Caveats in Brain Controllability'. In: *NeuroImage* 176 (Aug. 2018), pp. 83–91. DOI: 10.1016/j.neuroimage.2018.04.010. (Visited on 03/10/2023) (cited on pages 26, 29, 33).

[70] T. M. McKenna, T. A. McMullen, and M. F. Shlesinger. 'The brain as a dynamic physical system'. en. In: *Neuroscience* 60.3 (June 1994), pp. 587–605. DOI: 10.1016/0306-4522(94)90489-8. (Visited on 04/25/2023) (cited on page 27).

[71] Jason Z. Kim and Danielle S. Bassett. 'Linear Dynamics and Control of Brain Networks'. en. In: *Neural Engineering*. Ed. by Bin He. Cham: Springer International Publishing, 2020, pp. 497–518. DOI: 10.1007/978-3-030-43395-6_17. (Visited on 04/25/2023) (cited on page 27).

[72] S. Boccaletti et al. 'Complex networks: Structure and dynamics'. en. In: *Physics Reports* 424.4 (Feb. 2006), pp. 175–308. DOI: 10.1016/j.physrep.2005.10.009. (Visited on 06/05/2023) (cited on page 27).

[73] M. Chavez et al. 'Synchronization is Enhanced in Weighted Complex Networks'. In: *Physical Review Letters* 94.21 (June 2005). Publisher: American Physical Society, p. 218701. DOI: 10.1103/PhysRevLett.94.218701. (Visited on 08/07/2023) (cited on page 27).

[74] David Gfeller and Paolo De Los Rios. 'Spectral Coarse Graining of Complex Networks'. In: *Physical Review Letters* 99.3 (July 2007). Publisher: American Physical Society, p. 038701. DOI: 10.1103/PhysRevLett.99.038701. (Visited on 10/19/2022) (cited on page 27).

[75] Samir Suweis et al. 'Brain controllability: Not a slam dunk yet'. en. In: *NeuroImage* 200 (Oct. 2019), pp. 552–555. DOI: 10.1016/j.neuroimage.2019.07.012. (Visited on 02/16/2022) (cited on pages 29, 33).

[76] Julia Elina Stocker et al. 'Network controllability measures of subnetworks: implications for neurosciences'. en. In: *Journal of Neural Engineering* 20.1 (Feb. 2023). Publisher: IOP Publishing, p. 016044. DOI: 10.1088/1741-2552/acb256. (Visited on 03/07/2023) (cited on pages 29, 33).

[77] Cathie Sudlow et al. 'UK Biobank: An Open Access Resource for Identifying the Causes of a Wide Range of Complex Diseases of Middle and Old Age'. In: *PLoS Medicine* 12.3 (Mar. 2015), e1001779. DOI: 10.1371/journal.pmed.1001779. (Visited on 03/07/2023) (cited on page 31).

[78] Fidel Alfaro-Almagro et al. 'Image processing and Quality Control for the first 10,000 brain imaging datasets from UK Biobank'. en. In: *NeuroImage* 166 (Feb. 2018), pp. 400–424. DOI: 10.1016/j.neuroimage.2017.10.034. (Visited on 06/08/2023) (cited on page 31).

[79] J-Donald Tournier et al. 'MRtrix3: A fast, flexible and open software framework for medical image processing and visualisation'. en. In: *NeuroImage* 202 (Nov. 2019), p. 116137. DOI: 10.1016/j.neuroimage.2019.116137. (Visited on 06/07/2023) (cited on page 31).

[80] Mark Jenkinson et al. 'FSL'. en. In: *NeuroImage*. 20 YEARS OF fMRI 62.2 (Aug. 2012), pp. 782–790. DOI: 10.1016/j.neuroimage.2011.09.015. (Visited on 06/07/2023) (cited on page 31).

[81] Alexander Schaefer et al. 'Local-Global Parcellation of the Human Cerebral Cortex from Intrinsic Functional Connectivity MRI'. eng. In: *Cerebral Cortex (New York, N.Y.: 1991)* 28.9 (Sept. 2018), pp. 3095–3114. DOI: 10.1093/cercor/bhx179 (cited on pages 32, 50).

[82] Andrea I. Luppi and Emmanuel A. Stamatakis. 'Combining network topology and information theory to construct representative brain networks'. In: *Network Neuroscience* 5.1 (Feb. 2021), pp. 96–124. DOI: 10.1162/netn_a_00170. (Visited on 02/15/2023) (cited on page 32).

[83] B. T. Thomas Yeo et al. 'The organization of the human cerebral cortex estimated by intrinsic functional connectivity'. In: *Journal of Neurophysiology* 106.3 (Sept. 2011), pp. 1125–1165. DOI: 10.1152/jn.00338.2011. (Visited on 03/20/2023) (cited on pages 32, 43, 44).

[84] Robert E. Smith et al. 'The effects of SIFT on the reproducibility and biological accuracy of the structural connectome'. en. In: *NeuroImage* 104 (Jan. 2015), pp. 253–265. DOI: 10.1016/j.neuroimage.2014.10.004. (Visited on 06/07/2023) (cited on page 32).

[85] O. Agcaoglu et al. 'Lateralization of Resting State Networks and Relationship to Age and Gender'. In: *NeuroImage* 0 (Jan. 2015), pp. 310–325. DOI: 10.1016/j.neuroimage.2014.09.001. (Visited on 03/09/2023) (cited on page 35).

[86] Loes Janssen, Ruud G. J. Meulenbroek, and Bert Steenbergen. 'Behavioral evidence for left-hemisphere specialization of motor planning'. In: *Experimental Brain Research* 209.1 (2011), pp. 65–72. DOI: 10.1007/s00221-010-2519-5. (Visited on 05/04/2023) (cited on page 35).

[87] Paolo Bartolomeo and Tal Seidel Malkinson. 'Hemispheric lateralization of attention processes in the human brain'. en. In: *Current Opinion in Psychology*. Attention & Perception 29 (Oct. 2019), pp. 90–96. DOI: 10.1016/j.copsyc.2018.12.023. (Visited on 01/28/2022) (cited on page 35).

[88] Alexander T Sack and Teresa Schuhmann. 'Hemispheric Differences within the Fronto-Parietal Network Dynamics Underlying Spatial Imagery'. In: *Frontiers in Psychology* 3 (2012). (Visited on 08/24/2023) (cited on page 35).

[89] Orrin Devinsky. 'Right Cerebral Hemisphere Dominance for a Sense of Corporeal and Emotional Self'. In: *Epilepsy & Behavior* 1.1 (Feb. 2000), pp. 60–73. DOI: 10.1006/ebeh.2000.0025. (Visited on 08/24/2023) (cited on page 35).

[90] Yoav Benjamini and Yosef Hochberg. 'Controlling the False Discovery Rate: A Practical and Powerful Approach to Multiple Testing'. en. In: *Journal of the Royal Statistical Society: Series B (Methodological)* 57.1 (1995). _eprint: https://onlinelibrary.wiley.com/doi/pdf/10.1111/j.2517-6161.1995.tb02031.x, pp. 289–300. DOI: 10.1111/j.2517-6161.1995.tb02031.x. (Visited on 07/21/2023) (cited on pages 35, 60).

[91] Peter H. Donaldson, Nicole J. Rinehart, and Peter G. Enticott. 'Noninvasive stimulation of the temporoparietal junction: A systematic review'. en. In: *Neuroscience & Biobehavioral Reviews* 55 (Aug. 2015), pp. 547–572. DOI: 10.1016/j.neubiorev.2015.05.017. (Visited on 06/20/2023) (cited on page 38).

[92] Maxwell B. Wang et al. 'Brain network eigenmodes provide a robust and compact representation of the structural connectome in health and disease'. en. In: *PLOS Computational Biology* 13.6 (2017). Publisher: Public Library of Science, e1005550. DOI: 10.1371/journal.pcbi.1005550. (Visited on 08/30/2022) (cited on page 40).

[93] Leonardo L Gollo. 'Mapping how local perturbations influence systems-level brain dynamics'. en. In: (), p. 43 (cited on page 40).

[94] Lucina Q. Uddin et al. 'Functional connectivity of default mode network components: Correlation, anticorrelation, and causality'. In: *Human Brain Mapping* 30.2 (Jan. 2008), pp. 625–637. DOI: 10.1002/hbm.20531. (Visited on 02/14/2023) (cited on page 41).

[95] David Maillet et al. 'Large-scale network interactions involved in dividing attention between the external environment and internal thoughts to pursue two distinct goals'. In: *NeuroImage* 197 (Aug. 2019), pp. 49–59. DOI: 10.1016/j.neuroimage.2019.04.054. (Visited on 05/10/2023) (cited on pages 41–43).

[96] M. E. Raichle et al. 'A default mode of brain function'. en. In: *Proceedings of the National Academy of Sciences* 98.2 (Jan. 2001), pp. 676–682. DOI: 10.1073/pnas.98.2.676. (Visited on 12/07/2020) (cited on pages 41, 43).

[97] Emily L. Parks and David J. Madden. 'Brain Connectivity and Visual Attention'. In: *Brain Connectivity* 3.4 (Aug. 2013). Publisher: Mary Ann Liebert, Inc., publishers, pp. 317–338. DOI: 10.1089/brain.2012.0139. (Visited on 05/02/2023) (cited on page 41).

[98] Maurizio Corbetta and Gordon L. Shulman. 'Control of goal-directed and stimulus-driven attention in the brain'. en. In: *Nature Reviews Neuroscience* 3.3 (Mar. 2002). Number: 3 Publisher: Nature Publishing Group, pp. 201–215. DOI: 10.1038/nrn755. (Visited on 05/04/2023) (cited on pages 41, 42).

[99] John Dominic Medaglia et al. 'Brain and cognitive reserve: Translation via network control theory'. en. In: *Neuroscience & Biobehavioral Reviews* 75 (Apr. 2017), pp. 53–64. DOI: 10.1016/j.neubiorev.2017.01.016. (Visited on 09/26/2022) (cited on page 41).

[100] N. Dijkstra et al. 'Distinct Top-down and Bottom-up Brain Connectivity During Visual Perception and Imagery'. en. In: *Scientific Reports* 7.1 (July 2017). Number: 1 Publisher: Nature Publishing Group, p. 5677. DOI: 10.1038/s41598-017-05888-8. (Visited on 05/10/2023) (cited on page 41).

[101] M. Belén Pardi, Anna Schroeder, and Johannes J. Letzkus. 'Probing top-down information in neocortical layer 1'. English. In: *Trends in Neurosciences* 46.1 (Jan. 2023). Publisher: Elsevier, pp. 20–31. DOI: 10.1016/j.tins.2022.11.001. (Visited on 09/14/2023) (cited on page 41).

[102] Anna Schroeder et al. 'Inhibitory top-down projections from zona incerta mediate neocortical memory'. English. In: *Neuron* 111.5 (Mar. 2023). Publisher: Elsevier, 727–738.e8. DOI: 10.1016/j.neuron.2022.12.010. (Visited on 09/14/2023) (cited on page 41).

[103] Ahmad Abu-Akel and Simone Shamay-Tsoory. 'Neuroanatomical and neurochemical bases of theory of mind'. en. In: *Neuropsychologia* 49.11 (Sept. 2011), pp. 2971–2984. DOI: 10.1016/j.neuropsychologia.2011.07.012. (Visited on 05/04/2023) (cited on page 42).

[104] Caio Seguin, Adeel Razi, and Andrew Zalesky. 'Inferring neural signalling directionality from undirected structural connectomes'. en. In: *Nature Communications* 10.1 (Sept. 2019). Number: 1 Publisher: Nature Publishing Group, p. 4289. DOI: 10.1038/s41467-019-12201-w. (Visited on 08/29/2023) (cited on pages 45, 46).

[105] Giulia Bassignana et al. 'The impact of aging on human brain network target controllability'. eng. In: *Brain Structure & Function* 227.9 (Dec. 2022), pp. 3001–3015. DOI: 10.1007/s00429-022-02584-w (cited on page 45).

[106] Pragya Srivastava et al. 'Models of communication and control for brain networks: distinctions, convergence, and future outlook'. In: *Network Neuroscience* 4.4 (Nov. 2020), pp. 1122–1159. DOI: 10.1162/netn_a_00158. (Visited on 08/29/2023) (cited on page 45).

[107] Stephen J. Gotts et al. 'Two distinct forms of functional lateralization in the human brain'. en. In: *Proceedings of the National Academy of Sciences* 110.36 (Sept. 2013). DOI: 10.1073/pnas.1302581110. (Visited on 05/09/2022) (cited on page 49).

[108] Vyacheslav R. Karolis, Maurizio Corbetta, and Michel Thiebaut de Schotten. 'The architecture of functional lateralisation and its relationship to callosal connectivity in the human brain'. en. In: *Nature Communications* 10.1 (Dec. 2019), p. 1417. DOI: 10.1038/s41467-019-09344-1. (Visited on 03/18/2022) (cited on page 49).

[109] J. H. Martínez et al. 'Role of inter-hemispheric connections in functional brain networks'. en. In: *Scientific Reports* 8.1 (Dec. 2018), p. 10246. DOI: 10.1038/s41598-018-28467-x. (Visited on 02/01/2022) (cited on pages 49, 50, 54, 56).

[110] J. Aguirre, D. Papo, and J. M. Buldú. 'Successful strategies for competing networks'. en. In: *Nature Physics* 9.4 (Apr. 2013), pp. 230–234. DOI: 10.1038/nphys2556. (Visited on 05/09/2022) (cited on pages 50, 54, 56).

[111] Leila Cammoun et al. 'Mapping the human connectome at multiple scales with diffusion spectrum MRI'. en. In: *Journal of Neuroscience Methods* 203.2 (Jan. 2012), pp. 386–397. DOI: 10.1016/j.jneumeth.2011.09.031. (Visited on 05/18/2022) (cited on page 50).

[112] Xiaoxuan Yan et al. *Homotopic local-global parcellation of the human cerebral cortex from resting-state functional connectivity*. en. Pages: 2022.10.25.513788 Section: New Results. Feb. 2023. DOI: 10.1101/2022.10.25.513788. URL: https://www.biorxiv.org/content/10.1101/2022.10.25.513788v2 (visited on 03/01/2023) (cited on page 50).

[113] Rahul S. Desikan et al. 'An automated labeling system for subdividing the human cerebral cortex on MRI scans into gyral based regions of interest'. In: *NeuroImage* 31.3 (July 2006), pp. 968–980. DOI: 10.1016/j.neuroimage.2006.01.021. (Visited on 09/22/2023) (cited on pages 51, 81).

[114] Felix Janelle et al. 'Superior Longitudinal Fasciculus: A Review of the Anatomical Descriptions With Functional Correlates'. In: *Frontiers in Neurology* 13 (2022). (Visited on 09/22/2023) (cited on pages 51, 52).

[115] Lucía Vaquero et al. 'Arcuate fasciculus architecture is associated with individual differences in pre-attentive detection of unpredicted music changes'. In: *NeuroImage* 229 (Apr. 2021), p. 117759. DOI: 10.1016/j.neuroimage.2021.117759. (Visited on 09/22/2023) (cited on pages 51, 52).

[116] Gregory Hickok and David Poeppel. 'The cortical organization of speech processing'. en. In: *Nature Reviews Neuroscience* 8.5 (May 2007). Number: 5 Publisher: Nature Publishing Group, pp. 393–402. DOI: 10.1038/nrn2113. (Visited on 09/22/2023) (cited on page 51).

[117] Stephen M. Smith et al. 'Advances in functional and structural MR image analysis and implementation as FSL'. eng. In: *NeuroImage* 23 Suppl 1 (2004), S208–219. DOI: 10.1016/j.neuroimage.2004.07.051 (cited on page 51).

[118] K. Rojkova et al. 'Atlasing the frontal lobe connections and their variability due to age and education: a spherical deconvolution tractography study'. eng. In: *Brain Structure & Function* 221.3 (Apr. 2016), pp. 1751–1766. DOI: 10.1007/s00429-015-1001-3 (cited on page 51).

[119] Pedro Nascimento Alves et al. 'An improved neuroanatomical model of the default-mode network reconciles previous neuroimaging and neuropathological findings'. en. In: *Communications Biology* 2.1 (Oct. 2019). Number: 1 Publisher: Nature Publishing Group, pp. 1–14. DOI: 10.1038/s42003-019-0611-3. (Visited on 05/09/2023) (cited on page 51).

[120] Michel Thiebaut de Schotten et al. 'Damage to white matter pathways in subacute and chronic spatial neglect: a group study and 2 single-case studies with complete virtual "in vivo" tractography dissection'. eng. In: *Cerebral Cortex (New York, N.Y.: 1991)* 24.3 (Mar. 2014), pp. 691–706. DOI: 10.1093/cercor/bhs351 (cited on page 53).

[121] Vito Latora and Massimo Marchiori. 'Efficient Behavior of Small-World Networks'. In: *Physical Review Letters* 87.19 (Oct. 2001). Publisher: American Physical Society, p. 198701. DOI: 10.1103/PhysRevLett.87.198701. (Visited on 09/22/2023) (cited on page 53).

[122] M. E. J. Newman. 'Finding community structure in networks using the eigenvectors of matrices'. In: *Physical Review E* 74.3 (Sept. 2006). Publisher: American Physical Society, p. 036104. DOI: 10.1103/PhysRevE.74.036104. (Visited on 09/22/2023) (cited on page 53).

[123] Francisco Aparecido Rodrigues. 'Network Centrality: An Introduction'. en. In: *A Mathematical Modeling Approach from Nonlinear Dynamics to Complex Systems*. Ed. by Elbert E. N. Macau. Nonlinear Systems and Complexity. Cham: Springer International Publishing, 2019, pp. 177–196. DOI: 10.1007/978-3-319-78512-7_10. (Visited on 06/14/2023) (cited on pages 53, 54).

[124] Xi-Nian Zuo et al. 'Network centrality in the human functional connectome'. eng. In: *Cerebral Cortex (New York, N.Y.: 1991)* 22.8 (Aug. 2012), pp. 1862–1875. DOI: 10.1093/cercor/bhr269 (cited on pages 54, 65).

[125] Travis Martin, Xiao Zhang, and M. E. J. Newman. 'Localization and centrality in networks'. In: *Physical Review E* 90.5 (Nov. 2014). arXiv: 1401.5093, p. 052808. DOI: 10.1103/PhysRevE.90.052808. (Visited on 03/14/2022) (cited on pages 55, 56, 71).

[126] Ki-ichiro Hashimoto. 'Zeta Functions of Finite Graphs and Representations of p-Adic Groups'. In: *Automorphic Forms and Geometry of Arithmetic Varieties*. Ed. by K. Hashimoto and Y. Namikawa. Vol. 15. Advanced Studies in Pure Mathematics. Academic Press, Jan. 1989, pp. 211–280. DOI: 10.1016/B978-0-12-330580-0.50015-X. (Visited on 09/21/2023) (cited on page 55).

[127] Yasser Iturria-Medina et al. 'Brain Hemispheric Structural Efficiency and Interconnectivity Rightward Asymmetry in Human and Nonhuman Primates'. In: *Cerebral Cortex* 21.1 (Jan. 2011), pp. 56–67. DOI: 10.1093/cercor/bhq058. (Visited on 04/18/2023) (cited on pages 58, 64).

[128] Lucia Jajcay et al. 'Brain Functional Connectivity Asymmetry: Left Hemisphere Is More Modular'. In: *Symmetry* 14 (Apr. 2022), p. 833. DOI: 10.3390/sym14040833 (cited on pages 58, 64).

[129] Dick Schijven et al. 'Large-scale analysis of structural brain asymmetries in schizophrenia via the ENIGMA consortium'. In: *Proceedings of the National Academy of Sciences* 120.14 (Apr. 2023). Publisher: Proceedings of the National Academy of Sciences, e2213880120. DOI: 10.1073/pnas.2213880120. (Visited on 06/21/2023) (cited on pages 59, 64).

[130] José V Pardo, Shantal M Nyabwari, and Joel T Lee. 'Aging-Related Hypometabolism in the Anterior Cingulate Cortex of Cognitively Intact, Amyloid-Negative Seniors at Rest Mediates the Relationship between Age and Executive Function but Not Memory'. In: *Cerebral Cortex Communications* 1.1 (May 2020), tgaa020. DOI: 10.1093/texcom/tgaa020. (Visited on 06/22/2023) (cited on page 65).

[131] Xiang-Zhen Kong et al. 'Mapping cortical brain asymmetry in 17,141 healthy individuals worldwide via the ENIGMA Consortium'. eng. In: *Proceedings of the National Academy of Sciences of the United States of America* 115.22 (May 2018), E5154–E5163. DOI: 10.1073/pnas.1718418115 (cited on pages 65, 66).

[132] Katja Koelkebeck et al. 'The contribution of cortical thickness and surface area to gray matter asymmetries in the healthy human brain'. en. In: *Human Brain Mapping* 35.12 (2014). _eprint: https://onlinelibrary.wiley.com/doi/pdf/10.1002/hbm.22601, pp. 6011–6022. DOI: 10.1002/hbm.22601. (Visited on 09/29/2023) (cited on pages 65, 66).

[133] Donald E. Kirk. *Optimal Control Theory: An Introduction*. en. Google-Books-ID: onuH0PnZwV4C. Courier Corporation, Apr. 2012 (cited on page 75).

[134] Brian D. O. Anderson and John Barratt Moore. *Optimal Control: Linear Quadratic Methods*. en. Google-Books-ID: LgUqAQAAMAAJ. Prentice Hall, 1990 (cited on page 75).

[135] Fan Chung. 'Laplacians and the Cheeger Inequality for Directed Graphs'. en. In: *Annals of Combinatorics* 9.1 (Apr. 2005), pp. 1–19. DOI: 10.1007/s00026-005-0237-z. (Visited on 12/19/2022) (cited on page 76).

[136] Nathanaël Perraudin et al. *GSPBOX: A toolbox for signal processing on graphs*. arXiv:1408.5781 [cs, math]. Mar. 2016. DOI: 10.48550/arXiv.1408.5781. URL: http://arxiv.org/abs/1408.5781 (visited on 12/19/2022) (cited on page 76).